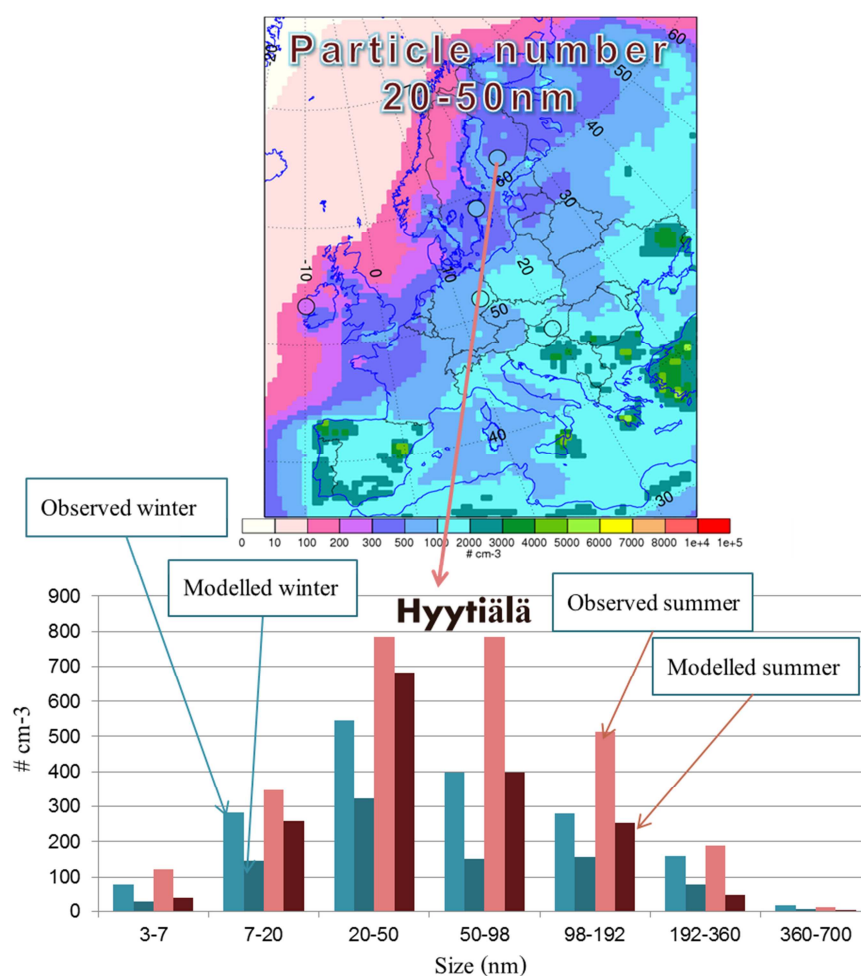# MATCH-SALSA

Multi-scale Atmospheric Transport and CHemistry model coupled to the SALSA aerosol microphysics model

Camilla Andersson, Robert Bergström, Cecilia Bennet, Manu Thomas, Lennart Robertson
Swedish Meteorological and Hydrological Institute, SE-60176 Norrköping, Sweden
Correspondence to: camilla.andersson@smhi.se

Harri Kokkola, Hannele Korhonen, Kari Lehtinen
Finnish Meteorological Institute, Kuopio Unit, P.O. Box 1627, FI-70211 Kuopio, Finland

Front:
Top panel: Mean particle number concentration in the size range 20-50nm modelled
with MATCH-SALSA (surfaces) and observed (filled circles) for 2007.
Bottom panel: Mean modelled (dark colors) and observed (bright colors) particle
number size distribution during winter (Oct-March) and summer (April-September)
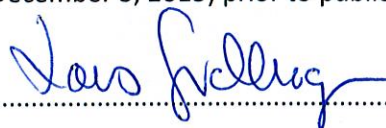half years of 2007 in the measurement site Hyytiälä in central Finland.

MATCH-SALSA

Multi-scale Atmospheric Transport and CHemistry model coupled to the SALSA aerosol microphysics model

Camilla Andersson, Robert Bergström, Cecilia Bennet, Manu Thomas, Lennart Robertson, Harri Kokkola, Hannele Korhonen and Kari Lehtinen

SUMMARY

This report presents a new aerosol dynamics version of a European scale Eulerian CTM, MATCH. The new model is called MATCH-SALSA, and includes aerosol microphysics and several options for nucleation, wet scavenging and condensation. The report entails model description, evaluation and sensitivity tests.

The new model reproduces observed higher particle number concentration (PNC) in central Europe and lower in remote regions. The model peak PNC occurs at the same particle size as the observed peak or at smaller sizes, which indicate missing growth. Total PNC is underestimated at some sites. The model performs well for particle mass, including SIA components. EC and OC are underestimated at many of the sites.

The results are sensitive to the fraction of SO_x emitted as H_2SO_4 and the optimum choice is site dependent. The model results are highly sensitive to whether organic nucleation is included or not. The model results are sensitive to amount of organic vapors in the condensation.

The model can be used in applications knowing the restrictions of what the model manages well and what needs further improvements, which is detailed in the report.

1. Introduction

The demand for improved representation of aerosols in atmospheric models has increased dramatically during recent years. This is partly due to the fact that more accurate and detailed aerosol mass and number size distributions, and information about chemical composition of the particles, are important for improving the estimates of the impact of particles on radiative forcing in climate models (e.g. Chen and Penner, 2005; Roesler and Penner, 2010). Further, aerosol particles have adverse effects on human health (e.g. Pope and Dockery, 2006), and it has been shown that aerosol size distribution, chemical composition and morphology may cause different health impacts (Schlesinger et al., 2006).

Aerosol dynamics need to be considered in order to describe particle mass and number concentrations accurately, including size distribution (Adams and Seinfeld, 2002). Size resolved PM data can be useful in both climate and health impact studies, and therefore there is a need to include a realistic description of aerosol dynamics in chemical transport models (CTMs) on the European scale.

This report presents a new aerosol dynamics version of a European scale Eulerian CTM. The new model is called MATCH-SALSA. The report includes model description, evaluation and sensitivity tests. In the final Section (7) of the report some questions are answered about the quality, use and applicability of the new model.

2. Description of MATCH-SALSA

We have implemented the sectional aerosol dynamics model SALSA (Kokkola et al., 2008) in the European scale CTM MATCH (Multi-scale Atmospheric Transport and Chemistry; Robertson et al., 1999). We call the new model MATCH-SALSA.

An earlier urban application of MATCH was applied to assess anthropogenic ultrafine particles in an urban environment, separated by seven monodisperse sizes (Gidhagen et al., 2005). Aersosol dynamics included water uptake, coagulation and dry deposition, but no nucleation or condensation. In earlier European scale MATCH versions (e.g. Robertson et al. 1999, Andersson et al. 2007; 2009), particles were handled with a simple bulk approach (with four size bins for primary particles), without any aerosol dynamic treatment (except hygroscopic growth in some model versions), but with dry and wet deposition of primary particles being dependent on particle size. The species treated were elemental carbon (EC), anthropogenic mineral dust, primary organic carbon (OC), sulfate, nitrate, ammonium and sea salt. Secondary organic aerosol was not included in the model. Particle number concentration (PNC) was not described.

In order to include aerosol dynamics in MATCH a computationally efficient version of the SALSA model was implemented in the framework of MATCH. It was implemented after the chemistry step (see Figure 1). The chemistry was adjusted slightly compared to earlier MATCH-versions, as described below.

SALSA describes aerosol hygroscopicity, nucleation, condensation and coagulation. The inclusion of SALSA improved MATCH through the inclusion of better size resolution, a description of mixing state and PNC, and a description of microphysics and particle aging. Other improvements are still under development, such as improved description of vertical transport of particles in clouds, inclusion of a terpene emission model, more detailed treatment of nitrogen gas-particle partitioning and more advanced description of aging and condensation of semivolatile organic gases.

The layout of MATCH-SALSA is illustrated in Figure 1. After initializations are completed the model iterates over time. The iterations are based on the meteorological time step where weather data are interpolated or read, new emissions are emitted and boundary concentrations are set. After this the emissions are injected and model transport fluxes are calculated with the internal sub-stepping time steps (dtadv and dtvdiff). Subsequently the model chemistry, aerosol microphysics and cloud droplet number concentration are calculated (based on the time step dtchem). Meteorological data are read at regular intervals while boundary conditions may be loaded at compound dependent intervals.

The operator-splitting approach for the different processes in MATCH-SALSA is illustrated in Figure 2. Since chemistry and aerosol dynamics are much more time consuming than the rest of the code, they are calculated with doubled time step as compared to the emission, transport and deposition.

A more detailed description of new model features, input data and model set up, that are used in the present study is given below.
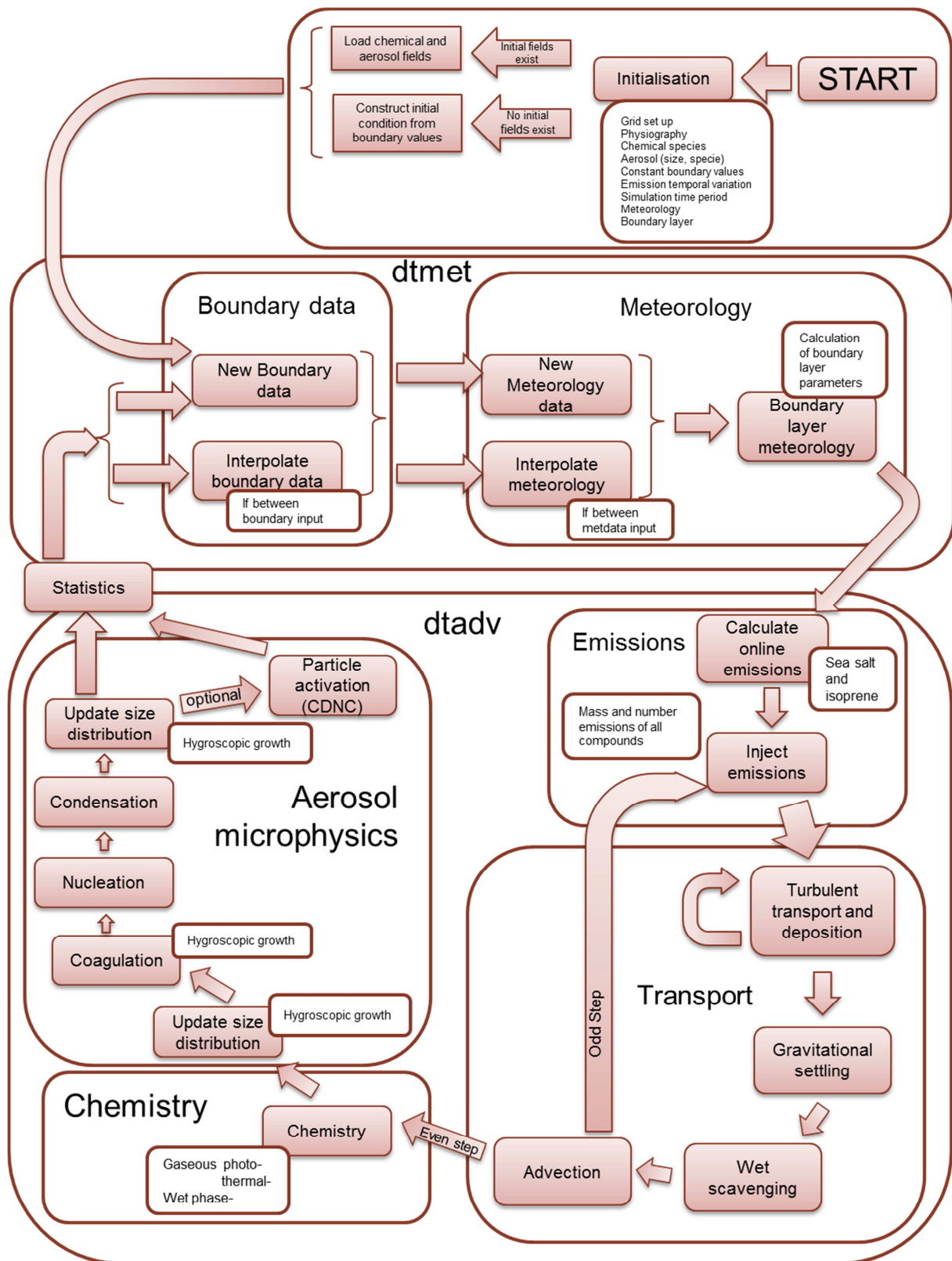
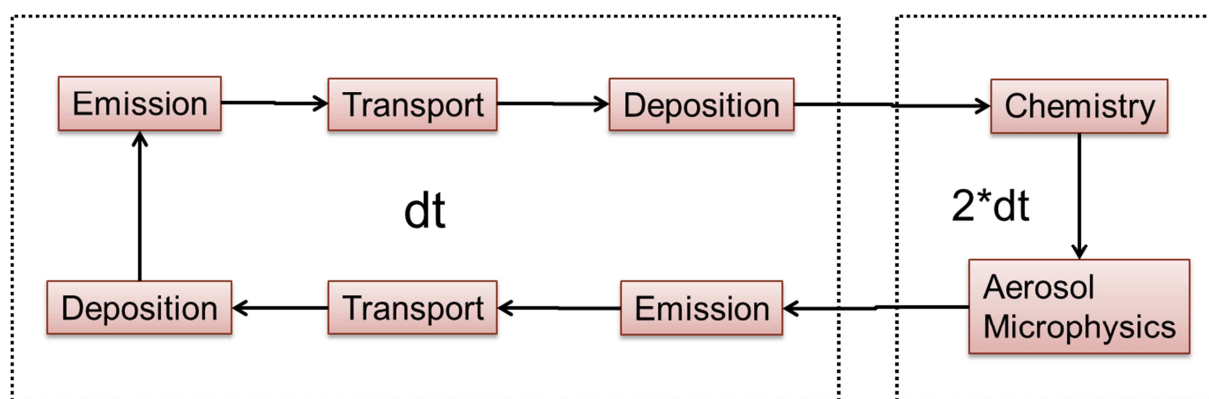**Figure 1. Data flow and time stepping in MATCH-SALSA.**

Figure 2. Details on model iteration and time stepping in MATCH-SALSA.

Emissions

Both biogenic and anthropogenic emissions are included in the model. Sea salt and isoprene emissions are calculated online, whereas anthropogenic and other emissions (volcanic sulfur, marine DMS and biogenic terpene) are given as input data to the model.

Sea salt emissions are modeled as described in Foltescu et al. (2005) but adjusted to a flexible number of size bins. For the smallest bins, up to the diameter of 1 µm the description by Mårtensson et al. (2003) was used. For larger sizes up to 10 µm in diameter the sea salt generation function was taken from Monahan et al. (1986). All particle components are emitted both as mass and number in the model. It is also possible to emit particles only as mass (without adding particle numbers); this option means that the emissions increase the size of existing particles through condensation.

Biogenic emissions of isoprene are calculated using the E-94 isoprene emission methodology proposed by Simpson et al. (1995). The model does not yet include wind-blown dust.

Transport

The transport model includes advective and turbulent transport. Particle number and mass are transported independently in MATCH-SALSA.

The advection-diffusion equation is solved in three dimensions for the atmospheric tracers through a Bott-type scheme (Bott 1989a, 1989b). The advection scheme is mass conserving and reduces numerical diffusion. This scheme was rewritten to be flexible to variable grid sizes and projections (Robertson et al., 1999). The vertical winds are calculated internally using the horizontal winds with a balancing procedure in order to assure that the transport of air is in mass-consistent balance with the input surface pressure tendencies (Heimann and Keeling, 1989).

Two formulations are used for the vertical turbulent exchange, depending on the stability in the boundary layer. For stable and neutral conditions the formulation follows Holtslag et al. (1995) and for unstable conditions the convective turnover time is used directly to determine the vertical turbulent exchange coefficient. The horizontal diffusive fluxes are assumed small compared to the horizontal advective fluxes and are therefore neglected. Deep convective transport is not included in the current model version. The transport scheme is described in more detail by Robertson et al. (1999).

Chemistry

The original MATCH photochemistry scheme (Langner et al., 1998) was, to a large extent, based on the EMEP MSC-W scheme (Simpson, 1992; Simpson et al., 1993), but with an alternative treatment of isoprene chemistry, using an adapted version of the Carter 1-product mechanism (Carter, 1996; Langner et al., 1998). A simplified mixture of a dozen representative compounds ("lumped molecules") is used to model the many different organic molecules emitted to the atmosphere (e.g., o-xylene represents all emitted aromatic species).

The gas-phase chemistry scheme in MATCH has remained mostly the same since 1998, but a number of reaction rates have been updated, taking into account new recommendations from IUPAC (Atkinson et al., 2006) and the Master Chemical Mechanism, MCM v3 (Jenkin et al., 1997; Saunders et al., 2003, via website: http://mcm.leeds.ac.uk/MCM); a few new gas phase components have also been added to the scheme. The revision of the MATCH chemistry scheme was based closely on the updates done in the EMEP MSC-W model, during 2008-2009, as documented by Simpson et al. (2012); the updated gas-phase reaction scheme in MATCH is mostly identical to the EMEP MSC-W EmChem09 scheme of Simpson et al. (2012), but for isoprene the scheme from Langner et al. (1998) is kept (with some reaction rates updated to IUPAC recommended values, Atkinson et al., 2006).

In addition to gas-phase chemistry, aqueous-phase oxidation of SO_2 in cloud water (based on Berge, 1992) and a few heterogeneous reactions for nitrogen compounds are included in the model. For MATCH-SALSA some further modifications related to particle formation have been made and the scheme used in the present work includes ca 140 thermal, wet and photolysis reactions, including about 60 different chemical species.

The chemistry code includes a very simple test scheme for secondary organic aerosol (SOA) formation from biogenic monoterpene emissions; α-pinene is used as a surrogate for all emitted monoterpenes. In the present study we assume rapid formation of condensable SOA after gas-phase oxidation of α-pinene (by O_3, OH or NO_3; oxidation rates are based on MCM v3.2, http://mcm.leeds.ac.uk/MCM); a fixed SOA yield of 30% is assumed for all oxidation paths. This fraction is input to the OM condensation scheme in SALSA. Note that the simplified BSOA "scheme" used in the present study is only included to test the organic-aerosol parts of MATCH-SALSA, with minimal changes to the standard photochemistry scheme; it is not expected to model BSOA formation in a very realistic way compared to real-world conditions but, given the high uncertainties in mono-terpene emissions (and the neglect of other BSOA-forming emissions), it was considered a reasonable approach for the development phase of MATCH-SALSA. A more detailed model for biogenic (and anthropogenic) SOA formation will be implemented in MATCH and MATCH-SALSA in the future.

Aerosol Microphysics

The aerosol dynamic model SALSA was included in MATCH; the combined model is called MATCH-SALSA. The aim of the MATCH-SALSA model is to describe aerosol mass and number concentrations, and particle size distribution features. The model is intended for coupling to climate models and radiative transfer calculations, and for estimation of human particle exposure.

The SALSA model was designed to obtain balance between computational efficiency and numerical accuracy. This was reached by keeping the tracer variables to a minimum by using a relatively coarse particle size resolution and including only the relevant chemical compounds in different particle size ranges (see Kokkola et al., 2008). The size resolution is varying across the size spectrum with higher resolution for particles that are crucial in cloud activation and for aerosol radiative properties. Aerosol number and mass concentrations are described by three ranges, divided into size bins with constant volume ratio. The number of bins in each range and the size limits of the bins are flexible. The first size range includes SO_4^{2-} and OC, the second and third size ranges includes sulfate (SO_4^{2-}), EC, OC, sea salt (NaCl) and mineral dust. SO_4^{2-} and OC are combined to calculate the water soluble fraction of the particles in the third size range. The hygroscopicity of the aerosol is calculated using the Zdanowskii-Stokes-Robinson method (Jacobson, 2002).

At the end of each microphysical time step the size distribution is updated to take into account growth or shrinkage of particles due to dynamic and chemical transformation processes. Nitrogen species are described by a simplified chemistry scheme without affecting the size distribution. They are currently handled outside SALSA. A more detailed description of the SALSA model is given by Kokkola et al. (2008) and Bergman et al. (2012), but the most important details are described below.

Nucleation schemes

Nucleation is simulated through an activation type nucleation formulation (Kulmala et al., 2006; Riipinen et al., 2007) and the formation rate of 3 nm particles (J3) is calculated according to Lehtinen et al. 2007. Nucleation is solved concurrently with condensation using the methodology of Jacobson (2002). This methodology takes into account the competition of nucleation and condensation in the mass transfer of volatile species between gas and particle phase.

There are other nucleation scheme options available for use in the model including for example binary nucleation (Vehkamaki et al., 2002), ternary nucleation (Napari et al., 2002a, 2002b) and activation of both H_2SO_4 and organic vapors (Paasonen et al., 2010). In a later section the model sensitivity is tested to some of these formulations.

Condensation

The scheme used for gas-to-particle transformation is the Analytical Predictor of Condensation scheme with saturation vapor pressure set to zero (Jacobson 1997). The method solved non-equilibrium transfer of semi-volatile compounds between gases and particles over a discrete time step. Since it requires no iteration, is mass conserving, and has been shown to be accurate over time step length of 7200 (Jacobson, 2005) it is very well suited for large scale atmospheric models such as MATCH.

Coagulation schemes

Coagulation is described using a semi-implicit scheme (Jacobson 1994). Similarly to the condensation scheme, a semi-implicit coagulation scheme does not require iteration and is mass conserving. Since coagulation is computationally the most time consuming microphysical process to simulate, coagulation between aerosol pairs for which coagulation efficiency is low are not taken into account. The detailed list of selected collision pairs in accounted for in coagulation routine are given in Kokkola et al., (2008).

Particle activation

Aerosols can act as cloud condensation nuclei altering the microphysical properties of clouds such as droplet number concentration, its albedo, effective radii and liquid water content; this impact on clouds is known as the indirect aerosol effect (Lohmann and Feichter, 2005, and references therein). To estimate the indirect aerosol forcing, it is necessary to incorporate the activation of aerosols into cloud droplets. For this, the MATCH-SALSA model can be run in an online coupled mode to a cloud activation model that computes cloud droplet number concentrations based on the prognostic parameterization scheme of Abdul-Razzak and Ghan (2002). This scheme is designed for models where a sectional representation of the aerosol size distribution is used. The number of particles activated to cloud droplets in each size section is determined by the particle size distribution, their number concentration and chemical composition as well as the updraft velocity and the maximum supersaturation of the air parcel. The parameterizations of Abdul-Razzak et al. (1998) and Abdul-Razzak and Ghan (2000, 2002) are a step forward to evaluate the sensitivity of droplet activation to both microphysical and dynamical factors because of the explicit link of updraft velocity and aerosol size distribution to cloud droplet number concentrations (Rissman et al., 2004).

Running the model with particle activation is optional. There is an option to use the resulting activated particle fraction in each size bin for calculation of incloud scavenging of particles.

Deposition

Dry deposition of trace gases are calculated with a resistance approach (Chamberlain and Chadwick, 1965) dependent on land use. Wet scavenging of most gaseous species is proportional to the precipitation intensity. For ozone, hydrogen peroxide and sulfur dioxide in-cloud scavenging is calculated using Henry's law equilibrium; sub-cloud scavenging is neglected for these species.

Wet and dry deposition of gases is described further in Andersson et al. (2007). More detailed descriptions of dry and wet deposition of *particle* species are given here.

Particle dry deposition

Particle dry deposition is calculated according to the model proposed by Zhang et al. (2001). Zhang et al. (2001) used a simplified empirical parameterization for all deposition processes. Particle growth at high humidity is included as well as dependency on land use class. The modeled dry deposition velocity (V_d) is a sum of gravitational settling velocity (V_g) and a term inversely proportional to the aerodynamic (R_a) and surface resistance (R_s)

$$V_d = V_g + \frac{1}{R_a + R_s}$$

The surface resistance is parameterized here as dependent on the collection efficiencies due to Brownian diffusion (E_B), impaction (E_{IM}) and interception (E_{IC}). For Brownian diffusion (E_B)

$$R_s = \frac{1}{\varepsilon_0 \mu_* (E_B + E_{IM} + E_{IC}) R_1}$$

Where R_1 is a correction factor representing the fraction of particles that stick to a surface, since particles larger than 5 µm may rebound when hitting the surface. ε_0 is an empirical constant and is

taken as 3 for all land use classes (as in Zhang et al. 2001). μ_* is the friction velocity. The Brownian diffusion is a function of the Schmidt number (Sc) and a collection efficiency parameter (γ):

$$E_B = Sc^{-\gamma}$$

where γ is dependent on land use. Impaction is dependent on the stokes number (St), here modeled through the equation introduced by Peters and Eiden (1992)

$$E_{IM} = \left(\frac{St}{\alpha + St}\right)^\beta$$

The β parameter in the impaction was set to 2 for all land use classes as in Zhang et al (2001). The α parameter depends on season and land use class (see Table 1). The Stokes number is simulated as in Zhang et al. (2001), with different expressions for vegetated and smooth surfaces.

Table 1. Dry deposition parameters for land use dependent particle dry deposition calculation.

	α	γ	A Apr-Sept (Oct-Mar)
Pasture	1.2	0.54	2.0E-3 (5.0E-3)
Arable	1.2	0.54	2.0E-3 (5.0E-3)
beech+oak	0.8	0.56	5.0E-3 (10.0E-3)
deciduous	0.8	0.56	5.0E-3 (10.0E-3)
low veg	1.2	0.54	2.0E-3 (5.0E-3)
rural	1.2	0.54	5.0E-3 (5.0E-3)
spruce	1.0	0.56	2.0E-3 (2.0E-3)
pine	1.0	0.56	2.0E-3 (2.0E-3)
wet land	2.0	0.54	10.0E-3 (10.0E-3)
mountain	50.0	0.54	-
urban	1.5	0.54	10.0E-3 (10.0E-3)
sea	100.	0.50	-
forest	0.8	0.56	5.0E-3 (5.0E-3)
noveg	50.0	0.54	-

The collection efficiency of interception is

$$E_{IC} = 0.5 \left(\frac{d_p}{A}\right)^2$$

where d_p is the particle diameter and A depends on season and land use surface.

Particle wet scavenging

Particles are wet deposited through incloud (W_{IC}) and subcloud (W_{SC}) scavenging. The incloud scavenging in the model depends on the fraction of cloud water (Cloud Liquid Water Content, CLWC) or ice (Cloud Ice Water Content, CIWC) that is precipitated (P) in each grid box, the solubility (F_s) of each particle size bin, the fraction of the box that is covered by cloud (CC) and the concentration of particles (c_i).

$$\frac{dc_i}{dt} = -(W_{IC} + W_{SC})$$

$$W_{IC} = -c_i \Lambda^{IC}{}_i$$

$$\Lambda^{IC}{}_i = F_s \frac{CC * P}{(CLWC + CIWC)}$$

In MATCH-SALSA the solubility is assumed to be the fraction of particles that are activated as cloud droplets. In the base case version of MATCH-SALSA the solubility of the particles is parameterized following Seinfeld and Pandis (1997), which means that in-cloud particles larger than 80nm in diameter will be activated as cloud droplets. This is of course a simplification; in reality the activated fraction depends on meteorological conditions. A more advanced formulation, which is more CPU-time consuming, is also implemented in the model. In this formulation the parameter F_s is calculated in each time step for each grid point, using a model that describes particle activation. Here F_s is the activated fraction of each particle class. The results from these two formulations are compared in Section 6 of this report.

The subcloud scavenging in the model is treated in a similar way as by Dana and Hales (1976). In MATCH-SALSA a simplified approach is used where a monodisperse washout coefficient is calculated for each particle bin and a standard rain drop spectrum[a] is assumed for all precipitation. The washout coefficient (i.e., the fraction of a species that is removed by precipitation below clouds) depends on precipitation amount and takes into account particle collection by Brownian diffusion, inertial impaction and interception. The total wet deposition is the sum of the incloud and subcloud scavenging.

Alternatively, much simpler, parameterized, formulations for the wet scavenging can be used, and the effects of using such parameterizations are investigated in sensitivity tests in Section 6.

---

[a] A representative frontal rain spectrum is used, R_g=0.02 cm, Σ_g=1.86 (Dana and Hales, 1976).

3. Model setup

In this section we describe the setup of the base case simulation using MATCH-SALSA. This simulation is evaluated thoroughly against measurements in Section 4. The settings and input for other simulations (sensitivity tests etc.) are described in corresponding sections of the report.

A horizontal model resolution of 44km was used in this study. For this resolution we use a 10 minute model time step for transport and deposition, whereas chemistry and aerosol microphysics is calculated every 20 minutes (doubled time step as described in Section 2).

The following sections describe the settings for aerosol microphysics, input data and boundary conditions that were used in the base case simulations. The emissions that were used in the base case simulation are also shown, as well as the other emissions that were used in the sensitivity tests.

Aerosol microphysics settings
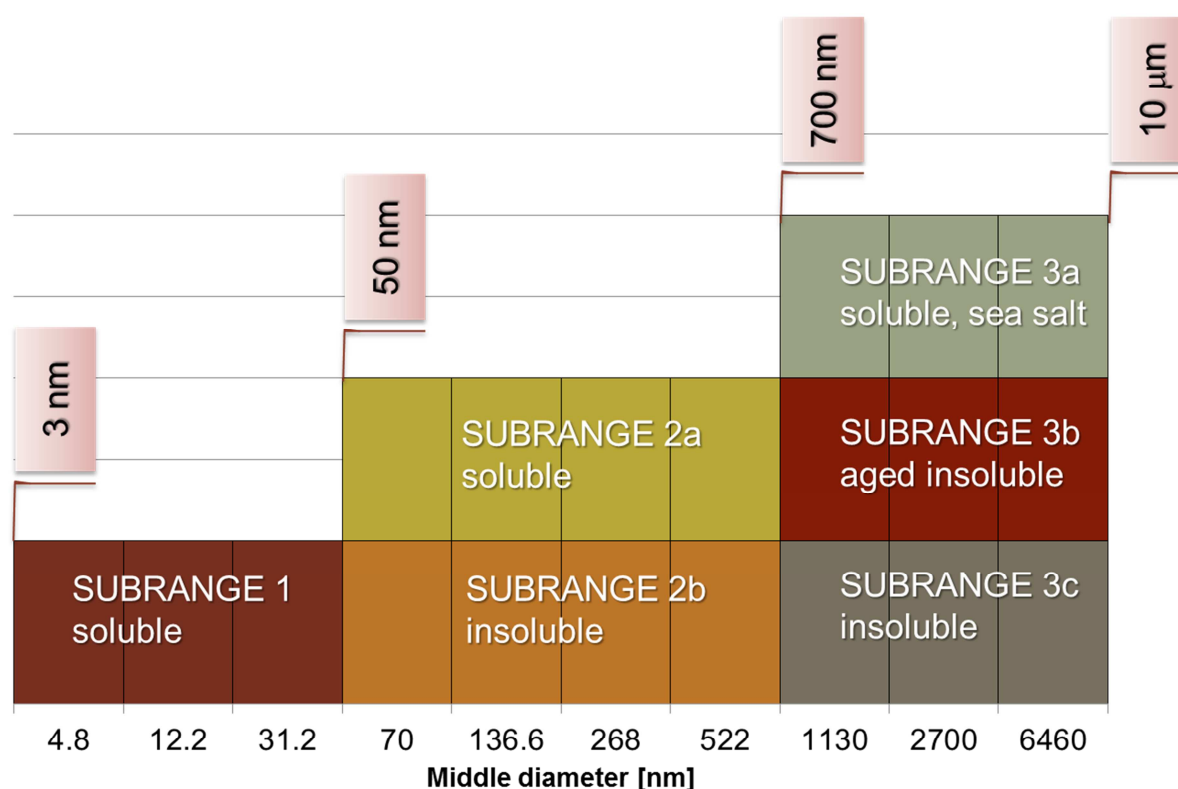
Figure 3. Aerosol division into bins in the three SALSA subranges in the base case set up of MATCH-SALSA.

As detailed in the model description, the size distribution and chemical speciation in MATCH-SALSA were divided into three subranges. The size limits of the ranges and the number of bins in each subrange are adjustable in the code. The following settings were used in this report (see Figure 3): The first subrange, consists of Nucleation and Aitken mode particles and was chosen to cover the diameter interval 3-50nm, with three log-normally distributed size bins; the second subrange, consists of hygroscopic (soluble) and non-hygroscopic (insoluble) accumulation mode particles, and covered the diameter interval 50-700nm, with four bins each for the two particle types; the third

subrange, includes sea salt particles, hygroscopic (aged insoluble) and non-hygroscopic (insoluble) coarse mode particles and covered the diameter size range 700nm-10µm, with three size bins for each of the three particle types. Thus, there were in total 20 size bins. However, in order to decrease the computational demand not all chemical components are included in all bins.

Boundary conditions

The concentrations of gaseous and particle species at the lateral and top boundaries of the model domain were set as described in Andersson et al. (2007). However, for organic matter (OM) the southern, western and northern boundary concentrations were set to the mass size distribution and totals of marine OM during different seasons as described by O'Dowd et al. (2004). These values were set at the first model level and linearly interpolated to the top and eastern boundaries where the OM concentration was set to zero. The corresponding PNCs were also introduced at the southern, western and northern lateral boundaries. The size-resolved boundary concentrations of OC are shown in Table 2.

Table 2. Lateral and top boundary concentrations of organic matter. The lateral boundary values are valid for the bottom centre of the boundary and interpolated between the top and other lateral boundary values. Unit: mol OM mol^{-1} air.

Size bin	season	top/east	west/south/north
4 (50-98nm)	Mar-Nov	0.	3.0E-11
	Dec-Feb	0.	0.
5 (98-192nm)	Mar-Nov	0.	1.7E-10
	Dec-Feb	0.	0.
6 (192-374nm)	Mar-Nov	0.	6.7E-10
	Dec-Feb	0.	7.6E-11
7 (374-700nm)	Mar-Nov	0.	5.5E-10
	Dec-Feb	0.	6.2E-11
15 (0.7-1.25µm)	Mar-Nov	0.	6.0E-10
	Dec-Feb	0.	1.6E-10
16 (1.75-4.18µm)	Mar-Nov	0.	3.1E-10
	Dec-Feb	0.	0.
17 (4.18-10µm)	Mar-Nov	0.	2.6E-10
	Dec-Feb	0.	7.7E-11

Input emissions

Monthly biogenic emissions of monoterpenes (see Figure 4) were taken from the EMEP MSC-W (European Monitoring and Evaluation Programme Meteorological Synthesizing Centre - West) model (Bergström et al., 2012; Simpson et al., 2012). α-pinene is used as a surrogate species for all biogenic monoterpenes. The emissions were distributed with a fixed diurnal variation having a day-time maximum and a night-time minimum, based on the mean diurnal variation of the EMEP MSC-W

model emissions in Finland. The resulting diurnal variation is shown in Table 3. The treatment of the biogenic monoterpene emissions in the present study is, thus, very simplified and in the near future MATCH will be updated with an online model of the emissions. A more detailed description of the biogenic SOA formation will also be implemented, based on the models by Bergström et al. (2012).

0   10   100   1000   1e+4   2e+4   3e+4   4e+4   5e+4   7e+4   1e+5   2e+5   3e+5   5e+5   1e+6   5e+6   1e+7
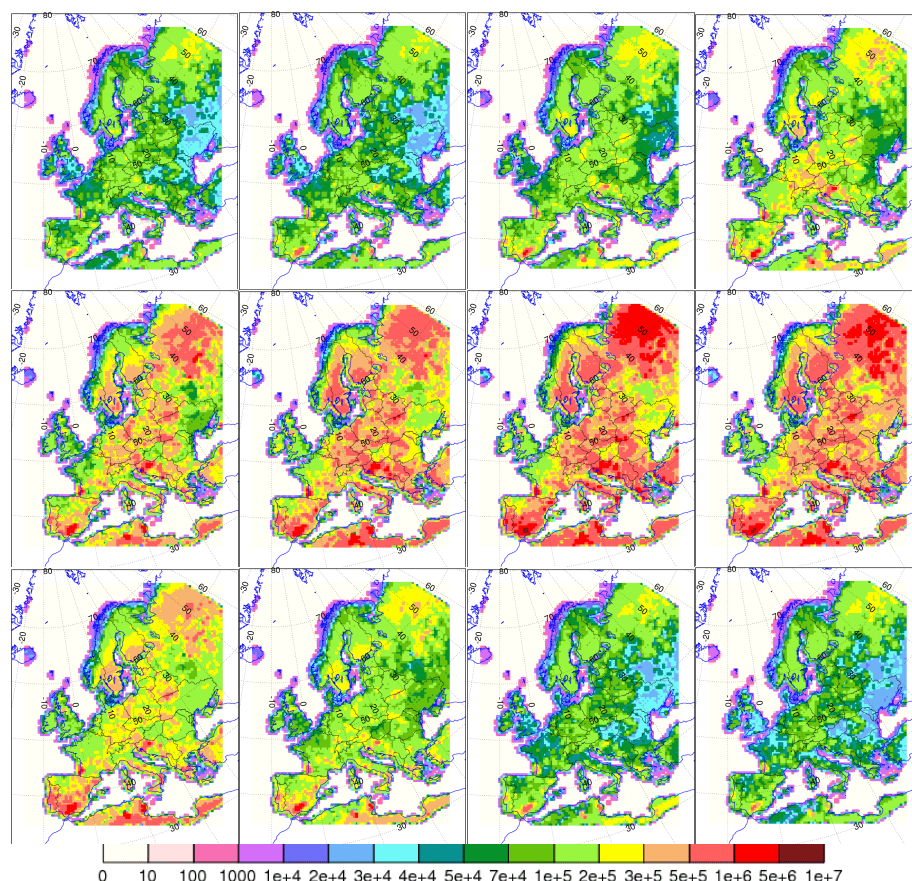
Figure 4. Monthly α-pinene emissions used in this study, based on EMEP MSC-W model results (Bergström et al., 2012). Unit: kg month[-1].

Table 3. Diurnal variation of emission of α-pinene emissions. Emission fraction, i.e. fraction of the total daily emission emitted *per hour*.

Time (h)	00-03	03-05	05-06	06-07	07-08	08-09	09-10
Emission fraction	0.008	0.007	0.014	0.041	0.064	0.073	0.076
Time (h)	10-12	12-13	13-14	14-15	15-16	16-17	17-18
Emission fraction	0.077	0.078	0.080	0.083	0.086	0.081	0.055
Time (h)	18-19	19-20	20-21	21-22	22-24		
Emission fraction	0.023	0.015	0.012	0.010	0.009		
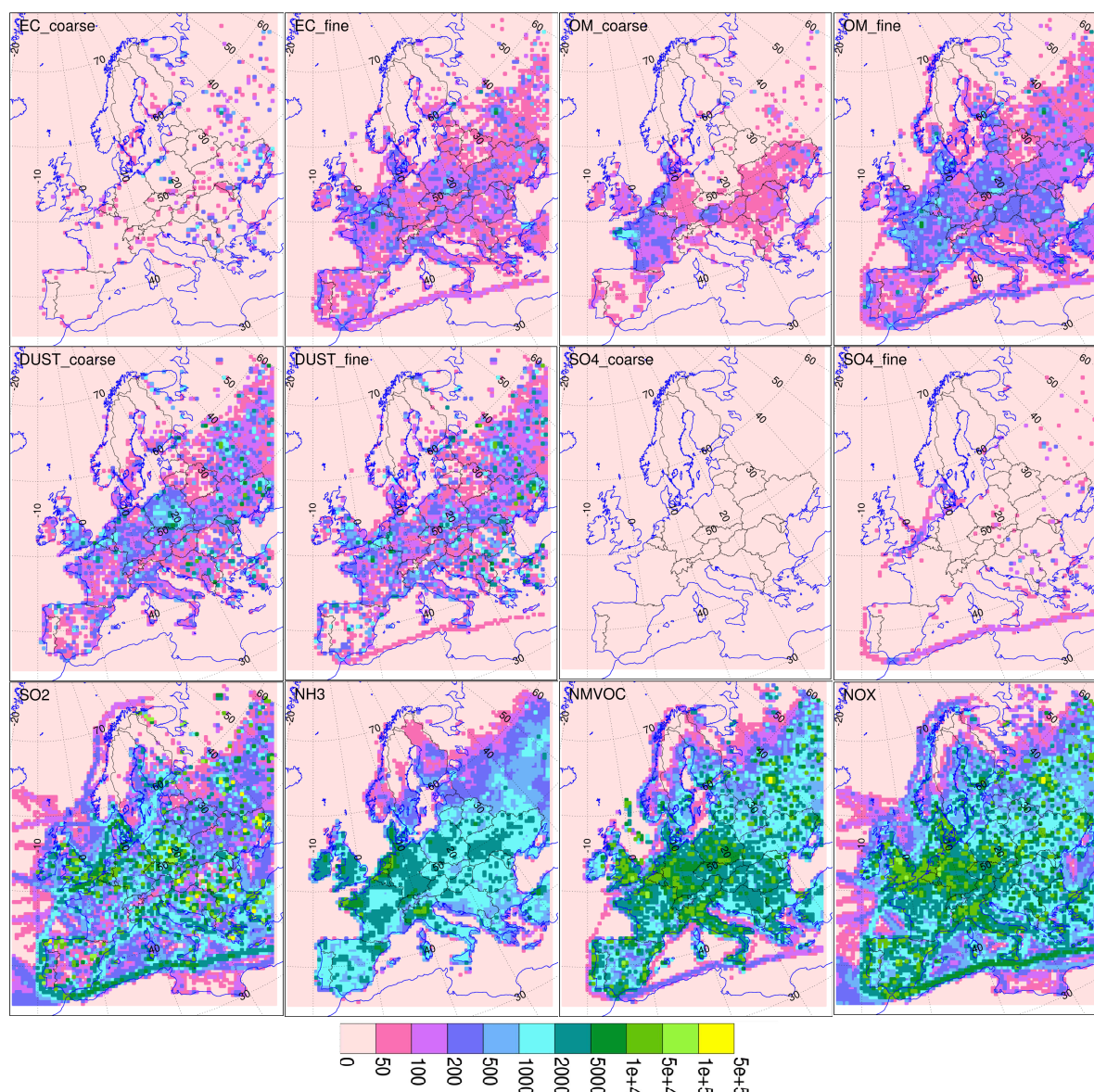
Figure 5. Annual anthropogenic emissions for 2007 from the TNO-MACC inventory (see text). Unit: tonnes year⁻¹.

The anthropogenic emissions used in the base case simulation are taken from the TNO-MACC emission inventory (Kuenen et al., 2011; Pouliot et al., 2012; see also the MACC - Monitoring the Atmospheric Composition and Climate - project web page http://www.gmes-atmosphere.eu/). The emissions include oxidized sulfur compounds (SOx), nitrogen oxides (NOx), ammonia (NH₃), carbon monoxide (CO), non-methane volatile organic compounds (NMVOC), EC, OM and other inorganic primary particles (DUST). The emissions of gaseous species are split between 11 SNAP sectors (EMEP/EEA 2009), whereas the primary particle emissions are split between the first 10 SNAP sectors (EMEP/EEA 2009) and a separate sector for international shipping. The TNO-MACC emissions are given as annual totals (Figure 5); seasonal, weekday and diurnal variations of the emissions are based on results from the GENEMIS project (http://genemis.ier.uni-stuttgart.de/; Friedrich and Reis, 2004).

15

The particle emissions of EC and OM[b] were distributed over different particle sizes according to sector resolved mass size distributions described by Visschedijk et al. (2009). They describe the size distribution of mass-based emissions for different SNAP sectors. Most SNAP Sectors are described by uni-modal distributions, except SNAP sector 4 (production processes) and international shipping that are described by bimodal distributions. The size distributions of EC and OM (see Table 4) are identical except for SNAP sector 9 (waste treatment and disposal).

Table 4. Parameters for distribution of EC and OM mass on particle sizes

SNAP	EC		OM		Number of modes (FRAC^1:FRAC^2)
	M (mode, mobility nm)	σ	M (mode, mobility nm)	σ	
1	120	0.5	120	0.5	unimodal
2	200	0.7	200	0.7	unimodal
3	120	0.5	120	0.5	unimodal
4	80(1) 1500(2)	0.6(1) 1(2)	80(1) 1500(2)	0.6(1) 1(2)	bimodal $(\frac{1}{6}:\frac{5}{6})$
5[c]	-	-	-	-	-
6[c]	-	-	-	-	-
7	140	0.45	140	0.45	unimodal
8	140	0.45	140	0.45	unimodal
9	100	1	200	1.5	unimodal
10	180	0.7	180	0.7	unimodal
internat shipping	200(1) 900(2)	0.5(1) 0.5(2)	200(1) 900(2)	0.5(1) 0.5(2)	bimodal $(\frac{11}{21}:\frac{10}{21})$

The distribution of the EC and OM mass are lognormal distributions, according to

$$\mu = \ln(Me^{\sigma^2})$$

$$E^i(D) = \frac{FRAC^i}{D\sqrt{2\pi}\sigma}e^{-\frac{(\ln D - \mu)^2}{2\sigma^2}}$$

where the particle size distribution, $E^i(D)$, is given as a function of the mobility diameter D. The three parameters: M, the mode (peak); σ, the standard deviation; and FRAC^i, the mass fraction in each mode, are given in Table 4. e^μ is the median (expected) value in the lognormal distribution.

Fine dust (with particle diameter below 2.5 µm) was distributed on the largest accumulation mode size in the non-soluble class. The distribution was parameterized using the mode and σ_{log} of the log-normal distributions. The resulting total model domain emissions of anthropogenic particle mass and number per size in the model are shown in Figure 6.

---

[b] OM emissions are assumed to be distributed over different particle sizes in the same way as OC.
[c] No EC or OM emissions in SNAP sectors 5 and 6 (extraction and distribution of fossil fuels and solvent use).
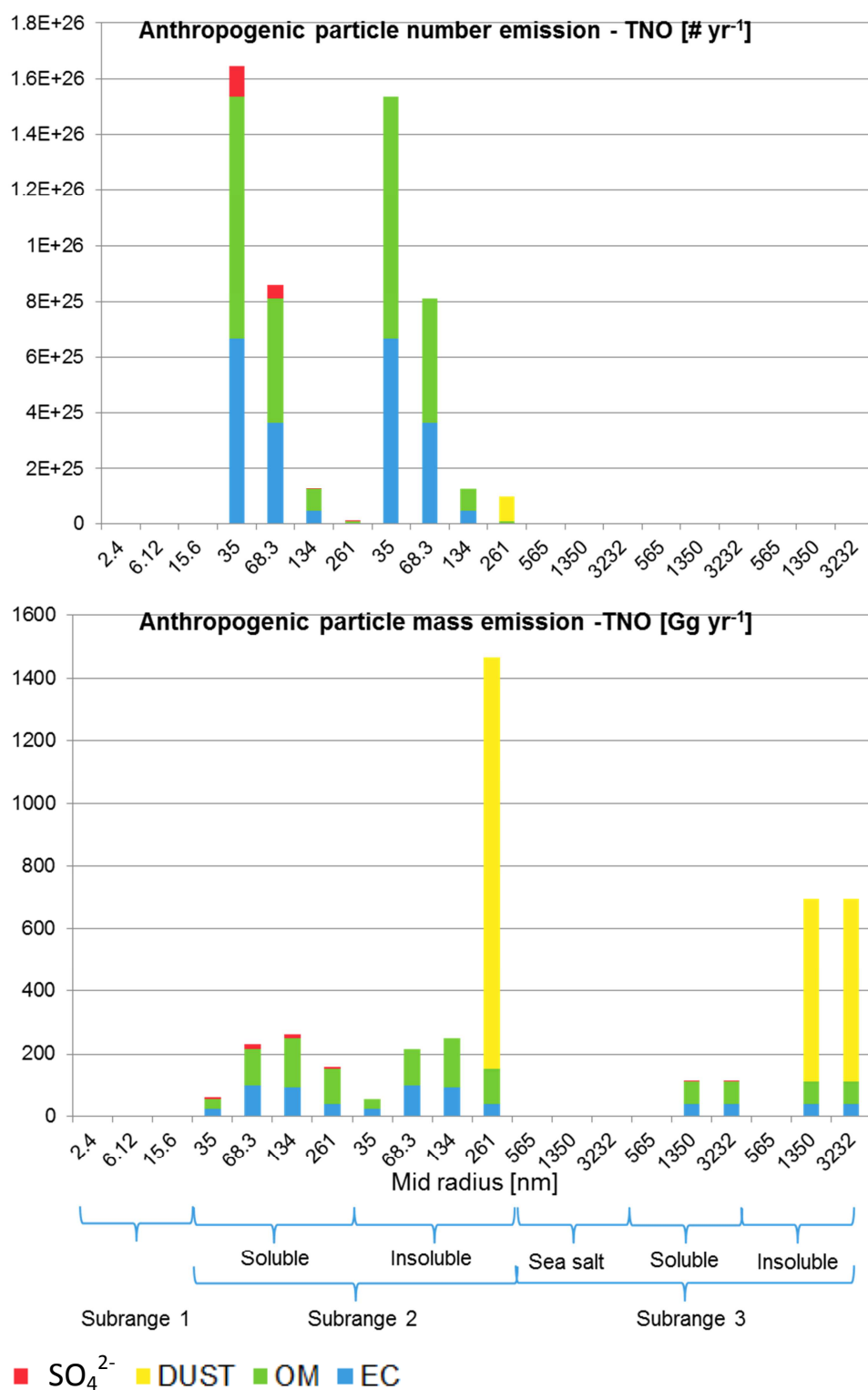
Figure 6. Annual anthropogenic size resolved particle number (top) and mass (bottom) emissions summed over the model domain. Note that particle number and mass emissions due to primary sea salt are not included in the diagrams.

The emissions of SO_x were split into 99% SO_2 and 1% H_2SO_4. The distribution of SO_x emissions between SO_2 and more oxidized compounds was discussed by Spracklen et al. (2005); the fraction of SO_2 increases with grid resolution and is typically set to between 95-100% in European scale models.

The impact of the distribution between SO_2, H_2SO_4 and SO_4^{2-} on the modeled PNC is investigated in Section 6 of this report. The processes through which SO_2 forms particulate sulfate (oxidation, followed by nucleation and condensation of H_2SO_4) add to the total PNC but may also shift the size distribution to larger sizes. The H_2SO_4 nucleation forms many small particles that either coagulate with each other or with larger particles. H_2SO_4 can also condense on already existing particles. These processes are competing. Therefore we chose to distribute emitted sulfate mass over particle sizes in the same manner as OM. The corresponding numbers of particles were also emitted in each bin.

NO_x was emitted as 95% NO and 5% NO_2. NMVOC emissions were divided into 10 surrogate compounds, using SNAP-sector specific distributions.

Meteorological data

Meteorology is input at regular time intervals; here we used three-hourly fields from the HIRLAM (Hi-Resolution Limited-Area Model; Undén et al., 2002) weather forecast model. The input meteorology is interpolated to hourly resolution. The model is set up covering Europe with a spatial resolution of 44km. In the vertical the model follows the model levels of the meteorological input data, using the lowermost 22 model levels up to about 5km height. The lowest model level is ca 60m thick.

4. Evaluation of MATCH-SALSA

Statistical metrics

In this section we present evaluation of MATCH-SALSA. This was conducted by comparing model results to measurements extracted from the measurement data bases EBAS (http://ebas.nilu.no) and EMEP (http://www.emep.int) for the year 2007. In the following sections we describe the model performance for particle species and total particle mass. We use the normalized mean bias (%bias), defined as the deviation in mean values (M^i) relative to the observed mean given in per cent, expressed as

$$\%bias = 100 \cdot \frac{M^{mod} - M^{obs}}{M^{obs}}$$

The %bias thus shows whether the model overestimates or underestimates on average.

We also want to know if the model adequately reproduces spatial and temporal variations. For this we determine the global correlation coefficient (also known as the Pearson correlation coefficient, r), expressed as

$$r(mod, obs) = \frac{C(mod, obs)}{\sqrt{V(mod, mod)V(obs, obs)}}$$

where C(mod, obs) is the covariance between all valid observed and modeled values at all stations and V(mod,mod) and V(obs,obs) are the modeled and observed variance. The root mean square error, RMSE is a measure of the combined variation and bias errors. Here we have used CV(RMSE), which means the RMSE normalized to the observed mean (also known as the coefficient of variation of the RMSE), expressed as,

$$CV(RMSE) = 100 \cdot \frac{\sqrt{\frac{1}{N} \sum_{i=1}^{N} (x_{mod}^i - x_{obs}^i)^2}}{M_{obs}}$$

The mean average of the variables at each station is used to form the spatial %bias, R and CV(RMSE) Thus, the spatial measures evaluate how well the model represent geographical variations, whereas the global measures also take into account the model performance on the temporal scale.

In the following section we evaluate the model through discussing model scores for these metrics. As the model was developed in terms of particle treatment, and especially aerosol dynamic processes, we focus on describing and discussing evaluation results for size resolved particle numbers and speciated particle components.

Measurement data

The measurement data that were used to evaluate the particle number size distribution, particle mass ($PM_{2.5}$ and PM_1), EC and OC were extracted from EBAS. The stations used in the evaluation of particle number size distribution, PM_1, $PM_{2.5}$, EC and OC are summarized in Table 5. Secondary

inorganic aerosol (SIA) species were evaluated against available measurements in the EMEP network for 2007[d].

Table 5. Measurement sites used in the model evaluation of EC, OC, PM_1, $PM_{2.5}$, PM_{10} and PNC. Further details can be found on the web sites of ebas (http://ebas.nilu.no) and EMEP (http://www.emep.int). In the evaluation of sulfur and nitrogen components all sites in the EMEP database were used, except for sites deviating more than 250m vertically from the modeled level.

Country		Code	Lat	Lon	Altitude	Components	Comment
Austria	Ilmitz	AT02	47.77	16.77	117	PM_1, $PM_{2.5}$	
Czech Rep.	Kosetice	CZ03	49.58	15.08	534	EC, OC	in PM_{10}
						$PM_{2.5}$	
Denmark	Lille Valby	DK41	55.69	12.13	10	PM_1, $PM_{2.5}$	
Finland	Hyytiälä	FI50	61.85	24.28	181	PNC	51 sizes, 3.160nm-1000nm
Finland	Virolahti II	FI17	60.53	27.69	4	PM_1, $PM_{2.5}$	
France	Puy de Dome	FR30	45.77	2.95	1465	EC, OC	in $PM_{2.5}$
Germany	Melpitz	DE44	51.53	12.93	87m	PNC	39 sizes, 3.7-859.4nm
						EC, OC	in PM_1, $PM_{2.5}$, PM_{10}
	Waldhof	DE02	52.80	10.76	74	PM_1, $PM_{2.5}$	
	Schauinsland	DE03	47.91	7.91	1205	$PM_{2.5}$	
Hungary	K-Puszta	HU02	48.97	19.58	125	PNC	46 sizes, 5.620nm-1000nm.
Ireland	Mace Head	IE31	53.33	-9.90	15	PNC	113 sizes, 8.1638nm-475.9047nm
						$PM_{2.5}$	
Italy	Montelibretti	IT01	42.10	12.63	48	EC, OC	in $PM_{2.5}$
						$PM_{2.5}$	
	Ispra	IT04	45.80	8.63	209	EC, OC	in $PM_{2.5}$
						$PM_{2.5}$	
Netherlands	Overtoom[e]	NL114	52.36	4.81	3	EC, OC	in $PM_{2.5}$
Norway	Birkenes	NO01	58.38	8.25	190	EC, OC	in $PM_{2.5}$, PM_{10}
Slovenia	Iskrba	SI08	45.57	14.87	520	$PM_{2.5}$	
Spain	Víznar	ES07	37.23	-3.53	1265	$PM_{2.5}$	
	Niembro	ES08	43.44	-4.85	134	$PM_{2.5}$	
	Campisabalos	ES09	41.28	-3.14	1360	EC, OC	in $PM_{2.5}$, PM_{10}
						$PM_{2.5}$	
	Cabo de Creus	ES10	42.32	3.32	23	$PM_{2.5}$	
	Barcarrola	ES11	38.48	-6.92	393	$PM_{2.5}$	
	Zarra	ES12	39.09	-1.10	885	$PM_{2.5}$	

[d] All available data for 2007 were used, except data from sites where the height of the first model level deviated more than 250m from the altitude of the measurement station.

[e] Overtoom is an urban background station in Amsterdam, the Netherlands.

	Paenausende	ES13	41.28	-5.87	985	PM$_{2.5}$	
	Montseny	ES1778	41.77	2.35	700	EC, OC	in PM$_{2.5}$, PM$_{10}$
	Els torms	ES14	41.40	0.72	470	PM$_{2.5}$	
	Risco Llamo	ES15	39.52	-4.35	1241	PM$_{2.5}$	
	O Saviñao	ES16	43.23	-7.70	506	PM$_{2.5}$	
Sweden	Aspvreten	SE12	58.80	17.38	20	PNC	11.1nm-417.8nm, 36 size bins.
						PM$_{2.5}$	
	Vavihill	SE11	56.02	13.15	175	PM$_{2.5}$	
Switzerland	Rigi	CH05	47.07	8.47	1031	PM$_1$, PM$_{2.5}$	
	Payerne	CH02	46.83	6.95	489	EC, OC	in PM$_{2.5}$
						PM$_1$, PM$_{2.5}$	
UK	Harwell	GB36	51.57	-1.32	137	PM$_{2.5}$	
						EC, OC	in PM$_{10}$
	Auchencorth Moss	GB48	55.79	3.24	260	PM$_{2.5}$	

For evaluating PNC, five stations were chosen to represent different parts of Europe; all the sites are classified as rural background sites. Two of the measurement sites: Melpitz (in eastern Germany) and K-Puszta (in central Hungary), are relatively close to regions with large emissions. Hyytiälä (in the inland of southern Finland) and Aspvreten (ca 70 km south west of Stockholm, in south eastern Sweden) were chosen as regional background stations occasionally impacted by aged particles due to transport from large emission sources in Europe. Mace Head was chosen to represent clean marine conditions. It is included to investigate the model performance in a clean marine air mass, occasionally influenced by long-range transport from continental Europe or emissions from the British Isles.
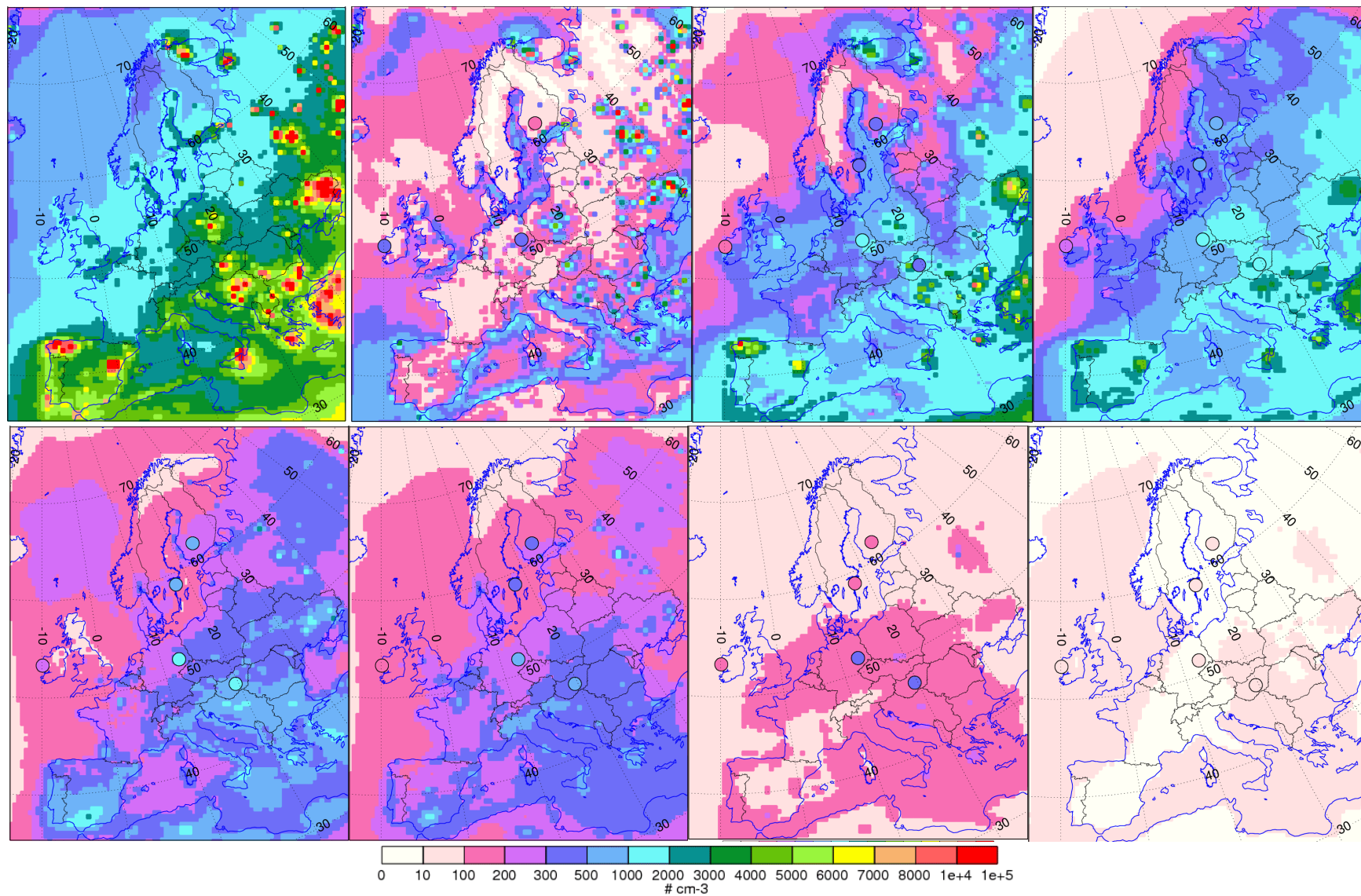
Figure 7. Calculated annual mean (2007) particle number concentration (PNC) in Europe. Top row from left to right: Total PNC (sum of all sizes), and PNC in size bins $PNC_{3<d<7nm}$, $PNC_{7<d<20nm}$, $PNC_{20<d<50nm}$. Bottom row from left to right: $PNC_{50<d<98nm}$ $PNC_{98<d<192nm}$, $PNC_{192<d<360nm}$, $PNC_{360<d<700nm}$. Observed annual mean PNC (filled circles) at the observation sites: Hyytiälä (Finland), Aspvreten (Sweden), Melpitz (Germany), K-Puszta (Hungary) and Mace Head (Ireland) when observed numbers exist in the indicated interval.

Model evaluation of particle number concentration (PNC)

Figure 7 shows the modeled annual mean PNC in Europe; both total PNC and the PNC in the different model size bins up to 700nm are shown. Corresponding measured annual mean PNC at the five observation sites are also displayed in circles for particle sizes where measurements are available.

The largest modeled total PNC are found in areas with high SOx emissions (e.g., areas around large point sources in Spain, Poland, south-eastern Europe, the Ukraine, Russia and the area around Etna; as well as along shipping routes around the Iberian Peninsula and the Gibraltar strait). These results are in line with previous other model studies (e.g. Spracklen et al., 2010; Yu and Luo, 2009).

For the whole grid, the total modeled PNC correlates strongest with SOx emissions (see Table 6). SOx is partly emitted as H_2SO_4 and partly as SO_2. H_2SO_4 is involved in new particle formation through nucleation, as well as in particle growth, which at least partly explains this correlation.

Table 6. Spatial (Pearson) correlation coefficient between total annual gridded emission and modeled annual mean total particle number concentration

Emitted specie	SOx	DUST coarse	EC fine	NOX	SO_4^{2-} fine	SO_4^{2-} coarse	DUST fine
r	0.53	0.49	0.46	0.44	0.43	0.40	0.39
Emitted specie	CO	NMVOC	EC coarse	OM fine	α-pinene	NH_3	OM coarse
r	0.39	0.36	0.35	0.34	0.19	0.14	0.12

The bins in the Aitken mode (particle diameters 7-20nm and 20-50nm) contribute most to the total PNC in the model. The highest PNC in the smallest, nucleating, bin are found in the urban areas in Russia and Belorussia. Increased values in this bin are also seen along the shipping lanes, as a result of relatively clean air combined with primary fine particle and SOx emissions. The Aitken mode PNC pattern is similar to the total PNC distribution, and the highest concentrations are found in areas in Spain, Turkey, Former Yugoslavia, Bulgaria, and north-eastern Russia, and around the volcano Etna. The highest accumulation mode (50-700nm) PNC is found in southern Europe. This is partly due to relatively large emissions of primary fine particles and SOx; but another important reason is less precipitation in southern Europe compared to the north and west, allowing accumulation mode particles to reside longer in the atmosphere.

Table 7. Statistics from evaluation of modeled (MATCH-SALSA) to observed daily mean particle number concentration for winter (January-March and October-December) and summer (April-September) half-years 2007. Percentages are given in relation to observed mean.

Measurement site		Aspvreten		Hyytiälä		Melpitz		K-Puszta		Mace Head	
Size interval[f] (nm)		20-374	50-374	3-700	50-700	3-700	50-700	7-700	50-700	7-374	50-700
winter	obs mean (1000 cm^{-3})	1.4	0.9	1.7	0.8	4.5	2.3	3.1	2.6	0.9	0.5
	mod mean (1000 cm^{-3})	0.7	0.4	0.9	0.4	1.6	0.5	3.7	0.9	0.8	0.4
	%bias	-51	-56	-49	-54	-66	-79	18	-67	-8	-20
	R	0.1	0.26	0.31	0.31	0.58	0.53	0.24	0.58	0.27	0.14
	CV(RMSE) (%)	77	91	72	84	75	93	88	75	120	150
	# days	179	179	177	177	171	171	101	101	172	172
summer	obs mean (1000 cm^{-3})	2.2	1.4	2.6	1.5	7.1	2.6	3.4	2.2	1.2	0.6
	mod mean (1000 cm^{-3})	1.2	0.5	1.6	0.7	3.7	1.0	7.4	1.8	1.5	0.3
	%bias	-48	-64	-37	-53	-47	-60	119	-20	17	-51
	R	0.05	0.46	0.31	0.53	0.66	0.59	0.36	0.4	0.52	0.6
	CV(RMSE) (%)	67	77	58	68	63	74	179	54	145	113
	# days	176	176	183	183	172	172	151	151	161	161

Overall performance

Evaluation statistics for daily total PNC and PNC in the accumulation mode (PNC$_a$) at the five measurement sites are presented in Table 7. The size ranges for PNC and PNC$_a$ vary between the stations depending on the measurement interval. We separate performance during summer half-years (April-September) from winter (October-March). The reason for this is the differences in both primary emissions and atmospheric processes between the seasons. For example there is more residential biomass burning emissions during winter than during summer, whereas there are more biogenic VOC emissions during summer. Both these sources are associated with large uncertainties in the emission inventory and the model. The chemical transformation of terpenes to secondary organic aerosol in the atmosphere is also a source of uncertainty.

Modeled total PNC is generally in moderate to poor agreement with the observations, at least at the time scale of daily mean concentrations. At most sites the normalized mean bias is large both in summer and winter and the correlation coefficients are low. The normalized root mean square error CV(RMSE) is above 50% at all stations in both seasons. The relatively poor agreement between model and observations is not unexpected considering the simplifications discussed earlier; especially the handling of secondary organic aerosol is crude in this MATCH-SALSA version, and mostly intended to give a first estimate of this potentially very important component of the PM; the model treatment of particulate nitrogen also needs further work. Both SOA and particulate nitrogen are important for new particle formation and for the growth of the particles to larger sizes.

---

[f] The lower limit of the measurement interval at Hyytiälä and Melpitz is 3.2nm and at Mace Head it is 8.2nm.

Particle number size distribution

At Aspvreten, Hyytiälä and Melpitz both the total and the accumulation mode PNC are underestimated for both summer and winter. At K-Puzta and Mace Head the accumulation mode is underestimated, whereas the mean total PNC is overestimated or close to the observed. This indicates that there are differences in model performance within the size spectra. This is illustrated in Figure 8, where both the modeled and measured mean PNC size distributions are shown at the five observation sites, for winter and summer.

From the size distribution it is clear that it is a common feature that the PNC is underestimated or on the same level as the measurements for the measurement sites, except for the very smallest sizes at K-Puszta and Mace Head, where the numbers are overestimated, both during winter and summer. The shape of the size distribution is captured well, but there is a tendency for a shift of the maximum to smaller sizes in the model than in the observations, especially during winter at K-Puszta and the summer at Mace Head. The reason for the maximum occurring at too small sizes is likely too little condensation in the model. This may be improved in future model versions that include a more realistic treatment of SOA formation and nitrogen condensation processes.

Spatial distribution of total and accumulation mode particle number

Bar diagrams of 6-month average (summer and winter) total and accumulation mode PNC, at the measurement sites, are shown in Figure 9; the annual mean PNC for the full model domain is shown in Figure 7.

The model captures the general features of higher total and accumulation mode PNC in central parts of Europe than in the outer parts of the model domain. Aspvreten and Mace Head have the lowest modeled and observed PNCs. However, looking in more detail at the stations there are some discrepancies.

Melpitz has the highest observed total PNC, followed by K-Puszta, during both winter and summer; the model predicts the highest PNC in K-Puszta followed by Melpitz. The highest observed accumulation mode PNCs are found at K-Puszta and Melpitz during both half-years (the PNC are at similar levels for both seasons and both sites, slightly higher at K-Puszta during winter and somewhat higher at Melpitz in summer). The model predicts maximum accumulation mode PNC at K-Puszta for both winter and summer, followed by Melpitz at a much lower level.

Thus the spatial distribution of PNC in the model is not in perfect agreement with the variation in the observations. There may be many reasons for this. One important reason for the high modeled total PNC at K-Puszta is the high rate of nucleation which is caused by the large emissions of SOx in the area. It is possible that choice of fractions of H_2SO_4 emission in the model is not well suited for the time scale from source to measurement site at this location. The matter of emission fractions of SO_2 and more oxidized states of SOx is further discussed in Section 6.
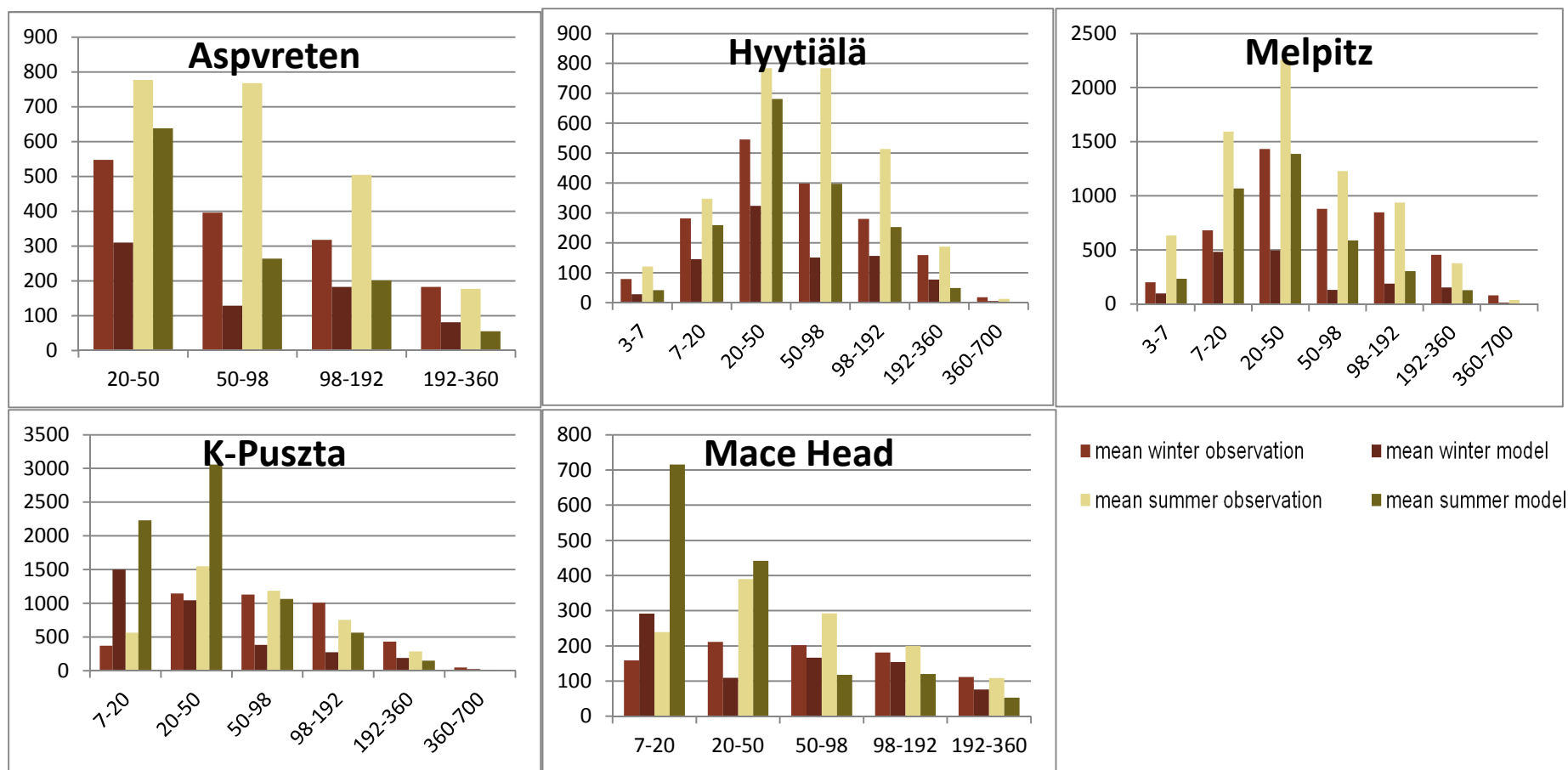
Figure 8. Modeled and measured winter (Jan-March, Oct-Dec) and summer (April-September) mean particle number concentration size distribution at five measurement sites in Europe during 2007. Unit: # cm^{-3}.
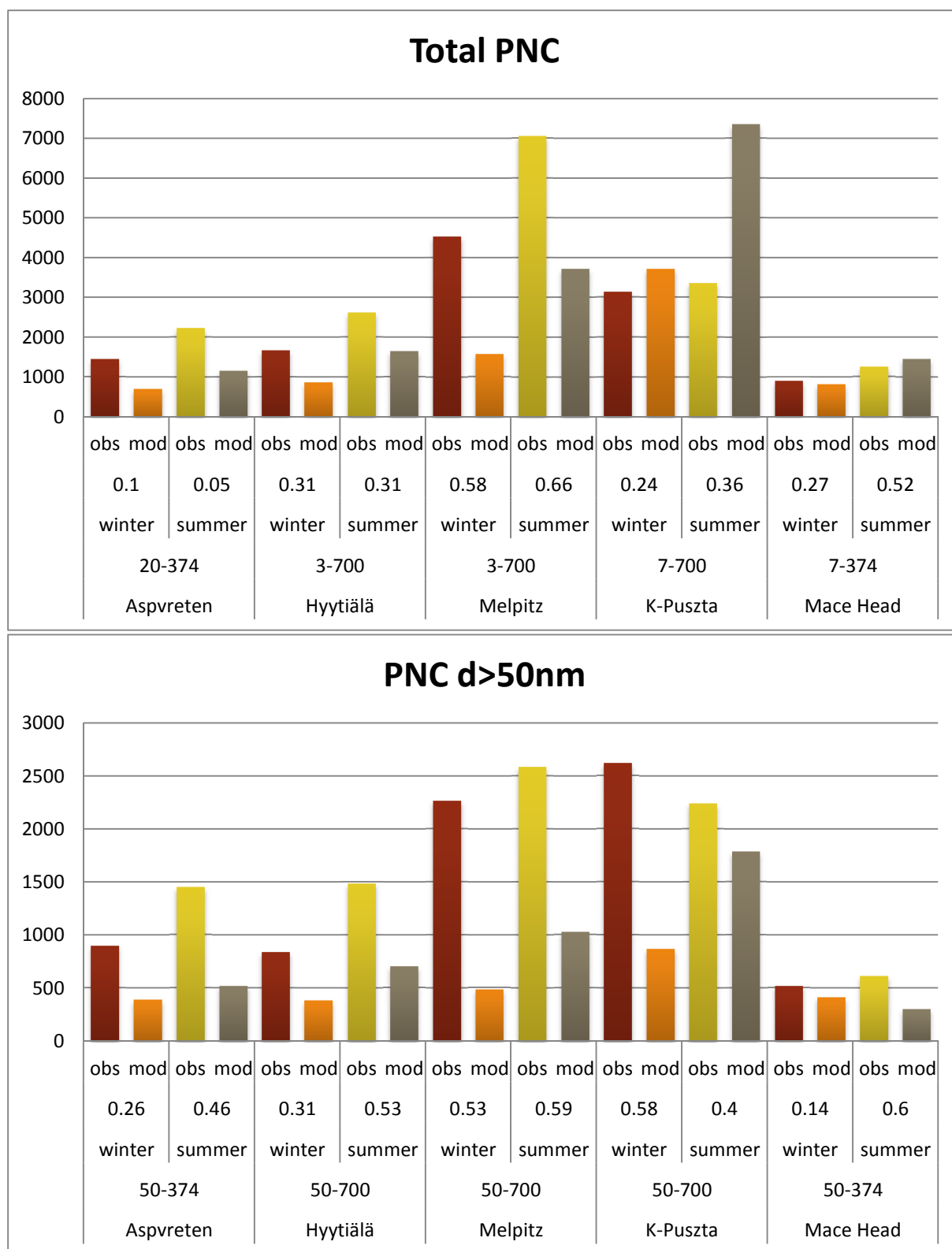
Figure 9. Mean particle number concentration (PNC) in winter and summer at five observation sites in Europe. Top panel: mean observed and modeled total PNC. Bottom panel: mean observed and modeled PNC in the accumulation mode. The interval above the observation site name indicates the particle size interval included, unit nm. The number above the season indication shows the (Pearson) correlation coefficient of daily mean PNC. Note that the size intervals differ between the stations: the size interval is used for both modeled and observed values.

Temporal evolution of the particle number concentration

Figure 10 shows the modeled and observed temporal variation of the daily mean PNC at five sites. The modeled PNC is shown as surfaces to indicate the evolution of the size spectra. New particle formation is evident in the model in the form of peaks in the very smallest particles sizes. These coincide with the observed maximum total numbers on some occasions, sometimes there is a shift of a few days. Often there are peaks in the observations when there are none in the model. Nucleation is a difficult process to capture in the model, since the model grid size is representative of a larger area, whereas the measurement station may be influenced by local emissions.

The best correlation between modeled and observed PNC is found at Melpitz (r=0.70) but the model underestimates PNC most of the time; observed PNC is almost always high at this site. At Mace Head some of the observed peaks are fairly well modeled but the overall correlation coefficient is modest (r=0.46); the timing of some peaks are shifted in the model compared to the observations and some model peaks are not seen in the observations and vice versa. The model grossly overestimates the total PNC at K-Puszta during summer, but the model temporal variation for particles sizes >20nm follows the measurements fairly well; during winter the model PNC is in better agreement with the observations. At Hyytiälä a lot of nucleation is observed; this is not captured by the model, possibly because of the simplified SOA scheme used in the present version of MATCH-SALSA, which is unlikely to model the effect of OM on nucleation in a realistic way.

Model evaluation of particle mass and composition

Simulated annual average PM_{10}, and the chemical components forming this mass, are displayed in Figure 11. The largest concentrations of PM_{10} are found at anthropogenic emission hotspots (e.g., northern Italy, Moscow and the eastern Ukraine) and over the Atlantic Ocean and parts of the Mediterranean Sea. The highest modeled concentrations over land are due to large anthropogenic emissions of primary inorganic aerosol (DUST), except in northern Italy, where there is a large contribution from ammonium nitrate, and in some sulfur emission hotspots in southeastern Europe where sulfate dominates PM_{10}. Over the oceans the largest contribution to PM_{10} is from sea spray particles; important sulfate contributions are also seen, especially around Etna and the eastern Mediterranean Sea.

In following subsections we present evaluation statistics for particle components, starting with SIA, moving on to elemental and organic carbon. Finally total PM_1, $PM_{2.5}$ and PM_{10} are evaluated.

Secondary inorganic aerosol (SIA)

Statistics from the evaluation for SIA components (particulate sulfate, SO_4^{2-}; nitrate, NO_3^-; and ammonium, NH_4^+) are shown in Table 8. Modeled and measured seasonal variations at the sites are displayed in Figure 12; the figure shows the monthly average over all measurement sites and the variation in monthly averages at the individual sites for the same month. In order to avoid biases due to possible incorrect separation of gas and particle phase nitrogen in the measurements, we also include evaluation results for total nitrate (TNO3: $HNO_3(g) + NO_3^-(p)$) and total reduced nitrogen (TNHx: $NH_3(g) + NH_4^+(p)$).
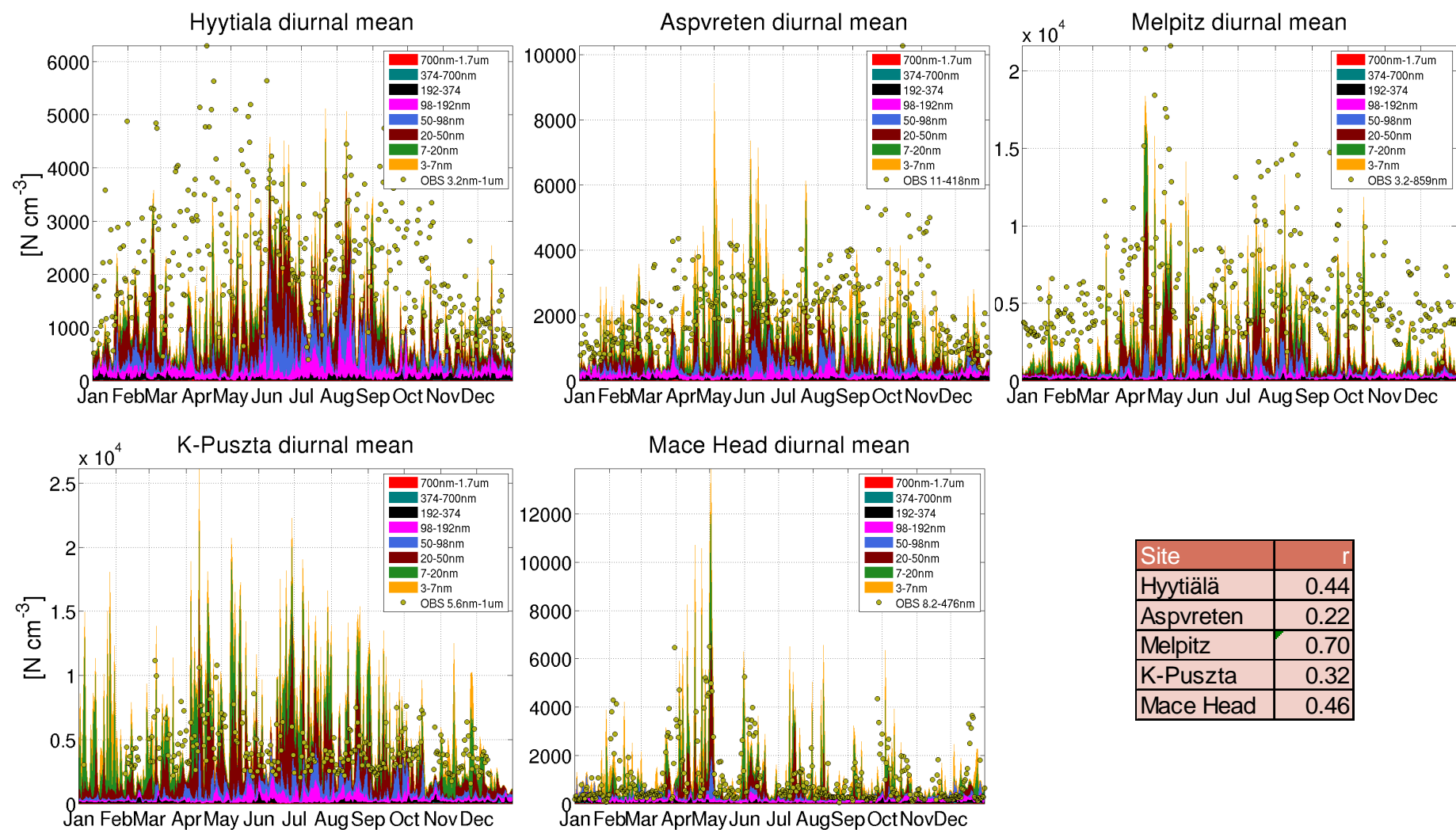
Figure 10. Observed and modeled daily mean particle number concentrations (PNC) at five sites in Europe. Modeled (surfaces) and observed (filled circles) daily mean PNC in size bins are displayed as a time series. See legend for colors representing the different size bins. Bottom right: (Pearson) correlation coefficient for evaluation of diurnal means during 2007.

Table 8. Comparison of modeled secondary inorganic aerosol (SIA) components to daily observed concentrations. Average results covering available measurements for the year 2007 (results for individual stations are given in the supplementary material). In addition to the SIA components also the total nitrate (TNO3=HNO$_3$(g)+NO$_3^-$(p)) and total reduced nitrogen (TNHx=NH$_3$(g)+NH$_4^+$(p)) are evaluated. The units for the concentrations are µg(S) m^{-3} for sulfate and µg(N) m^{-3} for the other species.

	Global/temporal						Spatial			
Measure:	Mean Obs	Mean Mod	%Bias	mean[g] r	mean[g] CV(RMSE)	#obs	%Bias	r	CV(RMSE)	#stns
Unit:	µg m^{-3}	µg m^{-3}	%		%		%		%	
SO$_4^{2-}$	0.63	0.65	4	0.52	46	16033	-6	0.57	53	52
NO$_3^-$	0.40	0.32	-21	0.44	49	7249	-22	0.83	48	23
TNO$_3$	0.49	0.40	-19	0.59	36	11039	-21	0.85	41	35
NH$_4^+$	0.72	0.64	-12	0.57	39	9728	-11	0.79	37	31
TNH$_x$	1.27	1.01	-21	0.53	40	10137	-20	0.87	38	32

Sulfate has a low mean bias (4%) whereas the average normalized RMSE (based on daily mean) is around 50%. The average correlation coefficient for the included sites is 0.52 and the spatial correlation (for the annual mean concentration at the stations) is 0.57. As can be seen in Figure A32 and Table A15 (in Appendix A), two stations are outliers, for which the model sulfate is more than twice the observed concentration (RU18: Danki, ca 95km south of Moscow and SK04: Stara Lesna in Slovakia). The reason for the large model bias at these sites is not known but it is likely that some emissions are overestimated in or near the grid boxes where the stations are located. Both the CV(RMSE) and the correlation coefficients are affected by these outliers, e.g. the spatial correlation coefficient improves significantly, it is 0.76 when they are removed from the data set.

The model tends to overestimate sulfate during November to February and underestimate during the rest of the year, i.e. the seasonal variation is stronger in the model (see Figure 12). The seasonal variation in sulfate is dependent on the variations in the emissions of SOx. A major emitting sector for sulfur is power plants with coal combustion. These emissions, and their seasonal variation, are dependent on the heating requirement, which is coupled to the winter temperatures and the duration of the cold season for a given year. The seasonal variation of these emissions in the model is a statistical description and not dependent on the particular winter temperatures a specific year. A warmer than average winter would lead to less seasonal variation in the real emissions, and thus over-prediction in winter and under-prediction in summer in the model. The year 2007 was exceptionally warm (European Climate Assessment & Dataset; Internet URL: http://eca.knmi.nl/; van Engelen et al., 2008), especially the winter 2006-2007 (http://www.ecmwf.int, ERA-Interim data set, as compared to the period 1979-2012), which could, at least partly, explain the low correlation. For most stations (47 out of 52) the modeled average sulfate is within ±50% of the observed concentration; the majority of those outside the span (four stations) are overestimated.

---

[g] Weighted average of correlation coefficients and CV(RMSE) at individual stations.
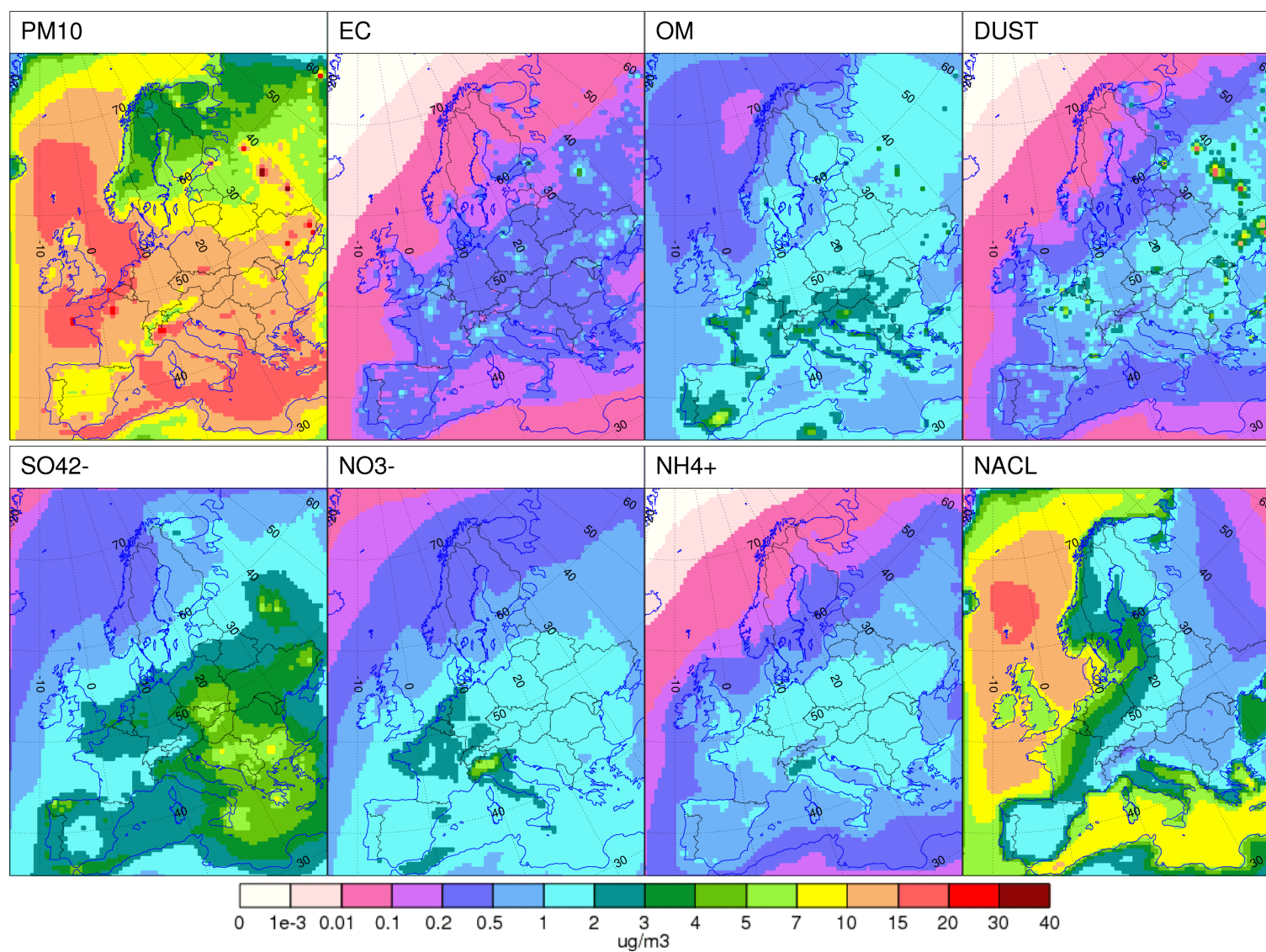
Figure 11. Modeled annual mean concentrations (for 2007) of PM_{10} (peak at 37.3 μg/m^3 in Moscow) and its particle components: elemental carbon (EC), organic matter (OM), anthropogenic dust (DUST), sulfate (SO_4^{2-}), nitrate (NO_3^-), ammonium (NH_4^+) and sea salt (NaCl). Unit: μg m^{-3}.

The model performance for the evaluated nitrogen compounds (NO_3^-, $HNO_3+NO_3^-$, NH_4^+ and NHx) at individual stations is of similar quality as for sulfate. First we return to the average statistics in Table 8. On average, the model underestimates the concentration of the nitrogen components by about 10-20%, while the RMSEs in most cases are a bit lower than for sulfate (range from 36 to 49% for the N-components). The average station correlation coefficients vary between 0.44 and 0.59, whereas the spatial correlation coefficients are higher (between 0.79 and 0.87).

For the nitrogen compounds, the modeled seasonal variations are not as strong as the observed variations. Especially the spring maxima in the observed nitrate and ammonium are not as strong in the model, whereas there is little or no bias during summer and fall. For total reduced nitrogen, there is a general underestimation throughout the year, except during early winter.

There can be several reasons for the deviations of the modeled seasonal variations from those observed. The underestimation of the spring time maximum could be due to missing (or underestimated) emissions; e.g., the model does not include emissions from open burning of biomass (agricultural burning and wildfires) and large fires may emit substantial amounts of NOx that will be transformed into nitric acid (and nitrate) in the atmosphere. The underestimation of nitrate may also be a secondary effect of underestimation of NH_3 leading to too little formation of particulate nitrate ($HNO_3(g)$ deposits much more rapidly than particulate nitrate). A third alternative is problems with too rapid dry and/or wet deposition of HNO_3 in the model; a very simplified dry deposition scheme for gases was used in these model calculations and it may overestimate deposition substantially (the deposition errors are likely to be different for different seasons); both the dry and wet deposition schemes in MATCH are being revised and it is likely that the revisions will lead to especially large changes in the modeled concentrations of nitrogen components; over-predicted wet scavenging of particles during spring is another possible explanation for the underestimated spring concentrations of nitrate and ammonium.

The behavior of reduced nitrogen is more complex. During summer the underestimation in TNHx is not followed by underestimation of ammonium. Some biogenic emission sources for ammonia are missing in the model and these are likely to have a strong seasonal variation. The model also overestimates deposition of reduced nitrogen since it does not yet account for soil saturation of ammonia; this will lead to too little ammonia in the model, especially during periods with high ammonium deposition (e.g., during periods when fertilizers are spread over agricultural areas). Improving the model for ammonia deposition and biogenic ammonia emission would likely improve the seasonal variation for total reduced nitrogen.

As for the spatial variation, the model underestimates the annual mean concentration at the sites with highest concentration somewhat, for the four evaluated nitrogen compounds (see Appendix A, Figure A33, Figure A34, Figure A35 and Figure A36); but the bias at most sites falls within 50% (see Appendix A, Table A16, Table A17, Table A18 and Table A19). The largest relative overestimation is for two stations measuring nitrate in Latvia (LV10 and LV16) where both model and measurements estimate low concentrations. The largest underestimation (around 90%) is at three stations measuring total reduced nitrogen in Norway (NO15, NO39 and NO55 [both NO15 and NO55 are influenced by local agricultural activities according to EMEP site description; thus, they may be less representative for N-components in a regional scale model]) and at one station measuring nitrate in Austria (AT02).
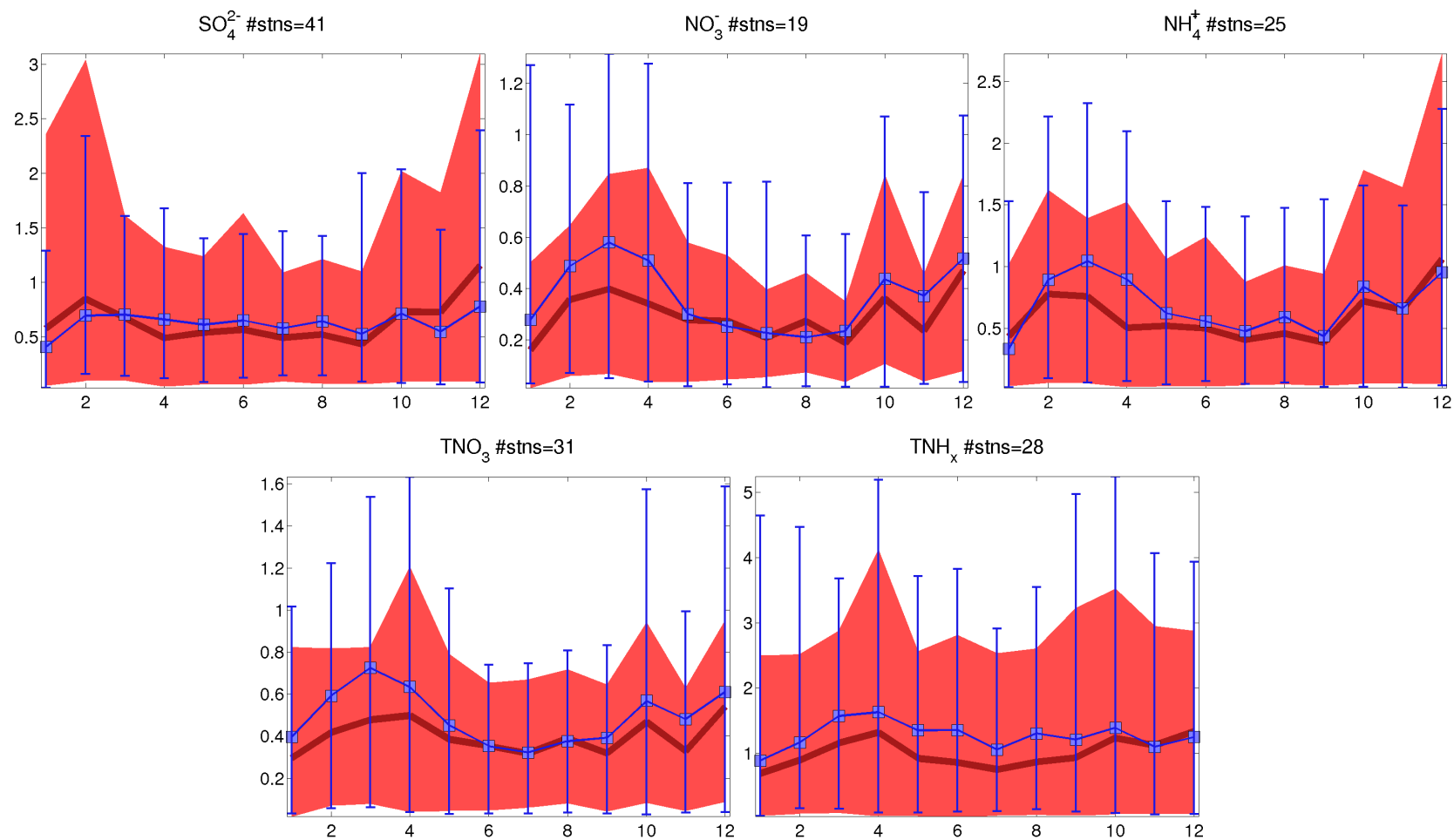
Figure 12. Monthly mean secondary inorganic aerosol (sulfate, SO_4^{2-}; nitrate, NO_3^-; and ammonium, NH_4^+), total nitrate (TNO3=HNO$_3$(g)+NO$_3^-$(p)) and total reduced nitrogen (TNHx=NH$_3$(g)+NH$_4^+$(p)) concentrations at EMEP observation sites in Europe. Observed average station mean concentrations, and the interval between maximum and minimum station means, are shown as blue squares and bars. The corresponding modeled average and max-min interval are illustrated with the red line and shaded area. Sites with less than 80% capture during the year were excluded from the comparison. Unit: μg(S/N) m^{-3}.

Elemental and organic carbon

In this section we evaluate elemental carbon (EC) and organic carbon (OC). The evaluation includes available measurements in ebas; 11 European sites were available for 2007 (see Table 5). The model describes organic matter (OM) rather than OC. In the evaluation we assume a OM:OC ratio of 1.4. The actual ratio is usually between 1.25 and 1.7, with a greater ratio for more aged OM (Turpin et al., 2000; Kupiainen and Klimont, 2007). Thus, the choice of a fixed OM:OC ratio will lead to model under- or overestimation depending on measurement site and time of year. Evaluation of EC and OC are shown in Figure 13 and Figure 14. The figures show the annual observed and modeled mean and daily correlation coefficients at individual measurement sites.

Both EC and OC are underestimated at many of the sites during the measurement periods. The underestimation is especially large at the Italian sites during winter for both EC and OC, and for EC at Melpitz. The reason for the underestimation (and in some cases overestimation) is likely to vary between the measurement sites and seasons. There is a generally higher correlation for EC than OC at the sites where both are measured. One of the reasons for this is that OC is more complicated to model than EC, since it is a combination of primary and secondary components, many of them semi-volatile.

We now turn to the model performance of daily EC and OC at individual stations. To restrict the number of figures we include only Ispra here (Figure 15); scatterplots and time-series of observed and modeled EC and OC at the other stations can be found in Appendix A (Figure A37 and Figure A38). We choose to show Ispra since it is one of two stations (Melpitz being the second) that measure daily EC and OC (in $PM_{2.5}$) during the whole year, and since the results at Ispra are of particular interest. The model performs well in describing what is observed at Ispra during summer but it greatly underestimates during wintertime. One reason may be underestimated residential wood combustion emissions (e.g. Bergström et al., 2012). Modeled and observed time-series of nitrogen dioxide (NO_2) are also included in Figure 15. For NO_2 there is also underestimation all year around, by 43% in summer and 51% in winter. There is a clear seasonality in both modeled and measured values. However, EC and OC have more pronounced underestimation during winter (-74 and -87%, respectively) than during summer (-20 and -37%, respectively), whereas the relative underestimation of NO_2 is fairly constant for all seasons. This seasonality in model EC and OC performance is very likely due to lacking emissions from one or more emission sectors, with greater emissions of EC and OC during winter, but relatively small contribution to NO_2. This work therefore strongly indicates underestimation of residential wood combustion emissions at least in the area around Ispra.

For the German site Melpitz (see Appendix A, Table A20 and Figure A37) EC is generally under-predicted throughout the year. OC is generally captured fairly well at the station, with underestimation of OC in PM_{10} during winter and overestimation for OC in $PM_{2.5}$ during summer. One reason for the relatively high EC measurements at Melpitz is that the measurement technique used at this site, to separate OC from EC, has no charring correction and is expected to lead to too high EC values and to underestimate OC (see Genberg et al., 2013, and references therein). There are large peaks during spring and late autumn of OC (and EC) in $PM_{2.5}$ and PM_{10}, which are clearly under-predicted (Appendix A, Figure A38). The peak in the beginning of April coincides with a vegetation fire episode (Genberg et al., 2013); the earlier peaks and the late autumn peaks are perhaps more likely due to residential combustion or other missing/underestimated sources. Stern et al. (2008)

compared five different chemical transport models to observations from northern Germany during highly polluted conditions. None of the models could reproduce the very high EC concentrations observed at Melpitz. Stern et al. (2008) suggested that the large underestimations of EC may be an indication that emissions in the central European region were underestimated during these episodes.

While EC and OC in $PM_{2.5}$ or PM_{10} are underestimated at many sites in Jan-Feb 2007, the variation and baseline of EC (but not OC) are captured well at Kosetice, Harwell and Campisabalos (Appendix A, Figure A37 and Figure A38).

Total particulate matter

In this section we evaluate total particulate matter for the sizes PM_1 and $PM_{2.5}$. The evaluation includes 28 measurement sites throughout Europe (Figure 16 and Appendix A, Table A21).

The model underestimates $PM_{2.5}$ by 14% (spatial average) and the spatial correlation coefficient is 0.64. The CV(RMSE) is 38%. The model underestimates $PM_{2.5}$ at the measurement sites with the highest observed annual mean (Appendix A, Figure A39). The underestimation of $PM_{2.5}$ can be due to a number of reasons including missing emissions, too short aerosol lifetime or too little secondary aerosol production. There is probably too little EC and OC in the model, at least at some of the sites, which can be explained by missing or underestimated emissions.

For PM_1 the annual means at the sites with the lowest concentration (Scandinavian sites NO01, FI17, DK41) are overestimated by the model. Out of the 35 evaluated annual means (PM_1 and $PM_{2.5}$) at the 28 stations, six means (at five stations) deviate by more than 50%. For PM_1 the overestimation for the three Scandinavian sites seems to be due to overestimation of sea salt. A closer look at modeled and measured PM_1 in Birkenes (Figure 17) shows that model peaks caused by sea salt are not seen in the observations. For this reason we also compare evaluation scores for modeled PM_1 and $PM_{2.5}$, with and without inclusion of sea salt aerosol in the total PM mass (Figure 18 and Appendix A, Figure A39 and Table A21). Many sites show improvement to the correlation coefficient for daily mean $PM_{2.5}$ or PM_1, which is an indication of too much sea salt at the wrong time. It may be due to too large sea salt emissions and/or too weak sink processes for the sea salt, since significant improvements in correlation are seen also at far inland sites. Further detailed evaluation of modeled sea salt against observed Na (in air and deposition) is needed.
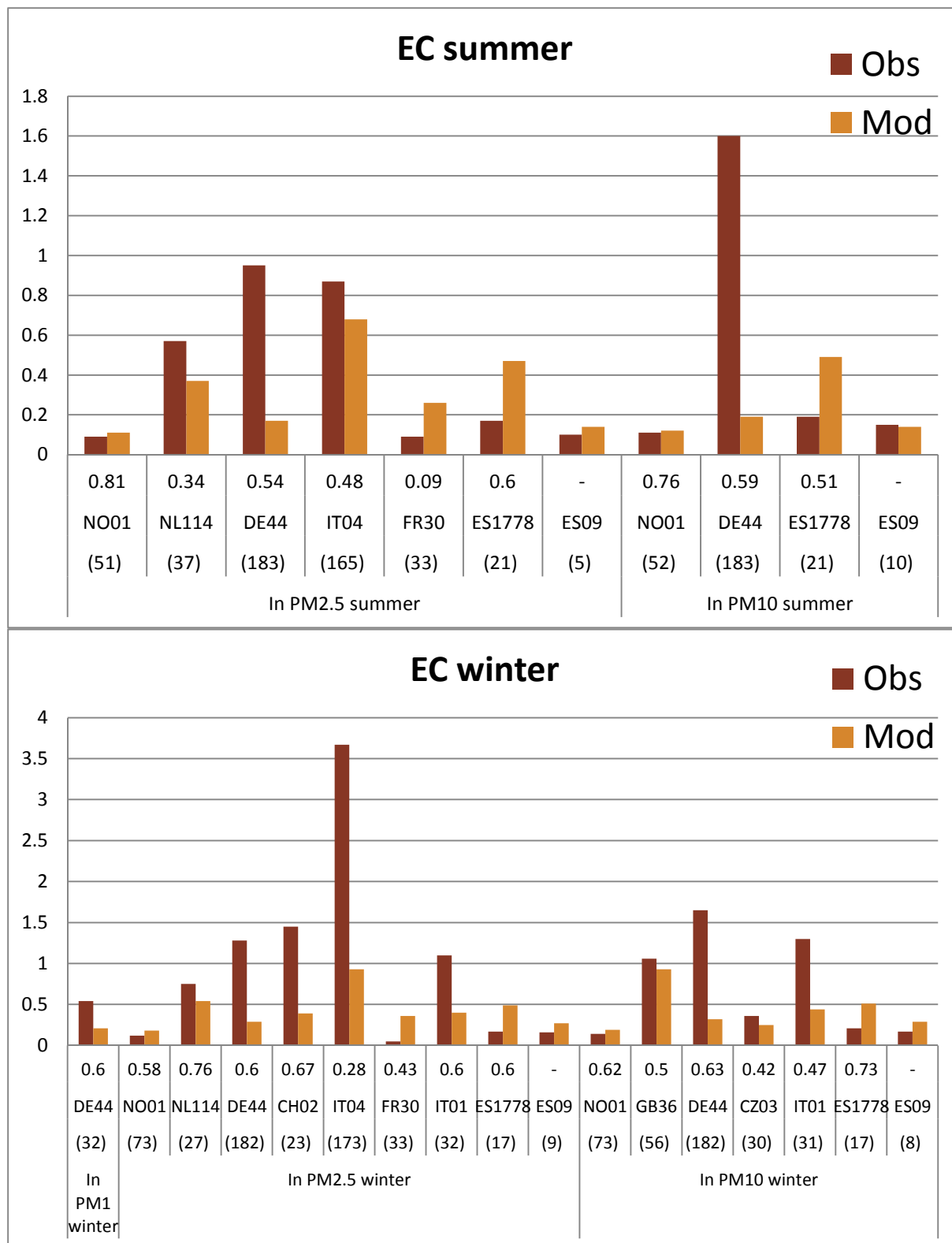
Figure 13. Evaluation of EC for 2007. Observed and modeled mean concentrations (unit: μg m^{-3}), correlation coefficients of daily mean concentrations are indicated below the bars. Measurement site codes as defined in Table 5. The number of daily mean values is indicated by the numbers in the parentheses. Correlation coefficients were calculated for measurement sites with more than 10 daily observations.

Figure 14. Evaluation of OC for 2007. Observed and modeled mean concentrations (unit: μg m⁻³), correlation coefficients of daily mean concentrations are indicated below the bars. Measurement site codes as defined in Table 5. The number of daily mean values is indicated by the numbers in the parentheses. Correlation coefficients were calculated for measurement sites with more than 10 daily observations.
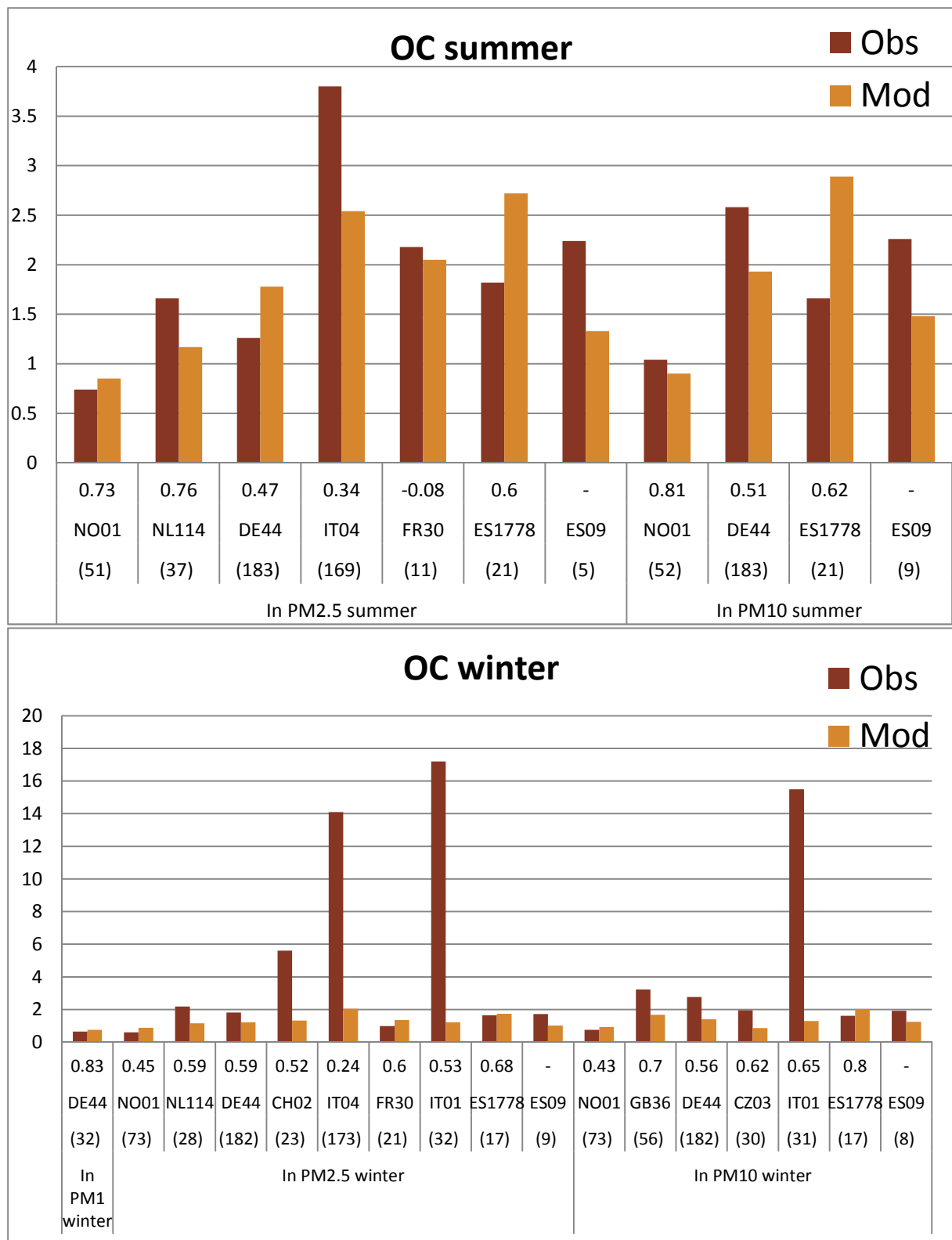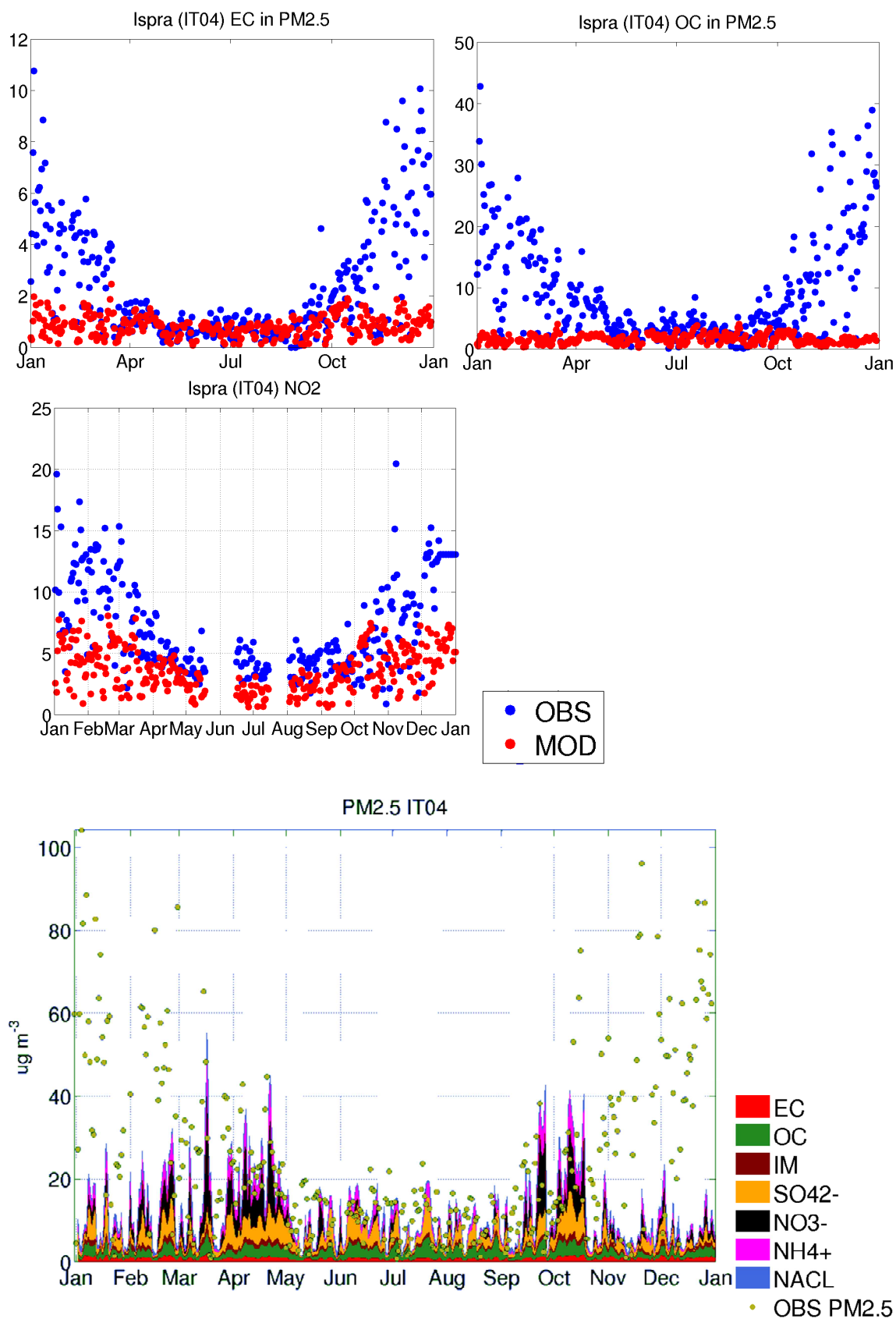
Figure 15. Observed and modeled time series at Ispra for daily EC (top left) and OC (top right) in PM$_{2.5}$, and NO$_2$ (middle) and modeled PM$_{2.5}$ constituents and observed PM$_{2.5}$ (bottom) during 2007. Modeled OM was scaled to OC using the factor 1.4. Unit: µg m^{-3}.
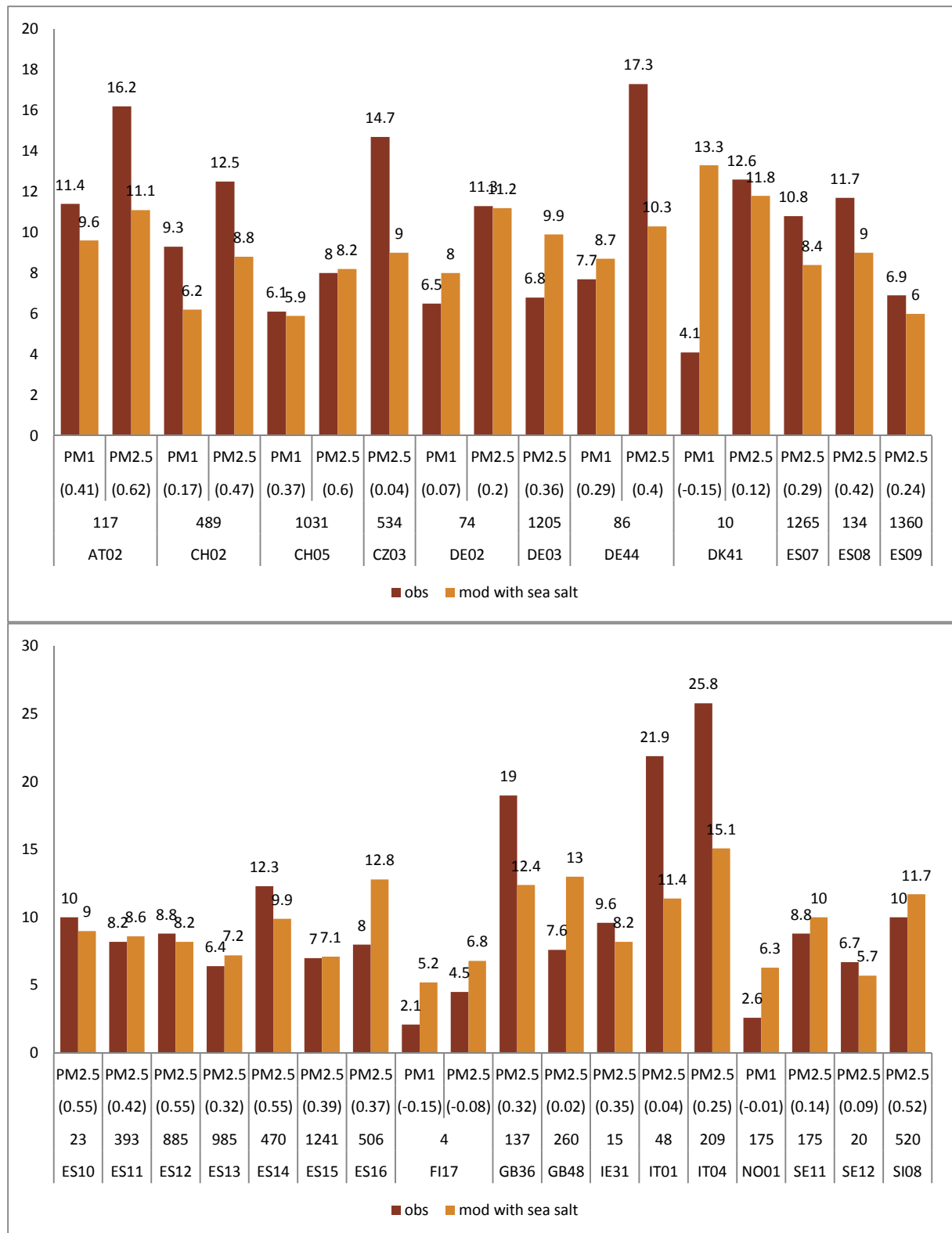
Figure 16. Evaluation of PM$_1$ and PM$_{2.5}$ for 2007. Observed and modeled mean concentrations (unit: μg m^{-3}); correlation coefficients of daily mean concentrations are indicated below the bars within parentheses. The elevation of each site is included below the correlation coefficients (unit: m above sea level). Station codes as defined in Table 5.
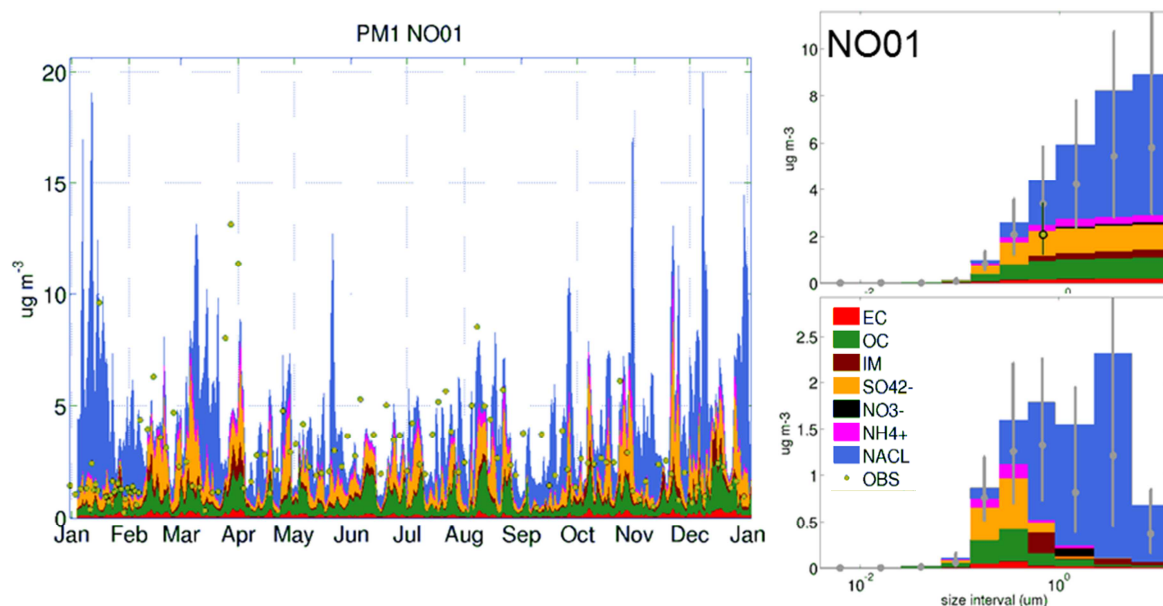
Figure 17. Modeled and observed PM$_1$ at Birkenes (NO01) for 2007. Time series of daily mean modeled PM$_1$ constituents (surfaces) and observed PM$_1$ (circles) (left hand side). Modeled 2007 annual mean PM constituent size distribution: accumulated over size bins up to the higher end of an indicated interval (top right panel) and mass per size bin (bottom right). Observed PM$_1$ (green dot with black ring). Modeled PM$_1$ constituents are shown as surface plots with different colors explained by the legend (in the bottom right panel). Modeled median and interquartile range (grey ring and error-bar in right hand panels). Observed median and interquartile range for PM$_1$ (green dot with black ring and error-bar in top right panels).

Conclusions on model performance

The MATCH model has been further developed to include aerosol microphysics, by including the aerosol dynamic model SALSA. The new features in MATCH-SALSA, compared to the standard MATCH model, include particle number size distribution and a simple treatment of biogenic secondary organic aerosol. The model performance is moderate to good, but improvements are needed in some areas. The model needs to be updated for online terpene emissions and better representation of SOA processes. Further, the model treatment of gas-particle partitioning of nitrogen can be improved. In Section 5 the new model is compared to the standard MATCH model.
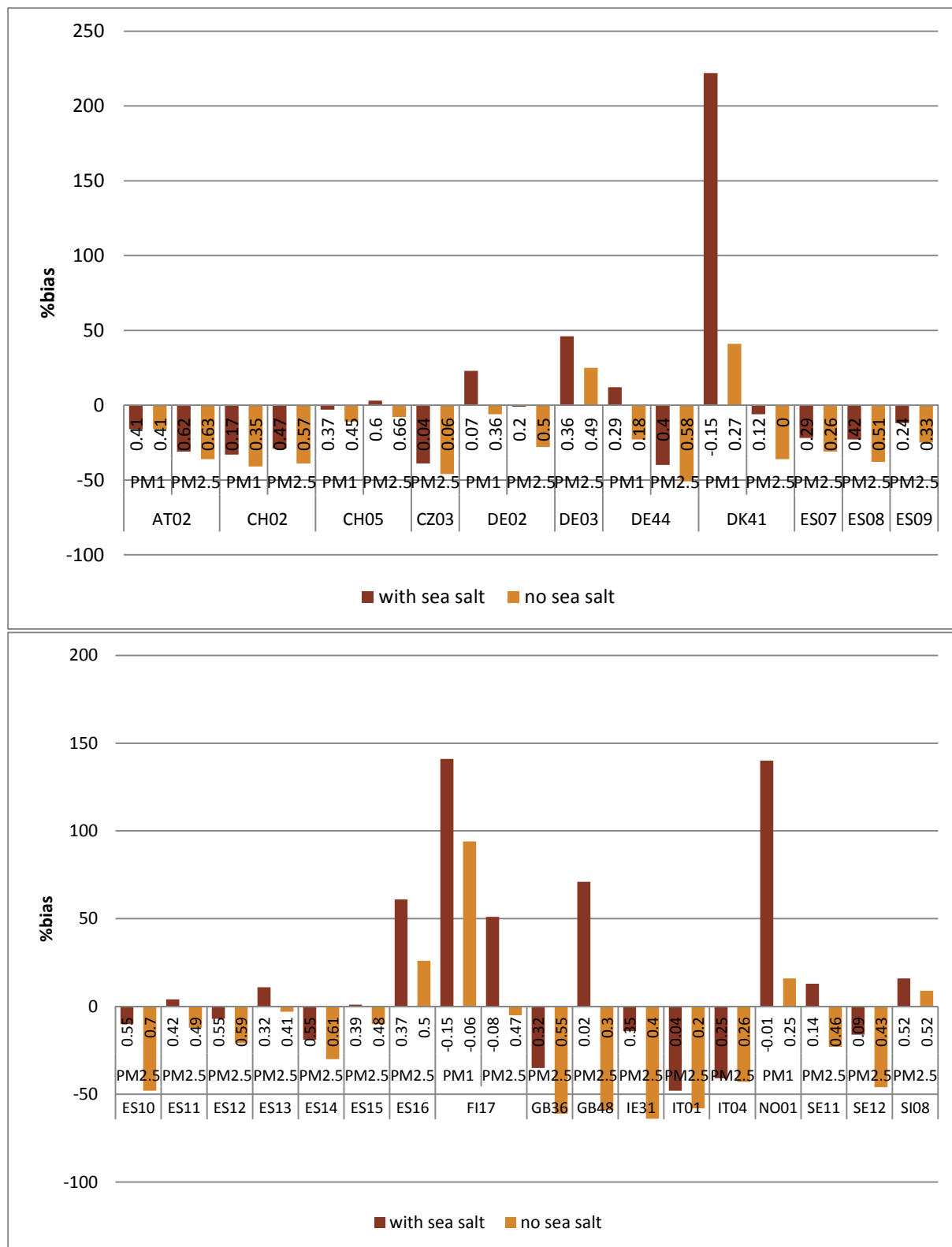
Figure 18. Comparison of evaluation scores for PM$_1$ and PM$_{2.5}$ when including or excluding sea salt particles in the PM mass. The bars show the %bias (unit: %; 0% is best score), the numbers below the zero %bias line is the correlation coefficient (r) when evaluating the daily mean values.

5. MATCH-SALSA compared to MATCH

The main improvement in MATCH-SALSA compared to the standard MATCH model is the inclusion of aerosol microphysics. This allows for a dynamic description of particle number concentrations. In the standard MATCH model particle dynamics is not described, except for size-dependent deposition. MATCH-SALSA describes new particle formation, through nucleation, and particle growth by condensation and coagulation. MATCH-SALSA has also been coupled to a cloud module describing the fraction of cloud activated particles; this was coupled to wet scavenging, as described in a sensitivity scenario in Section 6. The differences between MATCH and MATCH-SALSA are further detailed in Table 9.

Table 9. Main differences between MATCH-SALSA and the standard MATCH model

Process	MATCH	MATCH-SALSA
Particle size distribution	Primary particles: flexible, Secondary particles: 1 class.	Flexible number of nucleation-, aitken-, accumulation- and coarse particle classes; solubility of particle classes; cloud condensation nuclei/activated fraction of particles
Aerosol dynamics	Size dependent deposition.	Various descriptions of nucleation, condensation, coagulation, growth, size- and solubility-dependent wet and dry deposition, possibility for coupling between wet deposition and cloud droplet activated particle fractions.
Particle numbers	No description	Particle number in a flexible number of size intervals.
Particle mass/ chemical constituents	Primary particles: EC, OC, dust, sea salt Secondary particles: sulfate, nitrate, ammonium	Primary particles: EC, OM, dust, sea salt Secondary particles: sulfate, nitrate, ammonium, secondary organic aerosol

In order to evaluate improvements in MATCH-SALSA (MS), compared to "standard" MATCH (M), we performed a separate calculation with the MATCH model using the same methodology as the MATCH-SALSA base case simulation but turning off the SALSA model. This means that the M-case is similar to the standard MATCH model version which has been used in many applications. The two scenarios are detailed in Table 10.

Table 10. Model scenarios for comparing MATCH-SALSA to MATCH

Name	Description	Version
MS MATCH-SALSA	Standard MATCH-SALSA with TNO emissions.	S20BV86b
M MATCH	No SALSA No aerosol microphysics No SOA formation Closest resemblance to standard MATCH	S20BV68b

Particle Mass (PM$_{2.5}$)

The PM$_{2.5}$ concentrations from the two simulations are compared to each other and to observations at 27 European sites in Figure 19. Usually MS predicts higher PM$_{2.5}$ concentrations, which is expected since it includes SOA, which is not included in the M simulation. At some sites there is however higher concentration of sulfate in the M simulation than in MS. This is most likely a result of changes to the mass size distribution leading to changes in wet and/or dry deposition.

Modeled PM$_{2.5}$ is close to the observed or underestimated at most sites with both MS and M. At most sites the correlation coefficient for the MS run is either very similar to the M run or improved. The largest differences between MS and M are found at the Spanish sites where the MS results are clearly better correlated with the measurements. In Scandinavia and on the British Isles the correlation is generally poor in both model versions and there is little difference between MS and M.

Particle number

In most standard MATCH model simulations there is no representation of PNC, however in the M test run we do include PNC but only primary particle PNC is included. The SIA formed in the M-case is only added to the surface of already existing particles and therefore it does not add to the PNC. Measured and modeled total and accumulation mode PNC are presented in Figure 20.

There is less total PNC in winter than summer, both in the observations and in the model; this is due to weaker nucleation during winter. During summer, both accumulation mode PNC and total PNC are higher in MS than in M. New particles are formed in the nucleation routine, introduced in MS, and the condensation of H$_2$SO$_4$ and SOA in MS acts to grow the particle size distribution to accumulation mode sizes. During winter the total PNC is higher in MS than in M whereas the accumulation mode PNC is lower. This is due to less condensation in winter (especially less organic condensation) resulting in weaker growth of the newly formed small particles to larger sizes.

MS is generally better at describing the PNC at the measurement sites included in this study than what is simulated by the M-case: both the levels and correlation coefficients of total and accumulation mode PNC are better captured by MS. However, during winter the M-case is predicting higher accumulation mode PNC (i.e., slightly closer to the observed mean levels) but the correlation coefficient are worse for M than for MS. The lower PNC in MS is probably a result of the coagulation, which acts as a sink to particle numbers, combined with the weak condensation and nucleation during winter in this version of MATCH-SALSA.

Conclusions

MATCH-SALSA describes aerosol microphysical processes which are currently lacking in MATCH and therefore represents PNC better than a simulation similar to the standard MATCH model. PM$_{2.5}$ simulated by MATCH-SALSA shows some differences compared to MATCH, resulting from changes to the mass size distribution due to microphysical processing.

Figure 19. Observed (O) and modeled annual mean PM$_{2.5}$ concentration at European measurement sites. Modeled PM$_{2.5}$ also indicates chemical composition. Model versions are MATCH-SALSA (MS) and MATCH (M), see Table 10. The correlation coefficients of the daily mean PM$_{2.5}$ are given below the bars.
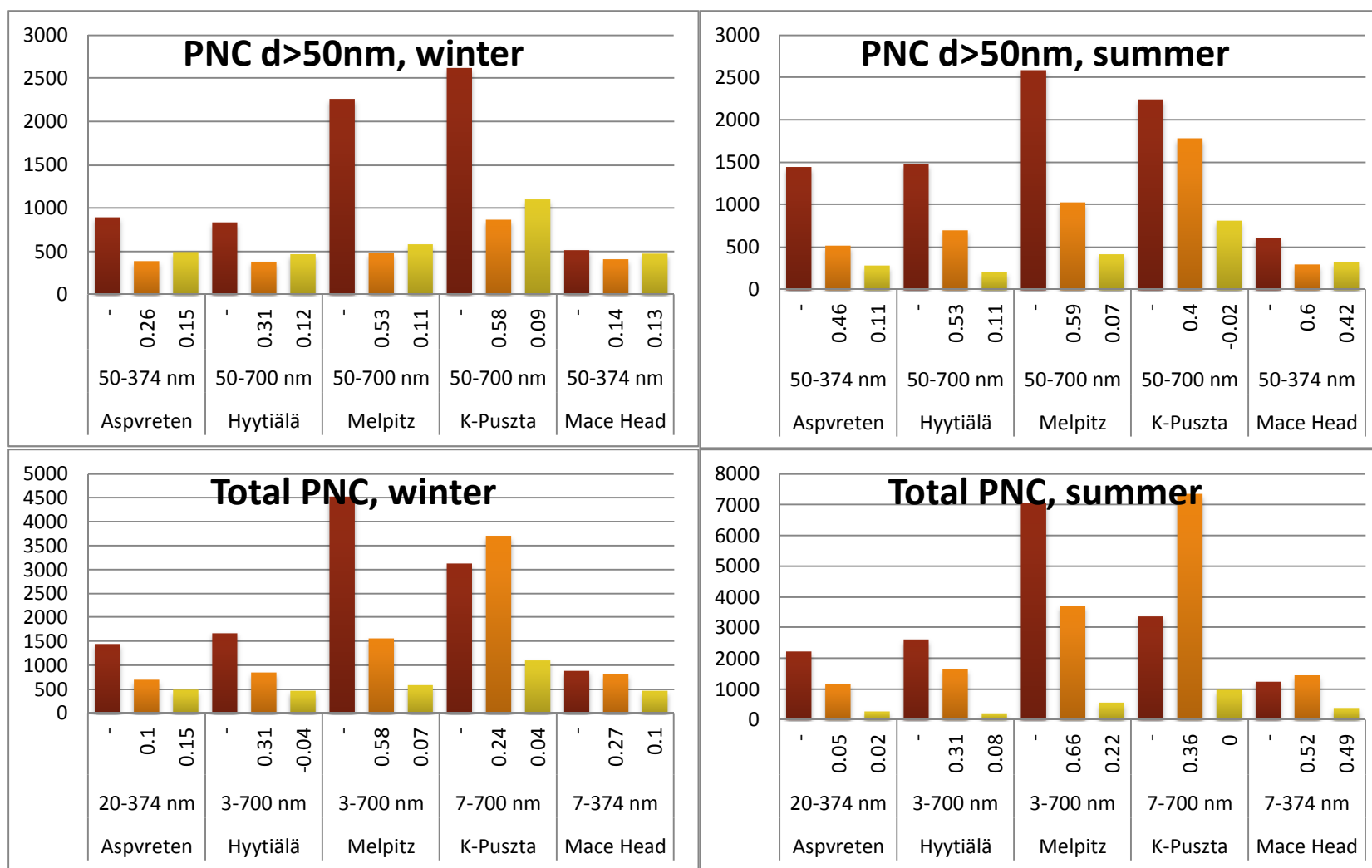
Figure 20. Observed (OBS) and modeled particle number concentration (PNC) in accumulation mode (diameter larger than 50nm; top row) and total PNC (bottom row) during winter (Jan-March and Oct-Dec, left panels) and summer (April-Sept, right panels) at five European measurement sites. The correlation coefficients of the daily mean PNC are given below the bars. Observations (dark red), and model versions: MATCH-SALSA (MS; orange) and MATCH (M; yellow), see Table 10. Note that the size intervals differ between the stations: the size interval is used for both modeled and observed values. Unit: # cm^{-3}.

6. MATCH-SALSA options – sensitivity tests and recommendations

A number of sensitivity tests were performed using MATCH-SALSA. The purpose of these tests was to understand how the model responds to different input data or model formulations affecting nucleation, growth and wet scavenging. The results from the sensitivity tests are presented in the following sections.

Nucleation

The distribution of SOx emissions between SO_2 and more oxidized compounds was discussed by Spracklen et al. (2005); the fraction of SO_2 increases with grid resolution and is typically chosen to be between 95-100% in European scale models. Here we investigate the impact of the distribution of SOx emissions between sulfur dioxide (SO_2), sulfuric acid (H_2SO_4) and sulfate (SO_4^{2-}) on the modeled PNC, since this choice has the potential to affect both nucleation and condensation in the model. Close to the source, SOx is emitted as SO_2 for most anthropogenic sectors. After emission, SO_2 is transformed to more oxidized species at a rate which depends on the ambient conditions. The ideal effective emission split between SO_2 and more oxidized states depends on the model resolution. Based on Spracklen et al. (2005) we chose 99% as SO_2 and 1% as H_2SO_4 in the base case simulation. The TNO emission data set already contained primary particulate sulfate, therefore we chose to emit the S(VI) as $H_2SO_4(g)$ (rather than $SO_4^{2-}(p)$), since H_2SO_4 can condense or nucleate in the microphysical routine in the model. We include tests where the fraction of SOx emitted as H_2SO_4 is increased to 5% (MS5) and decreased to 0% (MS0). Further, we also include a test where 1% is emitted as particulate sulfate instead of $H_2SO_4(g)$ (MS01).

MATCH-SALSA includes various nucleation schemes. Here we test for differences between the standard nucleation, which is activation type nucleation (MS), activation nucleation including both H_2SO_4 and organics (MSos), binary nucleation (MSb) and not including any nucleation (MS-).

Table 11. Model scenarios for comparing sensititvity to nucleation formulations and emissions affecting nucleation

Name	Description	Version
MS	Base case 1% SOx emissions as H_2SO_4. Activation nucleation of H_2SO_4.	S20BV86b
MS5	5% SOx emissions as H_2SO_4.	S20BV92
MSos	1% SOx emissions as H_2SO_4. Activation nucleation of H_2SO_4 and organics.	S20BV97
MS0	0% SOx emissions as H_2SO_4.	S20BV93
MS01	0% SOx emissions as H_2SO_4. 1% SOx emissions as $SO_4^{2-}(p)$.	S20BV94
MS-	1% SOx emissions as H_2SO_4. No nucleation.	S20BV96
MSb	1% SOx emissions as H_2SO_4. Binary nucleation.	S20BV95

The model sensitivity to these choices is investigated in this section, with settings as presented in Table 11. The resulting total and accumulation mode PNC for the sensitivity tests are presented in Figure 21 and Figure 22.
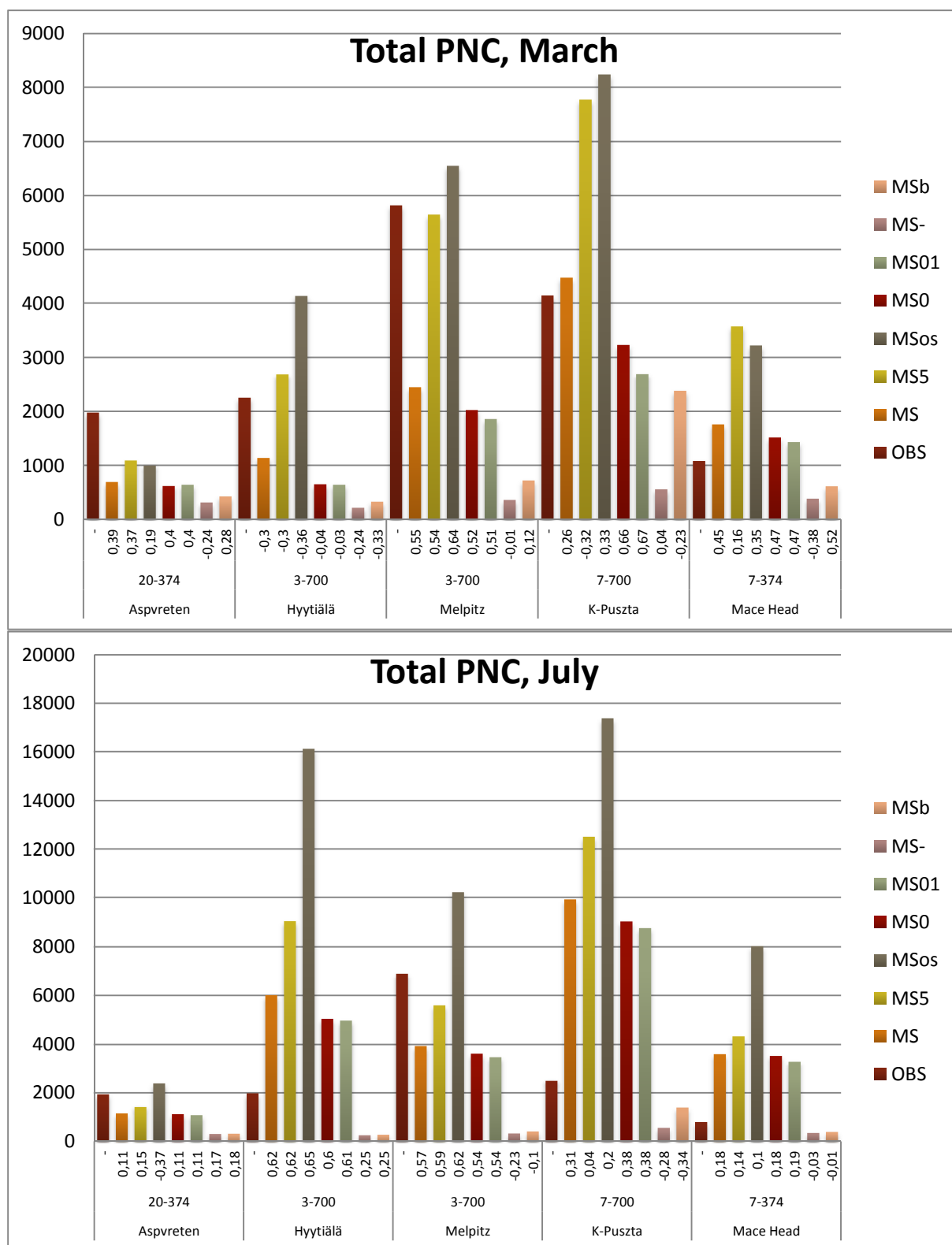
Figure 21. Mean observed and modeled total particle number concentration in March (top) and July (bottom) resulting from sensitivity tests on nucleation formulation and emission distribution of SOx between species. Note that the size intervals differ between the stations: the size interval is used for both modeled and observed values. Scenario notation: See Table 11. Unit: # cm^{-3}.

The amount of SOx emitted as H_2SO_4 affects both the total and the accumulation mode PNC, resulting in more PNC when increasing the H_2SO_4 fraction. However, including organic nucleation as well, results in even stronger increase in PNC than increasing the emitted H_2SO_4 fraction by 4% units. Choosing to emit all non-SO_2 as particulate sulfate instead of H_2SO_4 (g) leads to lower PNC, even slightly lower than when emitting all SOx as SO_2. The emitted sulfate will be condensed on available particle surfaces, thus not increasing PNC, whereas emitted SO_2 will form H_2SO_4 that will mainly act to increase the PNC.

Binary nucleation produces less PNC than the activation type nucleation, and most often the correlation coefficient is lower when using binary nucleation. Not including any nucleation always produces too little total and accumulation mode PNC with poor or no correlation to observations. The recommendation is to use activation type nucleation.

There is no clear single recommendation from the sensitivity tests on what choice is best. The fraction of H_2SO_4 that results in the best model performance (bias and correlation for total PNC) is site, and possibly season, dependent:

- Aspvreten: The correlation is fairly constant with H_2SO_4 fraction but the total and accumulation mode PNC is underestimated in March for all cases, whereas the bias is smaller in July. The total PNC correlation decreases when including organic nucleation: possibly the terpene emissions need improvements in this area.
- Hyytiälä: There is relatively good correlation for all activation nucleation cases for both accumulation mode and total PNC in July and some correlation also for accumulation mode PNC in March. Total PNC is severely overestimated in July.
- Melpitz: The correlation is (slightly) improved for the total PNC when including organic nucleation; for March the bias is also much smaller with organic nucleation than with activation type nucleation; for July, the increased model total PNC leads to an overestimation (of about the same magnitude as the underestimation when using activation nucleation), but the bias changes from underestimation to overestimation. Accumulation mode PNC is underestimated (especially in March) but a larger fraction of H_2SO_4 emissions decreases the bias, and results in higher correlation to observations in March. This could be a result of missing condensational growth in the model at this site. (This condensation may be due to other components than H_2SO_4, e.g., nitrogen compounds which are currently not included in the particle growth mechanism.)
- K-puszta: For total PNC, the model is best correlated with the observations when the H_2SO_4 emission fraction is 0%. Including organic nucleation leads to severe overestimation of the total PNC at K-puszta
- Mace Head: For total PNC the best correlation is obtained for the scenarios with low (0-1%) H_2SO_4 emission fractions; organic nucleation does not improve the performance. The total PNC is overestimated for all activation nucleation simulations at this site.
- General: For accumulation mode PNC the correlation is generally higher than for total PNC in both months (except Aspvreten in July). This may be an effect of the accumulation mode numbers being affected not only by nucleation and particle growth mechanisms, but also by primary particle emissions and long-range transport (LRT; the model usually captures the timing of LRT episodes well at regional background sites).

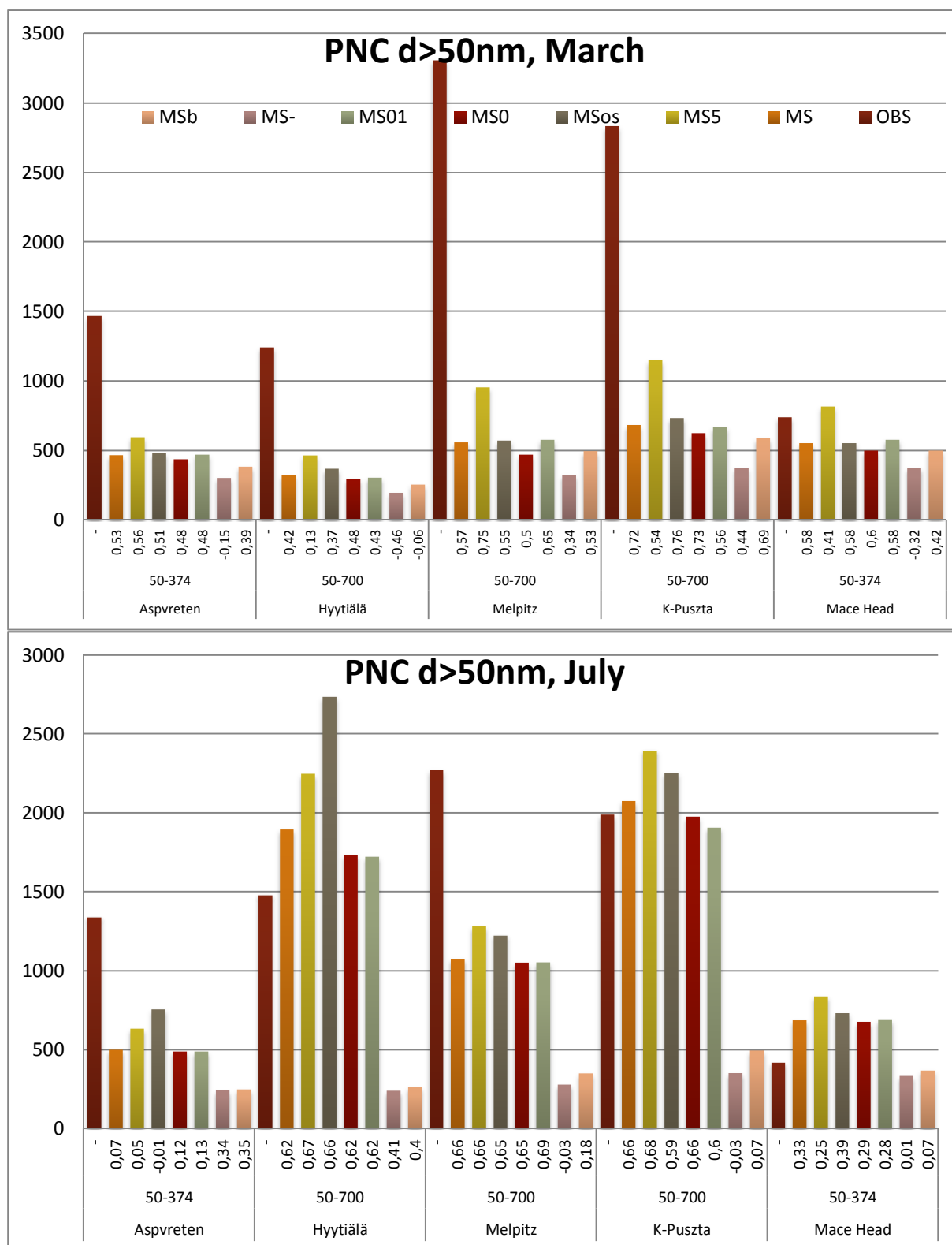**Figure 22. Mean observed and modeled accumulation mode particle number concentration (PNC) in March (top) and July (bottom) resulting from sensitivity tests on nucleation formulation and emission distribution of SOx between species. Note that the size intervals differ between the stations: the size interval is used for both modeled and observed values. Scenario notation: See Table 11. Unit: # cm^{-3}.**

The model is sensitive to organic nucleation. The model needs improvements including more realistic terpene emissions and SOA formation and gas-particle partitioning. Condensational growth also needs to be further developed, taking into account nitrogen partitioning and organic condensation needs to be treated in a more realistic way.

Condensation/coagulation

The PNC size distribution depends on primary emissions, new particle formation, condensation, coagulation and deposition. In the model the growth is represented by condensational growth by H_2SO_4 and organic vapors. The effects of varying H_2SO_4 emission fractions were treated in the previous section. Here we study the model sensitivity regarding different amounts of condensing organic vapors: 0% condensation of organic vapors (0TP), 10% (10TP), the base case 30% (MS), 50% (50TP), 100% (100TP), 1000% (1000TP). The 1000TP case is corresponding to an extreme upper boundary emission scenario, which we include since biogenic emissions are highly uncertain. Finally a test where the order of nucleation and condensation, and coagulation are switched (revcoag) is included.

Table 12. Model scenarios for comparing sensititvity to amount of condensable organic vapors and the order of coagulation

Case	Information	Version
0TP	0% condensable gases from oxidated α-pinene	S20BV104
10TP	10% condensable gases from oxidated α-pinene	S20BV107
MS	Base case 30% condensable gases from oxidated α-pinene	S20BV86b
50TP	50% condensable gases from oxidated α-pinene	S20BV108
100TP	100% condensable gases from oxidated α-pinene	S20BV106
1000TP	1000% condensable gases from oxidated α-pinene	S20BV103
revcoag	Coagulation after condensation/nucleation 30% condensable gases from oxidated α-pinene	S20BV101

The resulting total PNC and accumulation mode PNC for March and July are presented in Figure 23 andFigure 24. Increasing the amount of condensable organic gases increases the accumulation mode PNC from large underestimation, when having no condensable organic gases, to higher PNC. Depending on site the optimum amount varies. Increasing the amount of condensable gas also results in higher total PNC initially, but occasionally this trend is broken and the total PNC starts to decrease beyond some level. More organic gases cause smaller particles to grow, competing with coagulation. Stronger condensation means less loss of PNC due to coagulation and more accumulation mode particles due to growth. However, the incloud wet scavenging is stronger in the accumulation mode than in smaller sizes, causing a lowering of the total PNC once the PNC peak is moved to larger sizes. The trend is broken in K-Puszta in March, and at all sites except Mace Head in July. This is probably an effect of the organic gases being larger in July than in March in general, and lower in Mace Head than the other sites.

Figure 23. Mean observed and modeled total (top) and accumulation mode (bottom) particle number concentration (PNC) in March resulting from sensitivity tests on amount of available condensable organic vapor and order of coagulation versus nucleation and condensation. Note that the size intervals (as in Figure 21 and Figure 22) differ between the stations: the size interval is used for both modeled and observed values. Scenario notation: See Table 12.
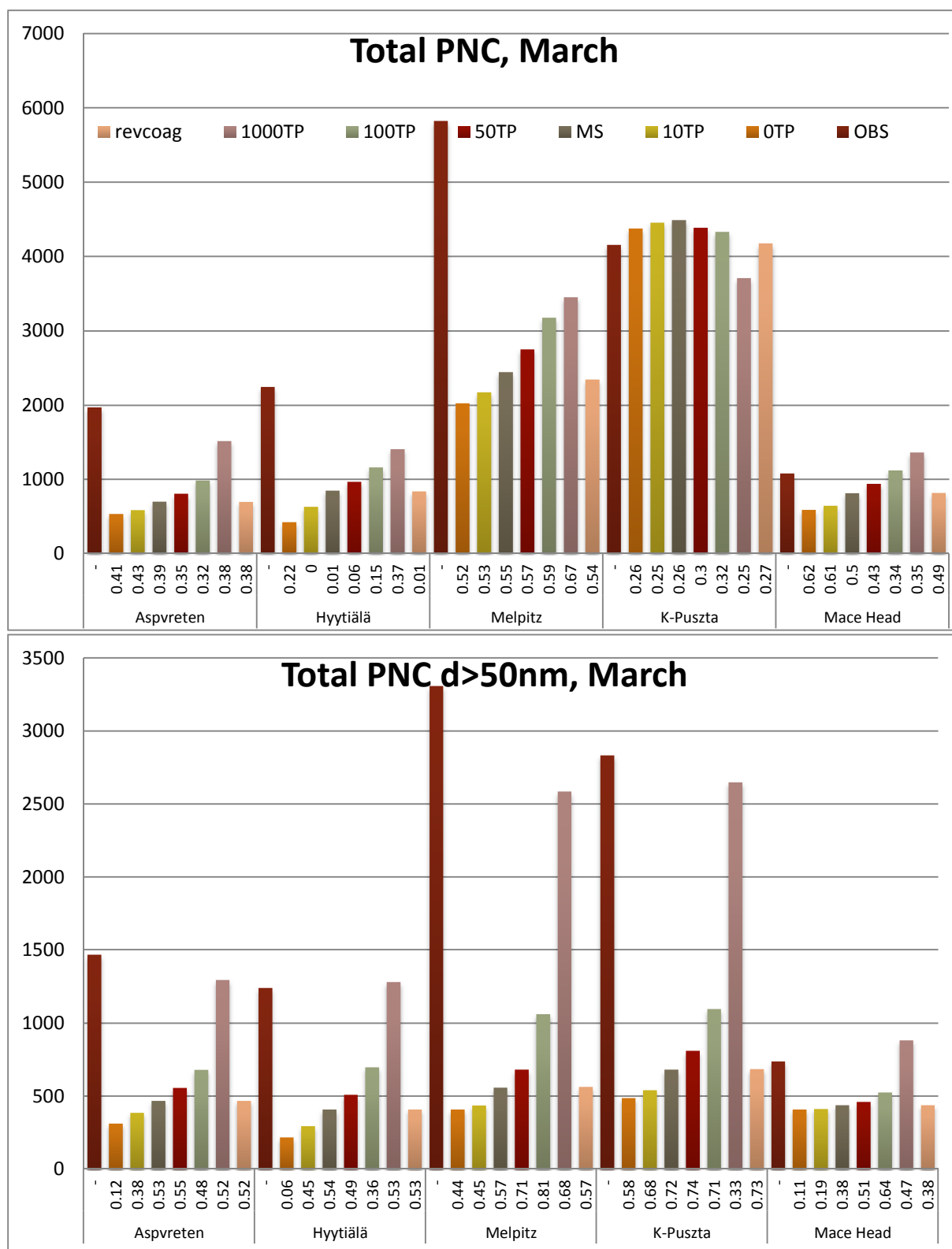
Figure 24. Mean observed and modeled total (top) and accumulation mode (bottom) particle number concentration in July resulting from sensitivity tests on amount of available condensable organic vapor and order of coagulation versus nucleation and condensation. Note that the size intervals (as in Figure 21 and Figure 22) differ between the stations: the size interval is used for both modeled and observed values. Scenario notation: See Table 12. Unit: # cm^{-3}.
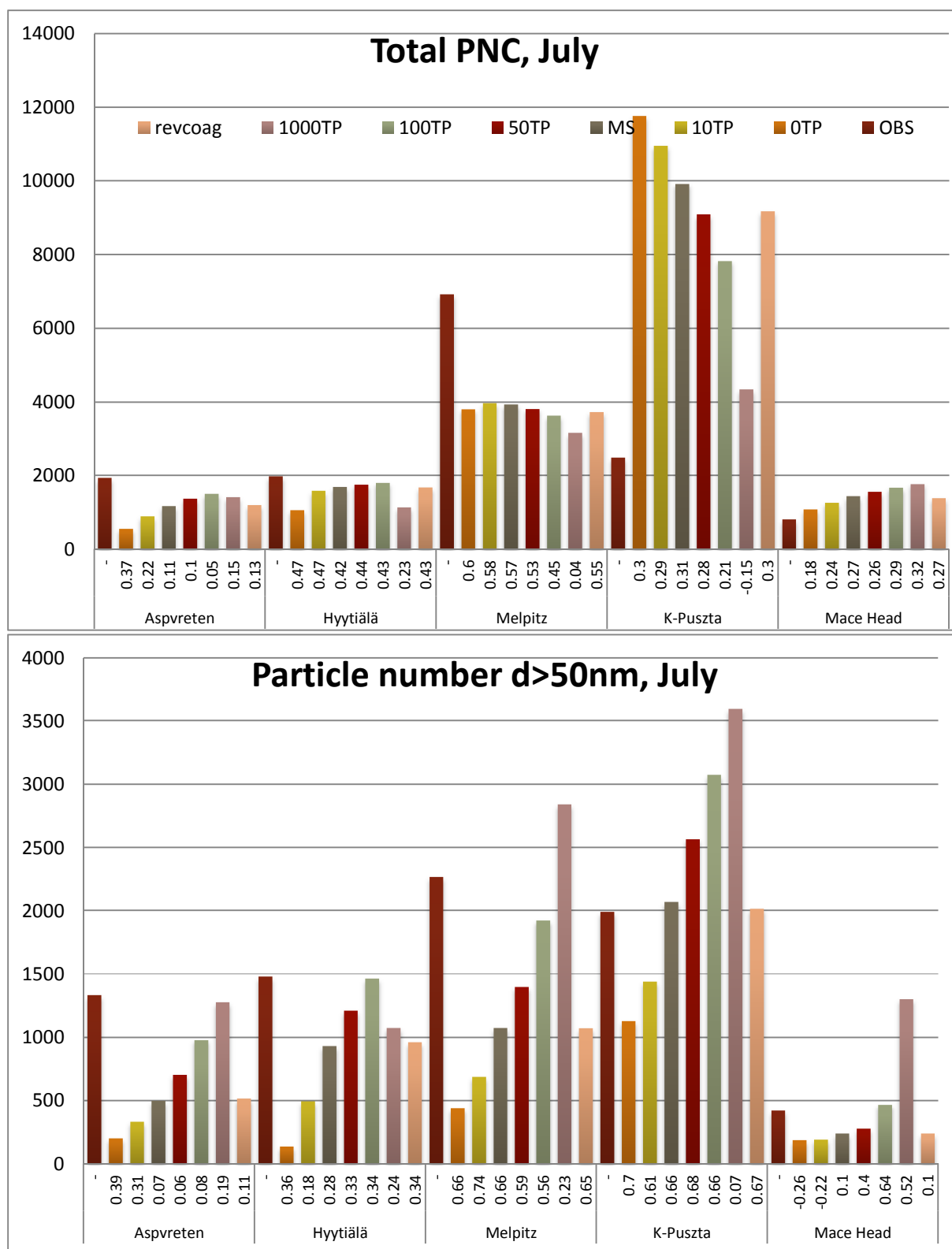
The model results are strongly sensitive to the amount of condensable gases and the amount that gives the best model performance in comparison to observations depends on site and season. Thus it is important to improve the model description on spatial and temporal variations and magnitude in terpene emissions as well as the description on condensable gases and possibly how these are interacting with particles, since they should both affect nucleation and condensation.

Wet scavenging

The change in concentration due to wet scavenging depends on both incloud and subcloud scavenging according to

$$\frac{dc_i}{dt} = -(W_{IC} + W_{SC})$$

where the incloud scavenging W_{IC} is described by

$$W_{IC} = -c_i \Lambda^{IC}{}_i$$

$$\Lambda^{IC}{}_i(D) = F_s(D)\frac{CC}{(CLWC + CIWC)} * P$$

where CLWC and CIWC are the cloud water content, P is the precipitation intensity in each grid box, CC is the fraction of the box that is covered by clouds and c_i is the concentration of particles. Particles larger than 80nm will be incloud scavenged, i.e. the factor F_s is 1 for these particles and 0 for smaller sizes. This is a simplification based on Seinfeld and Pandis (1997). We call the base case simulation *baseE*. A summary of this and all other cases in this section can be found in Table 13.

Table 13. Describing model scenarios for investigation of model sensititvity to wet scavenging parameterization

Case	Information	Parameters	Version
baseE	Base case in this section. As standard but with emissions from EMEP. Physical formulation with incloud and subcloud scavenging. Particles larger than 80nm are assumed to be activated as cloud droplets in the cloud with full efficiency.	*Fs(D>=80nm)=1* *Fs(D<80nm)=0*	S20BV87b
cloud	Formulation as baseE. Fraction of particles (per size, D) that are activated (Fa) as cloud droplets are wet scavenged.	*Fs=Fa(D)*	S20BV91b
L1	Constant wet scavenging factor for particles. More effective.	λ_i=2.78 × 10^{-4}	S20BV88b
L2	Constant wet scavenging factor for particles. Less effective.	λ_i =0.3 × 10^{-4}	S20BV90b

A more advanced formulation, which is more CPU-time consuming, is also implemented in the model. We call this simulation *cloud*. In this formulation the solubility parameter F_s in the incloud scavenging scheme is coupled to the particle activation formulation in the model. The number of particles activated to cloud droplets in each size section is determined by the particle size distribution, their number concentration and chemical composition as well as the updraft velocity and the maximum supersaturation of the air parcel. In this case F_s is the activated fraction, F_a, in the particle size fraction.

Two further sensitivity tests are included. These are not physically detailed, but based on a parameterized wet scavenging formulation. This formulation is not divided between incloud and subcloud scavenging, but rather using a wet scavenging coefficient, Λ_i, (that may differ between species). This coefficient describes the fraction of the compound that is wet scavenged according to

$$\frac{dc_i}{dt} = -c_i \Lambda_i$$

where c_i is the concentration of specie i and $\Lambda_i = \lambda_i \times P$, where P is the precipitation intensity at the surface and λ_i is a scavenging coefficient. Two different values of λ_i were tested. In one case (L1) a high wet scavenging coefficient was used ($\lambda_i = 2.78 \times 10^{-4}$) and in the other case (L2) a lower coefficient was used ($\lambda_i = 0.3 \times 10^{-4}$).

EMEP expert emissions (http://www.emep.int) were used in all the wet scavenging sensitivity tests. In Appendix B the EMEP particle mass (Figure B43) and number (Figure B44) emissions are compared to TNO emissions, which were used in the rest of the report. The number of particles emitted is slightly larger with the TNO inventory than with the EMEP emissions, due to the inclusion also of sulfate particles in the emissions from TNO. Dust was distributed differently on sizes in the two base case simulations. This should have no effect on the wet scavenging sensitivity tests, since the main fraction of dust is distributed on coarse mode and the largest accumulation mode sizes, which are always activated as cloud droplets within precipitating clouds. The coarse mode differences also have little effect on the particle number size distribution. For EC and OM, which are more important for PNC since they are mostly emitted as smaller particles, the size distribution was the same for both emission inventories (as described in Section 3).

The wet deposition sensitivity tests were performed for the three-year period 2007-2009. The reason for including more than one year is that the precipitation varies between years which may affect the model performance. For this reason, some evaluation statistics is presented separate between the years.

Evaluation of wet scavenging

Evaluation of precipitation is presented in Figure 25. There is greater variation in precipitation between the years in the model and the correlation is better for 2009 than for the other years. The precipitation is overestimated more for 2007 than for the other years, which could lead to an overestimation of wet scavenging for 2007.

Evaluation statistics of precipitation, and concentration in precipitation (CP) and wet deposition of SIA components based on baseE are presented in Table 14. Scatter plots of CP and wet deposition of oxidized sulfur (SOX_S), reduced nitrogen (NHX_N) and oxidized nitrogen (NOY_N) are shown in Figure 26. For SOX_S there is overestimation in CP, for NHX_N and NOY_N there is overall slight underestimation. The model tends to produce lower CP in 2007 than the other years, probably a result of over-predicted precipitation in that year. The wet deposition of nitrogen compounds is moderately overestimated, whereas the wet deposition of sulfur compounds is overestimated. For oxidized species the correlation is around 0.70, whereas it is lower for reduced nitrogen. The spatial distribution of nitrogen aerosol concentration in air is better captured than the wet deposition (with spatial correlation coefficient at around 0.80-0.90, see Table 8).
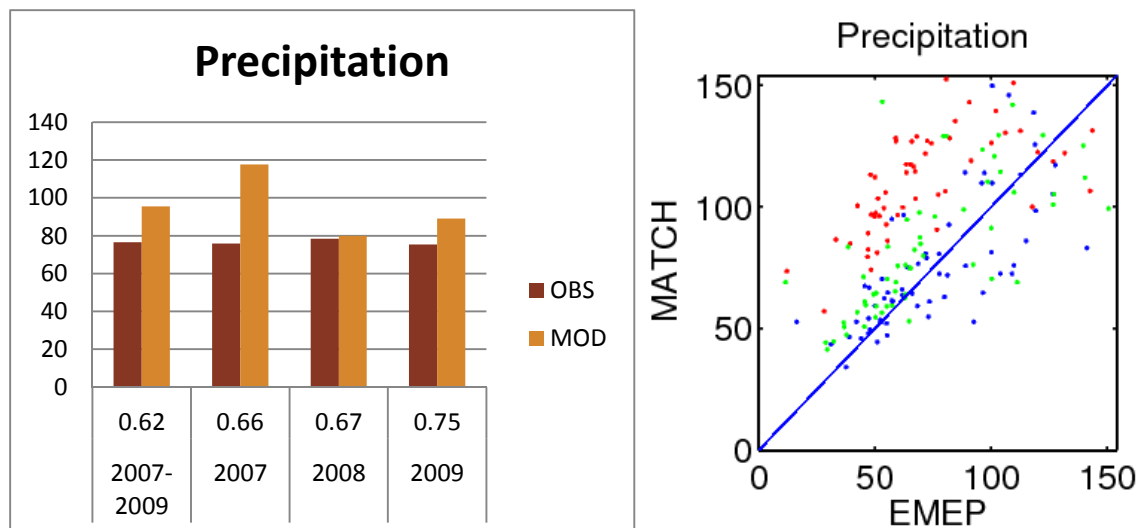
Figure 25. Modeled and observed precipitation during the years 2007-2009 at measurement sites in Europe. Left hand panel: Observed and modeled three-year mean and annual means for 2007-2009 over all EMEP measurement stations with more than 9 months of precipitation data. Spatial correlation coefficients (of 2007-2009 and annual precipitation at the measurement sites) are shown below the bars. Right hand panel: Modeled ("MATCH") versus observed ("EMEP") annual precipitation at measurement sites. Red: 2007, Blue: 2008, Green: 2009. Unit: mm month[-1].

Table 14. Evaluation statistics of annual mean precipitation, concentration in precipitation (CP) and wet deposition of oxidized sulfur (SOX_S), reduced nitrogen (NHX_N) and oxidized nitrogen (NOY_N), for the years 2007-2009, at measurement sites in Europe. The evaluation is conducted for MATCH-SALSA with EMEP emissions, baseE, and compared to measurements from the EMEP measurement network.

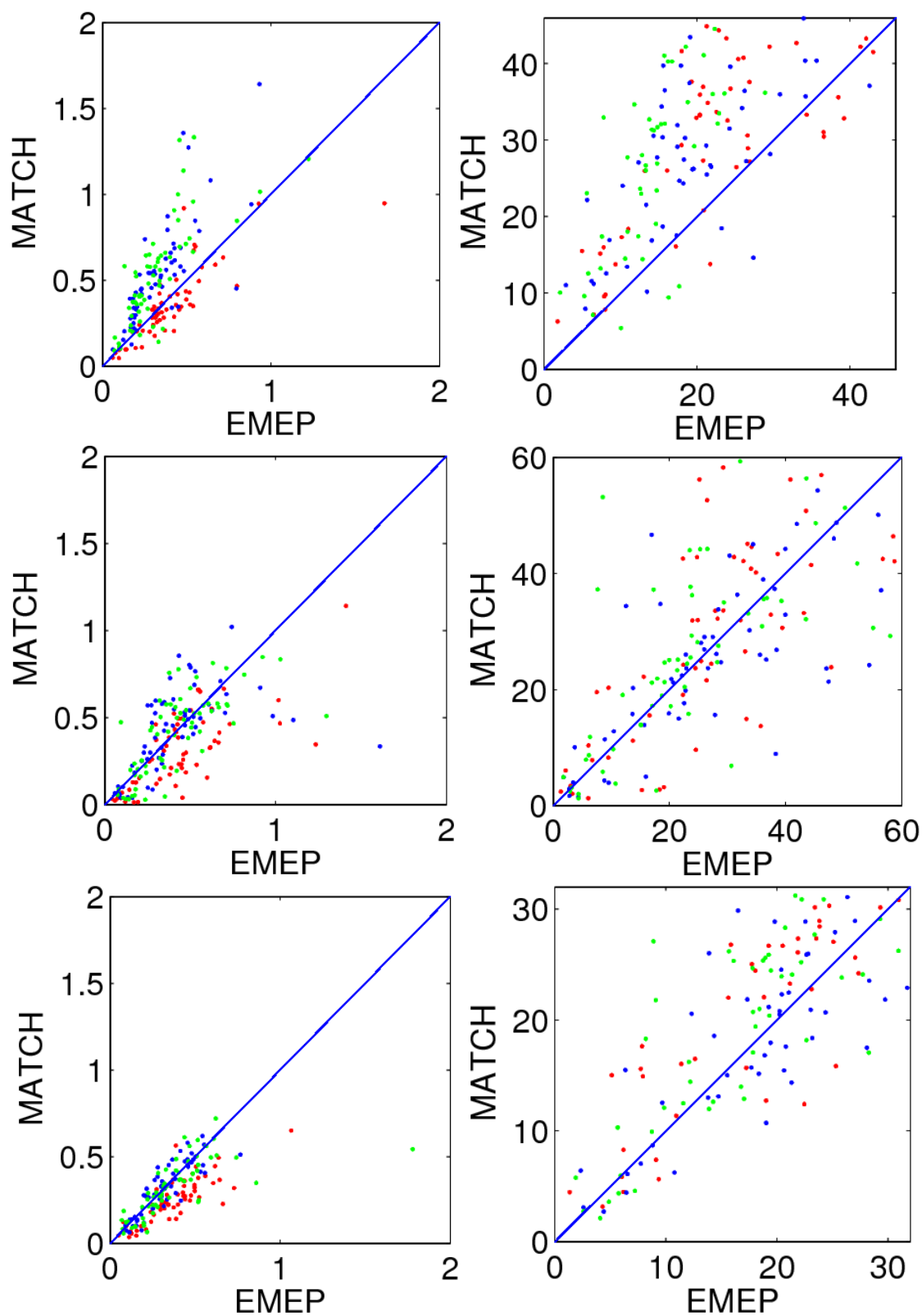|	SOX_S			NHX_N		NOY_N	
	prec.	CP	wet dep.	CP	wet dep.	CP	wet dep.
Mean (mod)	95	0.47	36	0.39	30	0.3	23
Mean (obs)	76	0.35	23	0.45	29	0.36	23
Variance (mod)	1308	0.08	442	0.05	428	0.02	128
Variance (obs)	1087	0.04	206	0.13	537	0.04	242
Abs error	28	0.18	14	0.17	11	0.09	7
Bias (%)	38	41	76	-6	20	-12	14
Correl. coefficient	0.62	0.67	0.70	0.39	0.48	0.71	0.74

Figure 26. Modeled (MATCH) versus measured (EMEP) annual mean concentration in precipitation (left) and wet deposition (right) of SOX_S (top row), NHX_S (middle row) and NOY_N (bottom row) at measurement sites in Europe. Red: 2007, Blue: 2008, Green: 2009. The model version is baseE (standard MATCH-SALSA with EMEP emissions).

Sensitivity to the wet scavenging parameterization for SIA components

The resulting CP and wet deposition of SOX_S, NHX_N and NOY_N for the sensitivity scenarios are presented in Figure 27, Figure 28 and Figure 29. The resulting level of SOX_S and NHX_N wet deposition and CP is similar between all versions except the L2 version for which both CP and resulting wet deposition is smaller, which leads to a smaller bias.

The spatial correlation for CP and wet deposition of SOX_S and NOY_N are clearly better than for NHX_N for the years 2007 and 2008. Differences in correlation are small between the different wet deposition schemes except for SOX_S in 2009, which seems to be less well modeled with the simple λ-schemes.

For NOY_N there is basically no variation in correlation coefficient between model versions, but the performance of CP during 2009 is worse than the other years.

As SOX_S is included in the microphysics of MATCH-SALSA, the results are most interesting for this component; (NOY_N and NHX_N may not be distributed on the right particle sizes in the present version of MATCH-SALSA, which may lead to incorrect deposition as well). The physical descriptions (cloud and baseE) lead to higher spatial correlation for 2009 (and marginally so for 2007) but the more advanced cloud activation scheme does not improve the wet scavenging results compared to the baseE case.
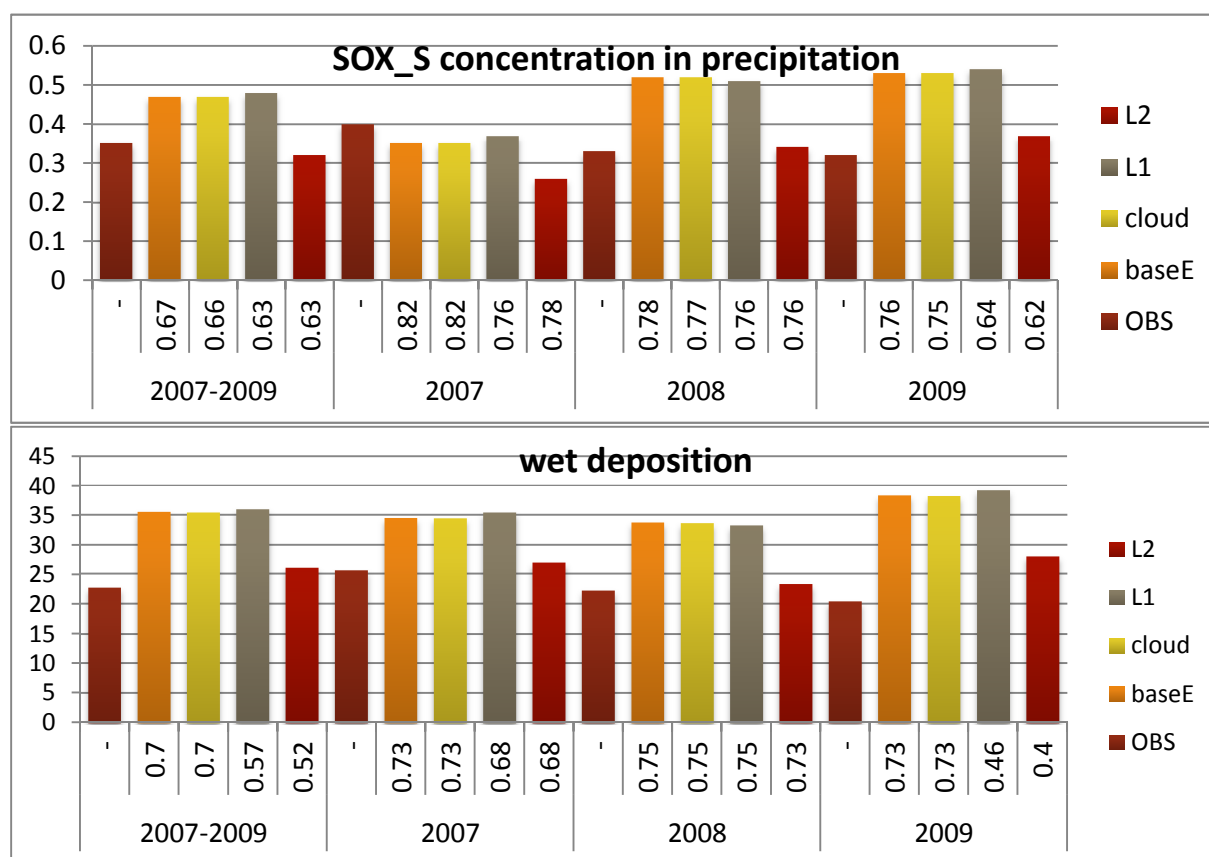

Figure 27. Observed (OBS) and modeled mean concentration in precipitation of oxidized sulfur (SOX_S) and annually accumulated SOX_S wet deposition. Correlation coefficient of annual values at all measurement sites is indicated below the bars. Model scenarios are described in Table 14. Units: concentration mgS l^{-1} and deposition mgS m^{-2} yr^{-1}.
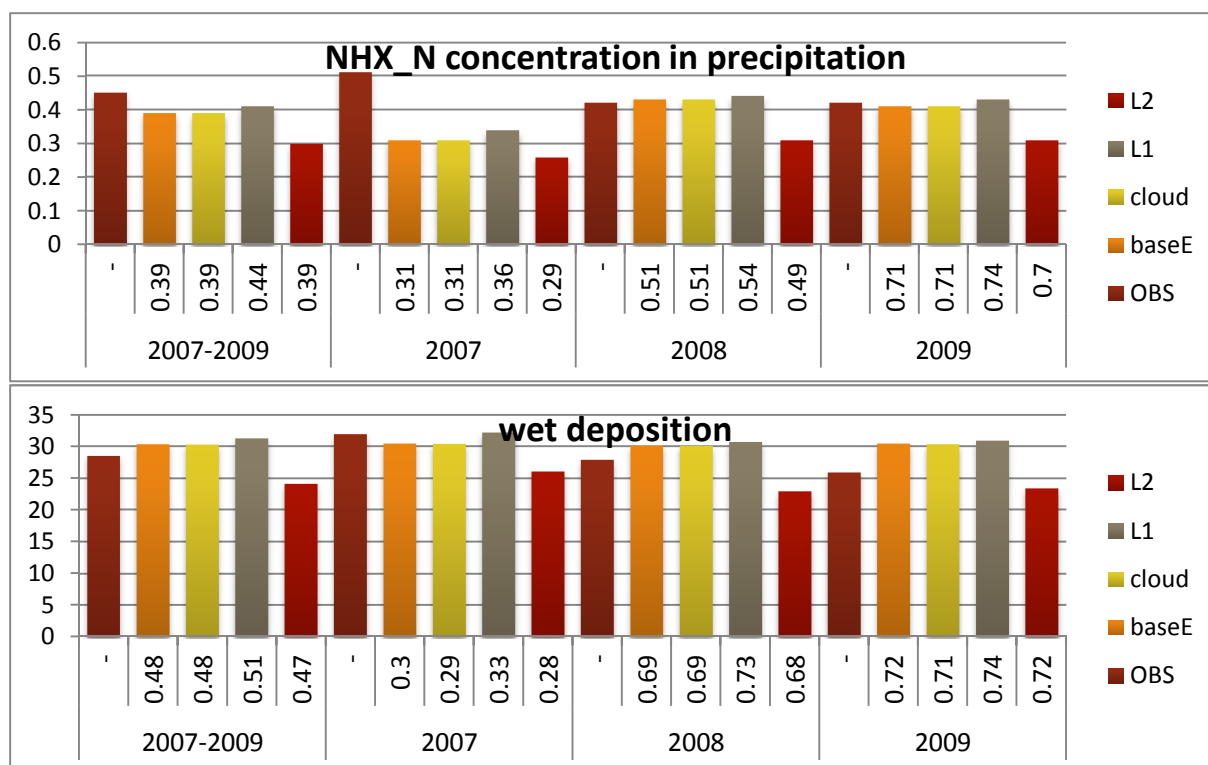
Figure 28. Observed (OBS) and modeled mean concentration in precipitation of reduced nitrogen (NHX_N) and annually accumulated NHX_N wet deposition. Correlation coefficient of annual values at all measurement sites is indicated below the bars. Model scenarios are described in Table 14. Units: concentration mgN l^{-1} and deposition mgN m^{-2} yr^{-1}.
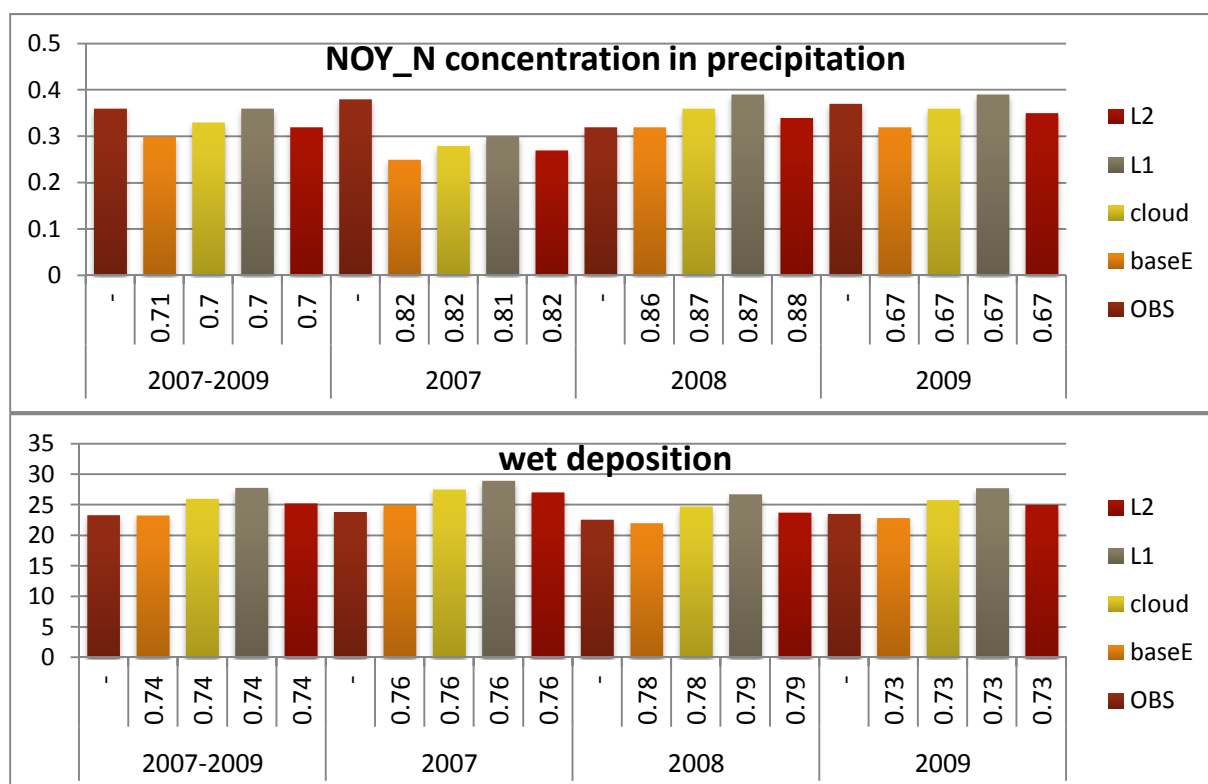

Figure 29. Observed (OBS) and modeled mean concentration in precipitation of oxidized nitrogen (NOY_N) and annually accumulated NOY_N wet deposition. Correlation coefficient of annual values at all measurement sites is indicated below the bars. Model scenarios are described in Table 14. Units: concentration mgN l^{-1} and deposition mgN m^{-2} yr^{-1}.

Sensitivity of particle mass (PM$_{2.5}$) to the wet scavenging parameterization

The model gives lower PM$_{2.5}$ concentrations when the L1 parameterization is used than with the other formulations (Figure 30). L2 results in higher PM$_{2.5}$ concentrations than the more advanced formulations, baseE and cloud. However, though the L1 often produces underestimation of annual mean, the correlation coefficient is generally higher for this formulation than for the other schemes. One of the reasons for this could be sea salt, which seems to be transported too far inland in the model, giving rise to peaks where there are no observed peaks, as was discussed in Section 4; the L1 scavenging ratio is expected to be too high for accumulation mode particles and this "error" may to some extent compensate for an error in the sea salt modeling.

Sensitivity of PNC to the wet scavenging parameterization

The L1 scheme resulted in higher total PNC during summer than the other formulations (Figure 31). All cases gave similar accumulation mode PNC for summer but for winter the L1 case gave lower levels than the other formulations. Due to the lower PM$_{2.5}$ concentration in the L1 parameterization, the small particles are probably not coagulated as efficiently, resulting in higher total PNC numbers in that scenario. At most sites, the correlation coefficients are similar for all tested wet deposition schemes.

When looking at long-term statistics the cloud activation scheme did not improve the modeled PNC or PM$_{2.5}$.

Recommendations based on the sensitivity tests

What are the optimum model settings for MATCH-SALSA?

- Use activation nucleation, at this stage without organic nucleation.
- Use the physical wet scavenging formulation (used in the base cases, MS and baseE).
- There is no need to use particle activation scavenging (cloud case), compared to the baseE formulation of particle scavenging.

What are identified as sensitive parameters?

- The results are dependent on fraction of SOx emitted as H$_2$SO$_4$ and the best choice is site dependent.
- The model results are highly sensitive to whether organic nucleation is included or not.
- The model results are sensitive to amount of organic vapors in the condensation.

Where should the focus be for future model improvements?

- The model is underestimating condensational growth, which may be at least partly due to the fact that nitrogen condensation is not affecting the particle microphysics. This needs to be improved in the model.
- An emission routine for biogenic monoterpenes is needed and a more realistic scheme for SOA formation should be tested. This will influence the model performance on total PNC through impacts on both nucleation and condensation.
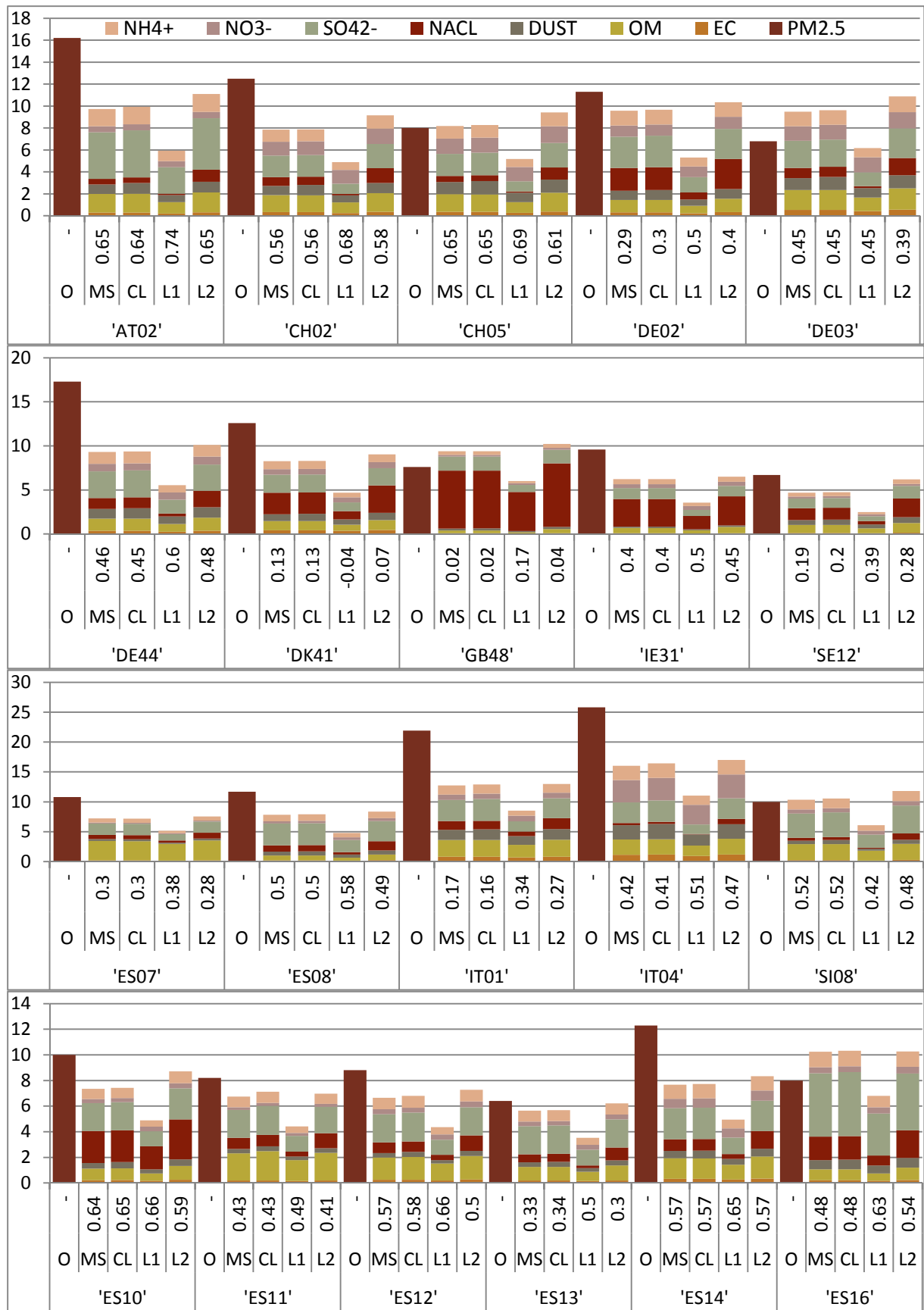
Figure 30. Observed (OBS) and modeled scenarios of annual mean particle mass (PM$_{2.5}$) concentration in air. Model scenarios are described in Table 14, but the MS case refers to the baseE case and CL means the cloud case. Unit: µg m^{-3}.
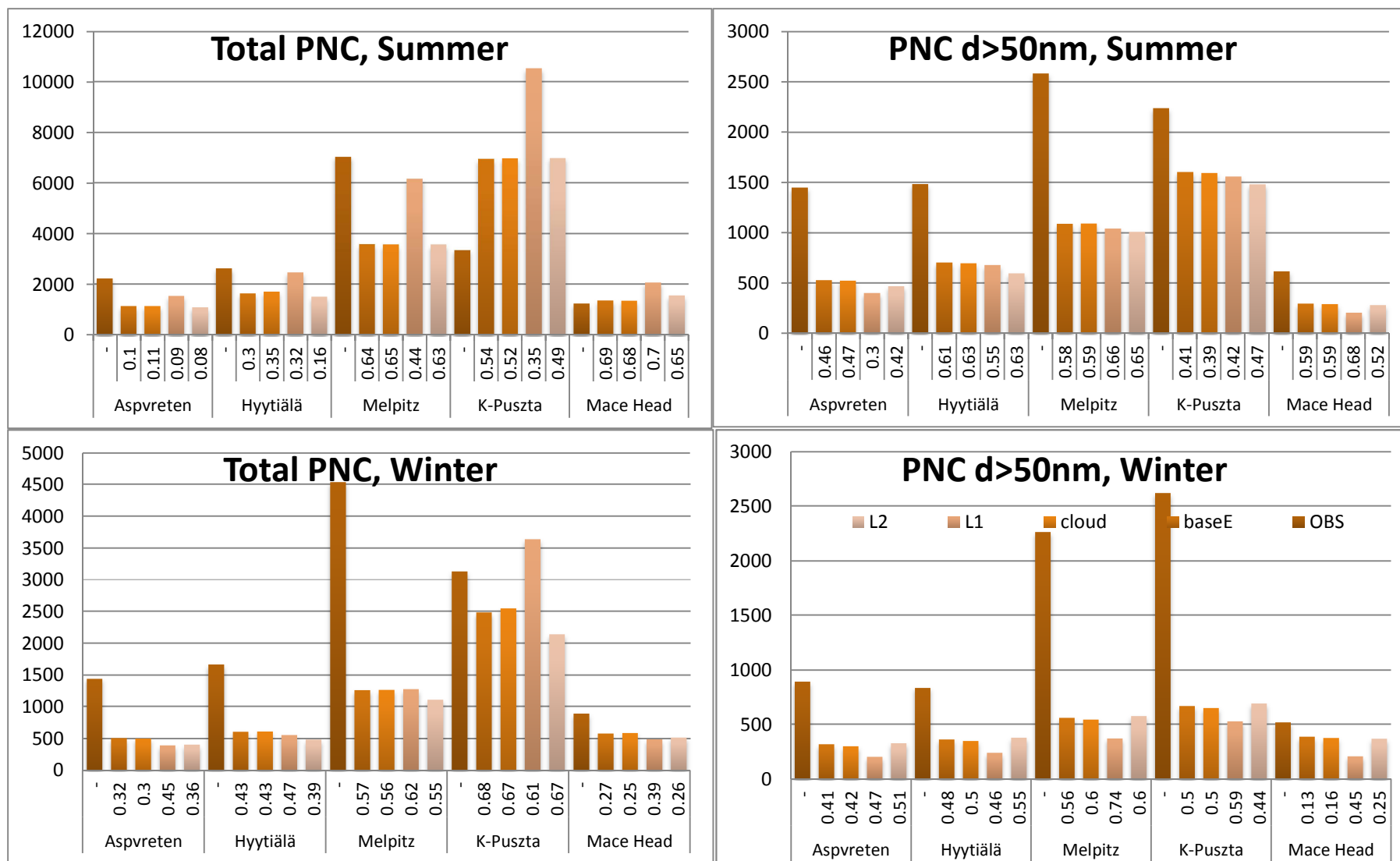
Figure 31. Spatial variation of observed and modeled (scenarios) summer (April-September; top row) and winter (January-March and October-December; bottom row) mean particle number concentration (PNC) for the year 2007. Left panels: Total PNC. Right panels: Accumulation mode PNC. Scenario notation: see Table 13. Unit: # cm^{-3}.

7. Overall Conclusions

What are the strengths and weaknesses of the new model?

We have implemented the sectional aerosol dynamics model SALSA (Kokkola et al., 2008) in the European scale CTM MATCH (Multi-scale Atmospheric Transport and Chemistry; Robertson et al., 1999). The new model is called MATCH-SALSA. It includes aerosol microphysics and several options for nucleation, wet scavenging and condensation.

In general the model reproduces observed higher particle number concentration (PNC) in central Europe and lower in remote regions. The model peak PNC occurs at the same particle size as the observed peak or at smaller sizes, which indicate missing growth. Total PNC is underestimated at some sites. The model performs well for particle mass, including SIA components. EC and OC are underestimated at many of the sites.

Where should the focus be for future improvements?

- A biogenic emission module for monoterpenes is needed to be able to treat SOA formation in a realistic way. Updating the biogenic SOA scheme will likely have a large impact on modeled PM2.5 and also affect the model performance for total PNC through impacts on nucleation and condensation.
- Nitrogen gas-particle partitioning should be coupled to the microphysics. This may improve the underestimated condensational growth.
- Open fire emissions from wildfires and agricultural activities (biomass burning) should be added to the model.
- Dust emissions should be included in the model.
- Processes affecting sea salt need further work and evaluation. This study has shown large modeled sea salt peaks that are not seen in the measurements. Both emissions and deposition of sea salt particles should be investigated.
- Emission inventories need to be improved, especially for EC and OC emissions.

Can we apply the new model?

The model can be used in applications knowing the restrictions of what the model manages well and what needs further improvements. Before using the model for simulating $PM_{2.5}$ the SOA formulation needs further improvements. Before using the model in future/trend simulations a model of biogenic emissions of terpenes need to be included in MATCH-SALSA. MATCH-SALSA is computationally heavier than MATCH, which also puts restrictions on when the model can be used.

How is MATCH-SALSA in comparison to MATCH?

The models should be used for different applications. When ozone photo chemistry or sulfur/nitrogen deposition is in focus, the standard MATCH model is still useful (and probably preferable because of the computational demands of MATCH-SALSA). When particle numbers are in focus then MATCH-SALSA is the only choice. For particle mass, it depends on the application.

What is the optimum model set up when running MATCH-SALSA?

- Use activation nucleation (at this stage without organic nucleation).
- Use the physical wet scavenging formulation.
- There is no need to use particle activation scavenging for model runs aimed at describing wet deposition and/or surface air quality.

What are identified as sensitive parameters?

- The results are dependent on fraction of SO_x emitted as H_2SO_4 and the optimum choice is site dependent.
- The model results are highly sensitive to whether organic nucleation is included or not.
- The model results are sensitive to amount of organic vapors in the condensation.

8. References

Abdul-Razzak, H. and S. J. Ghan, 2000: A parameterization of aerosol activation, 2. Multiple aerosol types, J. Geophys. Res., 105, 6837 – 6844.

Abdul-Razzak, H., S. J. Ghan, and C. Rivera-Carpio, 1998: A parameterization of aerosol activation, 1, Single aerosol type, J. Geophys. Res., 103, 6123 – 6132.

Abdul-Razzak, H., and S. J. Ghan, 2002: A parameterization of aerosol activation, 3. Sectional representation, J. Geophys. Res., 107, D3, 4026, 10.1029/2001JD000483.

Adams, P.J. and Seinfeld, J.H., 2002. Predicting global aerosol size distributions in general circulation models J Geophys Res D, 107 (D19), AAC 4-1-AAC 4-3.

Andersson, C., Langner, J., Bergström, R. 2007. Interannual variation and trends in air pollution over Europe due to climate variability during 1958-2001 simulated with a regional CTM coupled to the ERA40 reanalysis. *Tellus 59B*, 77-98.

Andersson, C., Bergström, R. and Johansson, C., 2009. Population exposure and mortality due to regional background PM in Europe – long-term simulations of source region and shipping contributions. Atmos. Env. 43, 3614-3620.

Atkinson, R; D. L. Baulch; R. A. Cox; J. N. Crowley; R. F. Hampson; R. G. Hynes; M. E. Jenkin; M. J. Rossi; and J. Troe, Evaluated kinetic and photochemical data for atmospheric chemistry: Volume II - gas phase reactions of organic species, 2006, *Atmos. Chem. Phys*., **6**, 3625-4055. http://www.atmos-chem-phys.net/6/3625/2006/ and http://www.iupac-kinetic.ch.cam.ac.uk/

Berge, E., 1992. Coupling of wet scavenging of sulphur to clouds in a numerical weather prediction model. *Tellus* **45B**, 1-22.

Bergström, R., Denier van der Gon, H.A.C., Prévôt, A.S.H., Yttri, K.E., and Simpson, D., 2012: Modelling of organic aerosols over Europe (2002-2007) using a volatility basis set (VBS) framework: application of different assumptions regarding the formation of secondary organic aerosol, Atmos. Chem. Phys., 12, 8499-8527, doi:10.5194/acp-12-8499-2012.

Bergman, T., Kerminen, V.-M., Korhonen, H., Lehtinen, K. J., Makkonen, R., Arola, A., Mielonen, T., Romakkaniemi, S., Kulmala, M., and Kokkola, H., 2012. Evaluation of the sectional aerosol microphysics module SALSA implementation in ECHAM5-HAM aerosol-climate model, *Geosci. Model Dev.*, **4**, 845-868, doi:10.5194/gmd-5-845-2012.

Bott, A. 1989a. A positive definite advection scheme obtained by nonlinear renormalization of the advective fluxes. Monthly Weather Review 117, 1006-1015.

Bott, A. 1989b. Reply. Monthly Weather Review 117, 2633-2636.

Carter, W.P.L., 1996. Condensed atmospheric photooxidation mechanism for isoprene, *Atmos. Environ.* **30**, 4275-4290.

Chamberlain, A.C. and Chadwick, R.C., 1965. Transport of iodine from atmosphere to ground. Tellus 18, 226-237.

Chen, Y. and Penner, J.E., 2005. Uncertainty analysis for estimates of the first indirect aerosol effect. Atmos Chem Phys 5, 2935-2948.

Dana, M. T. and Hales, J. M. 1976. Statistical aspects of the washout of polydisperse aerosols. *Atmos Environ* **10**, 45–50.

EMEP/EEA 2009. EMEP/EEA air pollutant emission inventory guidebook 2009. EEA technical report no 9.

Foltescu, V.L., Pryor, C.S. and Bennet, C. 2005. Sea salt generation, dispersion and removal on the regional scale. *Atmos Environ* 39, 2123-2133.

Friedrich, R. and Reis, S. (eds) 2004. Emissions of air pollutants – measurements, calculations and uncertainties. Springer. ISBN 978-3-540-00840-8.

Gidhagen, L., Johansson, C., Langner, J. and Foltescu, V., 2005. Urban scale modeling of particle number concentration in Stockholm. *Atmos Environ* 39, 1711-1725.

Genberg, J., Denier van der Gon, H. A. C., Simpson, D., Swietlicki, E., Areskoug, H., Beddows, D., Ceburnis, D., Fiebig, M., Hansson, H. C., Harrison, R. M., Jennings, S. G., Saarikoski, S., Spindler, G., Visschedijk, A. J. H., Wiedensohler, A., Yttri, K. E., and Bergström, R.: Light-absorbing carbon in Europe – measurement and modelling, with a focus on residential wood combustion emissions, Atmos. Chem. Phys., 13, 8719-8738, doi:10.5194/acp-13-8719-2013, 2013.

Heimann, M. & Keeling, C.D., 1989. A three-dimensional model of atmospheric CO2 transport based on observed winds. 2. Model description and simulated tracer experiments. In: Aspects of Climate Variability in the Pacific and the Western Americas (ed. DH. Peterson). American Geophysical Union, Washington DC, pp 237-275.

Holtslag, A.A.M., van Meijergaard, E. and De Rooy, W.C. 1995. A comparison of boundary layer diffusion schemes in unstable conditions over land. Boundary-Layer Meteorology 76, 69-95.

Jacobson, M. Z., 1994. Developing, coupling and applying a gas, aerosol, transport and radiation model to study urban and regional air pollution, Ph.D. thesis, Dept. of Atmospheric Sciences, University of California, Los Angeles.

Jacobson, M. Z., 1997. Numerical techniques to solve condensational and dissolutional growth equations when growth is coupled to reversible reactions, *Aerosol Sci. Technol*., 27, 491–498.

Jacobson, M. Z., 2002. Analysis of aerosol interactions with numerical techniques for solving coagulation, nucleation, condensation, dissolution, and reversible chemistry among multiple size distributions, *J. Geophys. Res*., 107, 4366, doi:10.1029/2001JC002044.

Jacobson, M.Z., 2005. Fundamentals of atmospheric modeling. Second edition. Cambridge university press.

Jenkin, M.E., Saunders, S.M., and Pilling, M.J., 1997. The tropospheric degradation of volatile organic compounds: a protocol for mechanism development, *Atmos. Environ*., **31**, 81-104, 1997.

Jönsson, O. et al., 2013. Air pollution episodes in Stockholm regional background air due to sources in Europe and their effects on human population. *Boreal Environ Res.* 18, 280-302.

Kokkola, H. et al., 2008. SALSA – a sectional aerosol module for large scale applications. *Atmos. Chem. Phys*. 8, 2469-2483.

Kuenen, J., Denier van der Gon, H., Visschedijk, A., van der Brugh, H., van Gijlswijk, R., 2011. MACC European emission inventory for the years 2003-2007. TNO report, TNO-060-UT-2011-00588.

Kulmala, M. et al., 2006. Cluster activation theory as an explanation of the linear dependence between formation rate of 3 nm particles and sulphuric acid concentration, *Atmos. Chem. Phys*., 6, 787–793, 2006, http://www.atmos-chem-phys.net/6/787/2006/.

Kupiainen, K. and Klimont, Z., 2007. Primary emissions of fine carbonaceous particles in Europe. Atmos Environ 41, 2156-2170.

Langner, J., Bergström, R. and Pleijel, H. 1998, European scale modeling of sulfur, oxidised nitrogen and photochemical oxidants. Model development and evaluation for the 1994 growing season. SMHI RMK 82. SMHI SE-60176 Norrköping, Sweden.

Lohmann, U. and J. Feichter, 2005: Global indirect aerosol effects: a review, Atmos. Chem. Phys, 5, 715-737.

Mårtensson, , E. M., Nilsson, E. D., de Leeuw, G., Cohen, L. H. and Hansson, H.-C. 2003. Laboratory simulations and parametrization of the primary marine aerosol production. *J. Geophys. Res.* **108**(D9), doi:10.1029/2002JD002263.

Monahan, E. C., Spiel, D. E. and Davidson, K. L. 1986. A model of marine aerosol generation via whitecaps and wave disruption. In: *Oceanic Whitecaps and Their Role in Air-Sea Exchange* (eds E. C. Monahan and G. Mac Niocaill). D Reidel, Norwell, MA, pp. 167–174.

Napari et al. 2002a, An improved model for ternary nucleation of sulfuric acid - ammonia- water, J. Chem. Phys., 116, 4221-4227.

Napari et al. 2002b. Parameterization of ternary nucleation rates for H_2SO_4 - NH_3 - H_2O vapors, J. Geophys. Res., 107(D19), AAC 6-1

O'Dowd, C.D., Facchini, M.C., Cavalli, F., Ceburnis, D., Mircea, M., Decesari, S., Fuzzi, S., Yoon, Y.J. and Putaud, J.-P. 2004. Nature 431, 676-680.

Paasonen, P, Nieminen, T. et al., 2010. On the roles of sulphuric acid and low-volatility organic vapours in the initial steps of atmospheric new particle formation. Atmos. Chem. Phys. 10, 11223-11242.

Peters, K. and Eiden, R., 1992. Modeling the dry deposition velocity of aerosol particles to a spruce forest. Atmos. Environ. 26 (14), 2555-2564.

Pope, C.A. and Dockery, D.W., 2006. Health effects of fine particulate air pollution: lines that connect. J Air and Waste Management Ass 56 (6), 709-741.

Pouliot, G., Thomas Pierce, T., Denier van der Gon, H., Schaap, M., Moran, M. and Nopmongcol, U., 2012. Comparing emission inventories and model-ready emission datasets between Europe and North America for the AQMEII project, *Atmos. Environ.* **53**, 4-14.

Riipinen, I. et al., 2007. Connections between atmospheric sulphuric acid and new particle formation during QUEST III, IV campaigns in Heidelberg and Hyytiälä, *Atmos. Chem. Phys.*, 7, 1899–1914, http://www.atmos-chem-phys.net/7/1899/2007/.

Rissman, T. A., A. Nenes and J. H. Seinfeld, 2004: Chemical Amplification (or Dampening) of the Twomey Effect: Conditions Derived from Droplet Activation Theory. J. Atmos. Sci., 61, 919–930.

Robertson, L., Langner, J. and Engardt, M. 1999. An Eulerian Limited-Area Atmospheric Transport model. Journal of Applied Meteorology 38, 190-210.

Roesler, E.L. and J.E. Penner 2010. Can global models ignore the chemical composition of aerosols? *Geophys. Res. Lett.* **17,** L24809. doi: 10.1029/2010GL044282.

Saunders, S. M., Jenkin, M. E., Derwent, R. G., and Pilling, M. J.: Protocol for the development of the Master Chemical Mechanism, MCM v3 (Part A): tropospheric degradation of non-aromatic volatile organic compounds, *Atmos. Chem. Phys.*, **3**, 161-180, doi:10.5194/acp-3-161-2003, 2003.

Schlesinger, R.B., Kunzli, N., Hidy, G.M., Gotschi, T. and Jerrett, M., 2006. The health relevance of ambient particulate matter characteristics: coherence of toxicological and epidemiological inferences. Inhal Toxicol 18 (2), 95-125.

Seinfeld, J.H. and Pandis, S.N., 1997. Atmospheric chemistry and physics. From air pollution to climate change. John Wiley and sons.

Simpson, D., 1992. Long-period modelling of photochemical oxidants in Europe. Model calculations for July 1995. *Atmos. Environ*. 26A, 1609-1634.

Simpson, D., Andersson-Skiöld, Y. and Jenkin, M.E. 1993. Updating the chemical scheme for the EMEP MSC-W oxidant model: current status. EMEP MSC-W Note 2/93.

Simpson, D., Guenther, A., Hewit, C.N. and Steinbrecher, R., 1995. Biogenic emissions in Europe. 1. Estimates and uncertainties. *J. Geophys. Res.* **100,** 22875-22800.

Simpson, D., Benedictow, A., Berge, H., Bergström, R., Emberson, L. D., Fagerli, H., Flechard, C. R., Hayman, G. D., Gauss, M., Jonson, J. E., Jenkin, M. E., Nyíri, A., Richter, C., Semeena, V. S., Tsyro, S., Tuovinen, J.-P., Valdebenito, Á., and Wind, P., 2012: The EMEP MSC-W chemical transport model – technical description, *Atmos. Chem. Phys*. 12, 7825-7865.

Spracklen, D.V., Pringle, K.J., Carslaw, K.S., Chipperfield, M.P. and Mann, G.W., 2005. A global off-line model of size-resolved aerosol microphysics: II. Identification of key uncertainties. *Atmos. Chem. Phys.* **5,** 3233-3250.

Spracklen, D.V., Carslaw, K.S., Merikanto, J. et al., 2010. Explaining global surface aerosol number concentrations in terms of primary emissions and particle formation. Atmos. Chem. Phys. 10 (10), 4775-4793.

Stern, R., Builtjes, P., Schaap, M., Timmermans, R., Vautard, R., Hodzic, A., Memmesheimer, M., Feldmann, H., Renner, E., Wolke, R., and Kerschbaumer, A.: A model inter-comparison study focussing on episodes with elevated PM10 concentrations, Atmos. Environ., 42 4567–4588, doi:10.1016/j.atmosenv.2008.01.068, 2008.

Tunved, P., Hansson, H.-C., Kerminen, V.-M., Ström, J., Dal Maso, M., Lihavainen, H., Viisanen, Y., Aalto, P.P., Komppula, M. and Kulmala, M. 2006. High natural aerosol loading over boreal forests. Science 312, 261-263.

Turpin, B.J. et al., 2000. Measuring and simulating particle organics in the atmosphere: problems and prospects. Atmos Environ 38 (18), 2983-3013.

Undén, P. et al., 2002. HIRLAM-5 Scientific Documentation. http://www.hirlam.org.

van Engelen, A, A. Klein Tank, G. van der Schrier and L. Klok, 2008. European Climate Assessment & Dataset (ECA&D), Report 2008, "Towards an operational system for assessing observed changes in climate extremes". KNMI, De Bilt, The Netherlands, 68pp.

Vehkamaki et al. (2002): An improved parameterization for sulphuric acid/water nucleation rates for tropospheric and stratospheric conditions, JGR, 107, D22, 4622.

Visschedijk, A.J.H., Denier van der Gon, H.,A.C., Dröge, R.., Van der Brugh, H., Kooter, I.M., 2009. A European high resolution and size-differentiated emission inventory for elemental and organic carbon for the year 2005. TNO report, TNO-034-UT-2009-00688-RPT-ML.

Yu F. and Luo, G., 2009. Simulation of particle size distribution with a global aerosol model: contribution of nucleation to aerosol and CCN number concentrations. Atmos Chem Phys 9 (20), 7691-7710.

Zhang et al (2001). Atmospheric Environment 35, 549-560.

Appendix A
Model quality

Table A15. Evaluation of MATCH-SALSA calculated particulate sulfate, $SO_4^{2-}(p)$, against observed (daily mean) concentrations in 2007 at regional background (EMEP) sites in Europe

Station	Obs	Mod	%bias	R	#Days
NO55	0.188	0.142	-24	0.35	361
FI36	0.211	0.134	-36	0.43	347
FI22	0.26	0.209	-20	-0.04	52
NO15	0.145	0.096	-34	0.41	348
SE05	0.177	0.106	-40	0.61	346
NO39	0.127	0.111	-13	0.22	362
FI37	0.352	0.293	-17	0.29	52
FI17	0.463	0.412	-11	0.66	363
FI09	0.283	0.334	18	0.75	340
NO01	0.277	0.35	26	0.63	365
SE14	0.622	0.5	-20	0.63	362
LV16	0.434	0.518	19	0.38	351
SE08	0.577	0.481	-17	0.70	352
DK08	0.726	0.557	-23	0.71	354
DK03	0.639	0.536	-16	0.71	357
DK31	0.689	0.486	-29	0.78	353
LV10	0.324	0.617	90	0.32	357
SE11	0.551	0.632	15	0.58	356
LT15	0.534	0.729	37	0.68	344
IE06	0.54	0.529	-2	0.13	347
GB02	0.448	0.467	4	0.41	353
DE01	0.851	0.599	-30	0.64	353
RU18	0.219	1.252	472	0.31	354
PL04	1.23	0.761	-38	0.64	364
DK05	0.789	0.695	-12	0.72	315
GB06	0.409	0.304	-26	0.68	221
DE09	0.774	0.707	-9	0.64	351
GB14	0.487	0.661	36	0.41	204
PL05	0.636	0.969	52	0.64	342
NL09	0.606	0.702	16	0.65	323
DE07	0.811	0.805	-1	0.70	364
IE05	0.489	0.502	3	0.08	347
IE08	0.724	0.739	2	0.29	365
NL08	0.765	0.842	10	0.79	186
IE01	0.512	0.304	-41	0.52	364
PL02	1.6	1.28	-20	0.48	361
NL10	0.717	0.895	25	0.46	270
GB07	0.763	0.807	6	0.46	242
GB13	0.529	0.556	5	0.70	164
FR09	0.992	0.916	-8	0.74	96
SK04	0.582	2.064	255	0.34	56
SK06	0.858	1.537	79	0.33	358
AT02	0.961	1.287	34	0.61	365
FR10	0.939	0.609	-35	0.37	317
FR14	0.739	0.616	-17	0.42	349

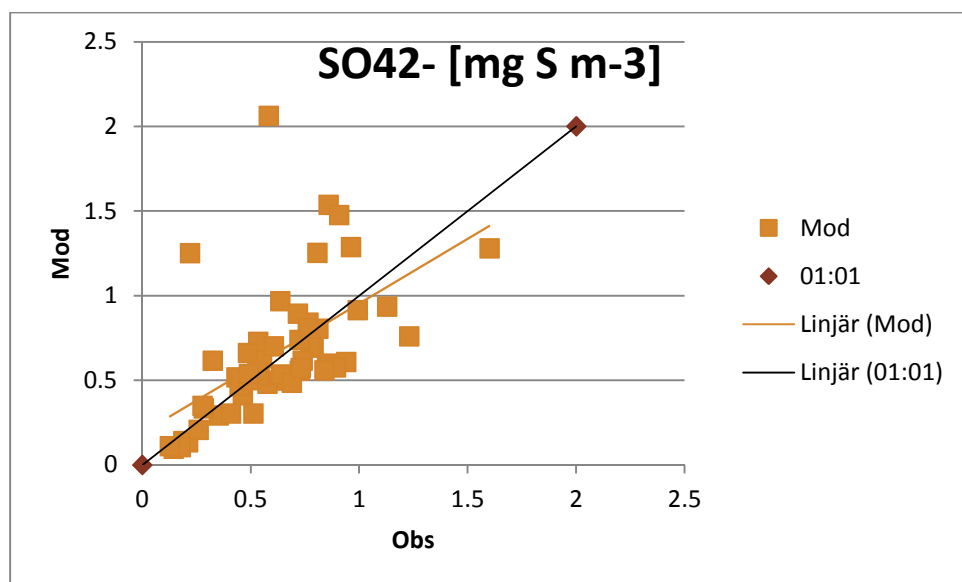| CH05	0.491	0.538	10	0.52	357
HU02	0.907	1.477	63	0.68	353
FR15	0.893	0.577	-35	0.54	355
FR17	0.73	0.573	-22	0.39	343
SI08	0.807	1.253	55	0.44	313
FR13	0.839	0.559	-33	0.41	103
IT01	1.128	0.936	-17	0.37	356

Figure A32. Scatter plot of the mean modeled and observed SO$_4{}^{2-}$(p) at the measurement sites in Table A15.

Table A16. Evaluation of MATCH-SALSA calculated particulate nitrate, $NO_3^-(p)$, against observed (daily mean) concentrations in 2007 at regional background (EMEP) sites in Europe

| Station	Obs	Mod	%bias	R	#Days
NO55	0.055	0.056	2	0.08	353
NO15	0.056	0.08	43	0.23	342
NO39	0.044	0.075	70	0.08	350
NO01	0.127	0.141	11	0.52	357
LV16	0.06	0.192	220	0.33	350
LV10	0.088	0.252	186	0.41	357
IE06	0.287	0.271	-6	0.29	349
DE01	0.76	0.41	-46	0.71	353
PL04	0.414	0.28	-32	0.59	364
DE09	0.64	0.375	-41	0.69	351
NL09	0.693	0.468	-32	0.65	331
DE07	0.489	0.364	-26	0.68	364
IE05	0.406	0.278	-32	0.27	349
IE08	0.455	0.569	25	0.21	365
NL08	0.843	0.718	-15	0.82	183
PL02	0.655	0.317	-52	0.67	361
NL10	0.97	0.574	-41	0.60	257
SK04	0.304	0.183	-40	0.74	56
SK06	0.32	0.271	-15	0.23	357
AT02	0.188	0.367	95	0.55	365
CH05	0.516	0.426	-17	0.69	26
HU02	0.39	0.387	-1	0.42	353
IT01	0.826	0.451	-45	0.37	356
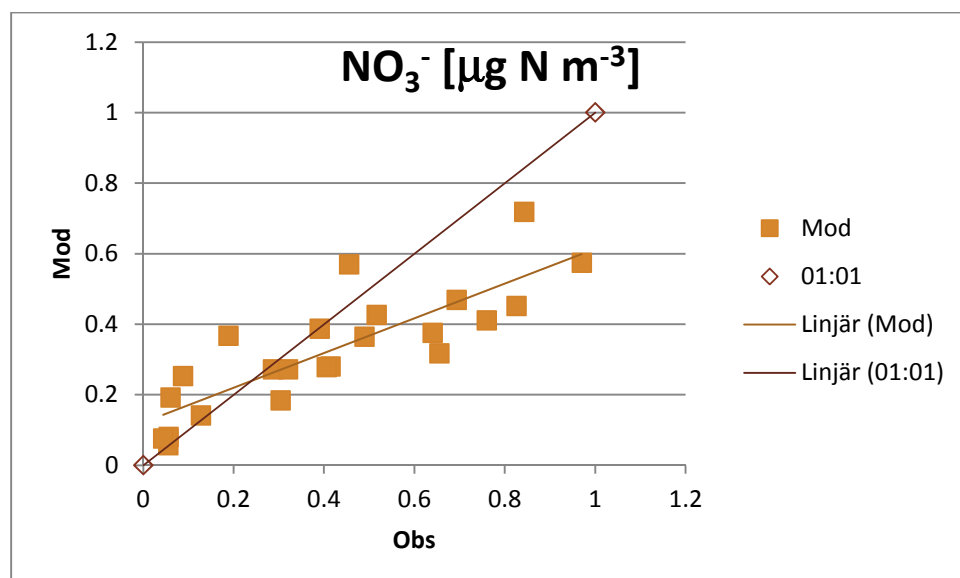
Figure A33. Scatter plot of the mean modeled and observed $NO_3^-(p)$ at the measurement sites in Table A16.

Table A17. Evaluation of MATCH-SALSA calculated total nitrate, $HNO_3(g)+NO_3^-(p)$, against observed (daily mean) concentrations in 2007 at regional background (EMEP) sites in Europe

Station	Obs	Mod	%bias	R	#Days
NO55	0.084	0.063	-25	0.13	351
FI36	0.041	0.062	51	0.51	326
FI22	0.049	0.084	71	0.22	50
NO15	0.091	0.092	1	0.32	342
SE05	0.042	0.083	98	0.49	342
NO39	0.064	0.094	47	0.13	350
FI37	0.15	0.176	17	0.07	49
FI17	0.216	0.212	-2	0.73	342
FI09	0.207	0.307	48	0.73	340
NO01	0.17	0.249	46	0.56	357
SE14	0.497	0.397	-20	0.73	361
LV16	0.304	0.27	-11	0.54	350
DK08	0.66	0.465	-30	0.72	351
DK03	0.67	0.455	-32	0.77	353
DK31	0.686	0.464	-32	0.78	351
LV10	1.229	0.593	-52	0.85	7
SE11	0.486	0.46	-5	0.71	357
LT15	0.587	0.411	-30	0.76	346
DE01	0.923	0.618	-33	0.74	353
PL04	0.538	0.467	-13	0.66	364
DK05	0.906	0.54	-40	0.71	315
DE09	0.849	0.561	-34	0.72	351
PL05	0.677	0.413	-39	0.54	343
DE07	0.683	0.537	-21	0.70	364
IE01	0.293	0.279	-5	0.64	364
PL02	0.818	0.446	-45	0.65	361
CH05	0.808	0.532	-34	0.78	362
SI08	0.291	0.579	99	0.27	310
FR13	0.645	0.446	-31	0.63	103
ES16	0.573	0.468	-18	0.69	343
ES10	0.687	0.666	-3	0.65	361
ES14	0.623	0.675	8	0.59	360
ES13	0.633	0.415	-34	0.34	357
ES12	0.495	0.563	14	0.59	351
ES11	0.506	0.463	-8	0.60	352

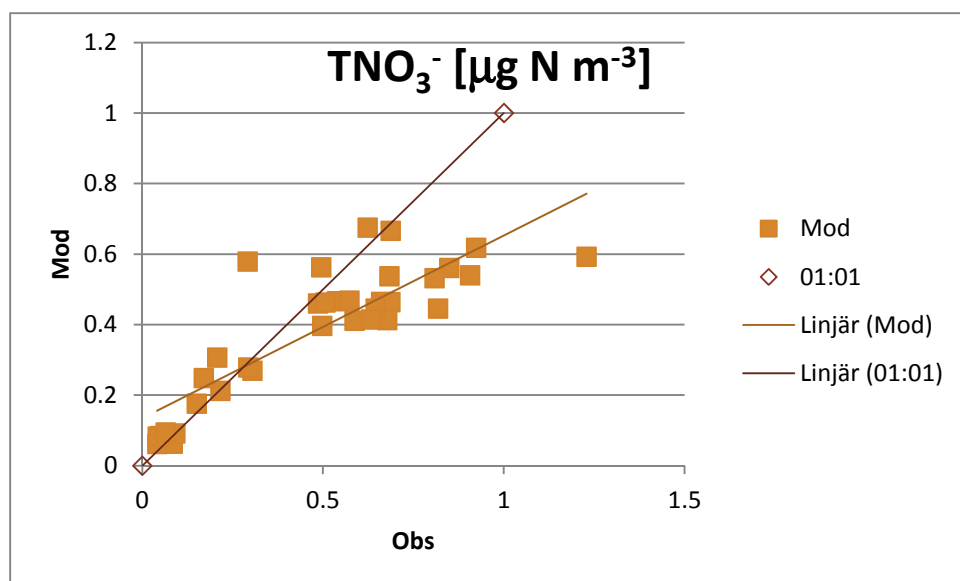**Figure A34. Scatter plot of the mean modeled and observed total nitrate = $HNO_3(g)+NO_3^-(p)$ at the measurement sites in Table A17.**

Table A18. Evaluation of MATCH-SALSA calculated particulate ammonium, $NH_4^+(p)$, against observed (daily mean) concentrations in 2007 at regional background (EMEP) sites in Europe

| Station	Obs	Mod	%bias	R	#Days
NO55	0.106	0.044	-58	0.44	351
FI36	0.087	0.066	-24	0.49	341
FI22	0.104	0.08	-23	0.31	52
NO15	0.076	0.061	-20	0.43	349
NO39	0.057	0.087	53	0.26	350
FI17	0.302	0.264	-13	0.72	363
FI09	0.187	0.19	2	0.69	339
LV16	0.616	0.417	-32	0.40	351
DK08	0.836	0.471	-44	0.80	355
DK03	0.98	0.615	-37	0.75	357
DK31	0.945	0.579	-39	0.82	352
LV10	0.525	0.536	2	0.45	354
IE06	0.728	0.424	-42	0.12	352
DE01	0.76	0.686	-10	0.76	352
RU18	0.39	0.722	85	0.44	355
PL04	0.9	0.656	-27	0.67	364
DK05	1.246	0.727	-42	0.74	314
DE09	0.706	0.771	9	0.76	350
NL09	1.08	0.866	-20	0.67	330
DE07	0.712	0.85	19	0.80	364
IE05	0.887	0.404	-54	0.22	352
IE08	0.74	1.029	39	0.25	362
NL08	1.352	1.232	-9	0.86	186
PL02	1.556	1.107	-29	0.59	348
NL10	1.464	1.135	-22	0.53	266
SK04	0.77	0.92	19	0.49	237
SK06	0.8	1.083	35	0.35	183
AT02	0.738	1.105	50	0.75	365
CH05	0.659	0.68	3	0.64	26
HU02	0.85	1.286	51	0.73	352
IT01	1.255	0.897	-29	0.62	356
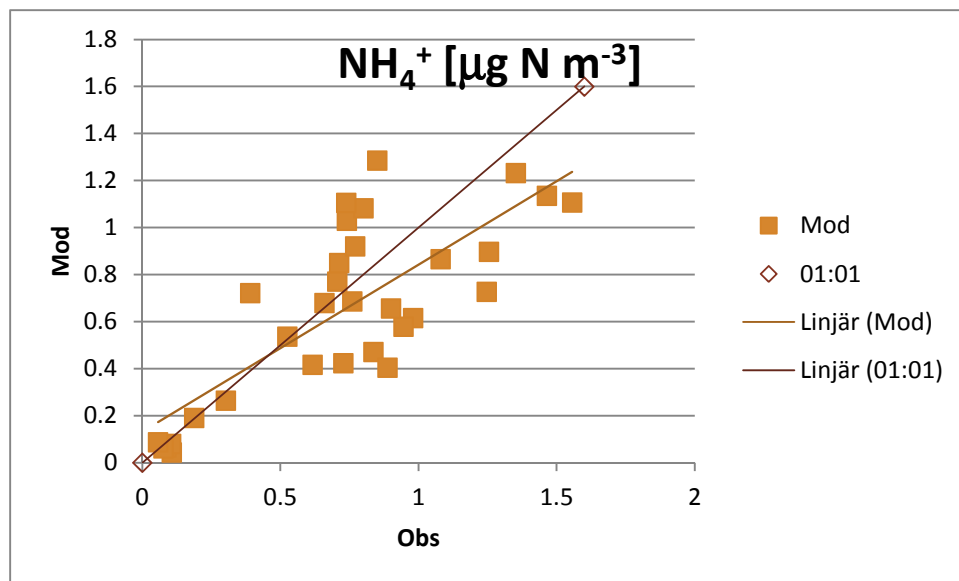
Figure A35. Scatter plot of the mean modeled and observed NH$_4^+$(p) at the measurement sites in Table A18.

Table A19. Evaluation of MATCH-SALSA calculated total reduced nitrogen, $NH_3(g)+NH_4^+(p)$, against observed (daily mean) concentrations in 2007 at regional background (EMEP) sites in Europe

| Station	Obs	Mod	%bias	R	#Days
NO55	0.539	0.057	-89	0.19	351
FI36	0.101	0.092	-9	0.47	347
FI22	0.128	0.092	-28	0.26	52
NO15	0.939	0.075	-92	0.13	348
SE05	0.162	0.085	-48	0.54	349
NO39	0.762	0.129	-83	0.36	350
FI37	0.278	0.23	-17	0.41	52
FI17	0.403	0.317	-21	0.68	363
FI09	0.242	0.221	-9	0.68	337
NO01	0.427	0.274	-36	0.65	347
SE14	0.698	0.629	-10	0.72	362
LV16	0.924	0.545	-41	0.45	351
LV10	1.033	0.843	-18	0.50	356
SE11	0.984	1.121	14	0.51	357
LT15	1.661	1.069	-36	0.64	346
DE01	2.011	1.311	-35	0.74	352
PL04	1.285	0.918	-29	0.73	364
DE09	1.757	1.415	-19	0.68	350
PL05	1.023	1.433	40	0.56	344
DE07	1.554	1.599	3	0.63	362
IE01	1.061	0.786	-26	0.67	364
PL02	2.977	1.877	-37	0.48	348
FR09	2.073	1.763	-15	0.76	96
CH05	1.912	2.35	23	0.73	362
SI08	0.987	1.703	73	0.32	311
FR13	1.901	1.554	-18	0.52	102
ES16	1.938	1.536	-21	0.60	356
ES10	1.408	0.723	-49	0.46	359
ES14	4.123	2.891	-30	0.49	345
ES13	1.202	1.472	22	0.57	358
ES12	1.536	1.163	-24	0.32	335
ES11	1.891	1.501	-21	0.39	361
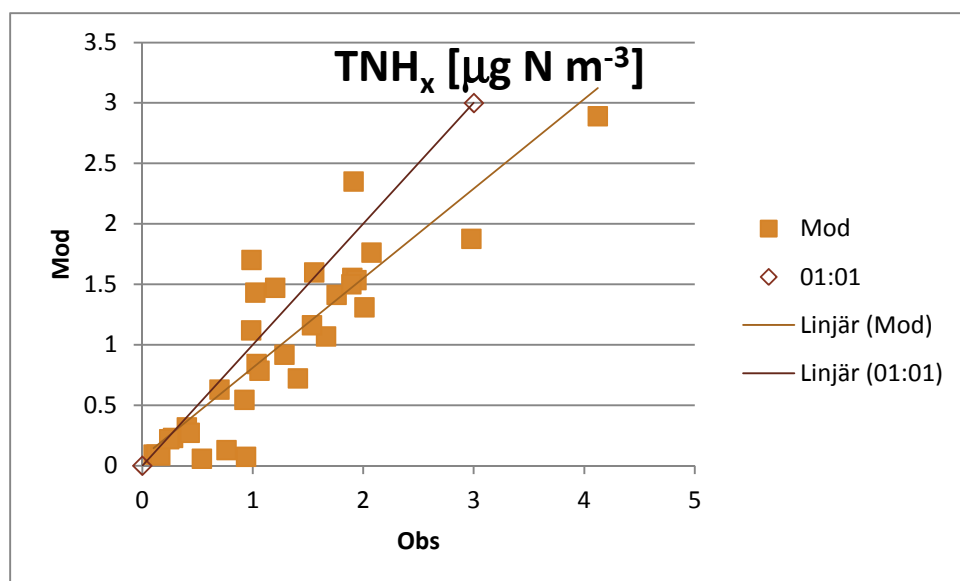
Figure A36. Scatter plot of the mean modeled and observed $NH_3(g)+NH_4^+(p)$ at the measurement sites in Table A19.

Table A20. Statistics from evaluation of the MATCH-SALSA simulated concentrations to daily observed EC and OC in PM$_1$, PM$_{2.5}$ and PM$_{10}$ for the year 2007. Percentage is given in relation to observed average. The spatial correlation is omitted for EC and OC due to the low number of stations.

		EC							OC						
	Stations[h]	Obs µg m^{-3}	Mod µg m^{-3}	bias (%)	MAE µg m^{-3}	MAE (%)	R	#meas	Obs µg m^{-3}	Mod µg m^{-3}	bias (%)	MAE µg m^{-3}	MAE (%)	R	#meas
In PM$_1$ winter	Melpitz	0.54	0.21	-60	0.33	60	0.60	32	0.65	0.76	18	0.23	36	0.83	32
In PM$_{2.5}$ winter	Birkenes	0.12	0.18	47	0.11	87	0.58	73	0.60	0.88	46	0.46	76	0.45	73
	Overtoom	0.75	0.54	-27	0.27	36	0.76	27	2.19	1.15	-48	1.25	57	0.59	28
	Melpitz	1.28	0.29	-77	0.99	77	0.60	182	1.81	1.21	-33	0.95	52	0.59	182
	Payerne	1.45	0.39	-73	1.06	73	0.67	23	5.61	1.33	-76	4.28	76	0.52	23
	Ispra	3.67	0.93	-75	2.76	75	0.28	173	14.1	2.04	-86	12.1	86	0.24	173
	Puy de Dome	0.05	0.36	556	0.31	556	0.43	33	0.99	1.35	36	0.46	46	0.60	21
	Montelibretti	1.10	0.40	-64	0.70	64	0.60	32	17.2	1.22	-93	16.0	93	0.53	32
	Montseny	0.17	0.49	181	0.32	181	0.60	17	1.64	1.74	6	0.48	29	0.68	17
	Campisabalos	0.16	0.27	65	0.10	65	-	9	1.73	1.01	-42	0.72	42	-	9
In PM$_{10}$ winter	Birkenes	0.14	0.19	38	0.10	75	0.62	73	0.76	0.92	22	0.48	63	0.43	73
	Harwell	1.06	0.93	-11	0.68	64	0.50	56	3.23	1.67	-48	1.65	51	0.70	56
	Melpitz	1.65	0.32	-80	1.33	80	0.63	182	2.77	1.40	-49	1.48	53	0.56	182
	Kosetice	0.36	0.25	-30	0.13	37	0.42	30	1.96	0.86	-56	1.13	58	0.62	30
	Montelibretti	1.30	0.44	-66	0.86	66	0.47	31	15.5	1.29	-92	14.2	92	0.65	31
	Montseny	0.21	0.51	143	0.30	143	0.73	17	1.61	2.03	26	0.57	35	0.80	17
	Campisabalos	0.17	0.29	71	0.12	71	-	8	1.92	1.25	-35	0.69	36	-	8
In PM$_{2.5}$ summer	Birkenes	0.09	0.11	27	0.03	40	0.81	51	0.74	0.85	14	0.31	42	0.73	51
	Overtoom	0.57	0.37	-36	0.24	42	0.34	37	1.66	1.17	-29	0.62	38	0.76	37
	Melpitz	0.95	0.17	-82	0.78	82	0.54	183	1.26	1.78	41	0.83	66	0.47	183
	Ispra	0.87	0.68	-21	0.35	40	0.48	165	3.80	2.54	-33	1.91	50	0.34	169
	Puy de Dome	0.09	0.26	171	0.18	192	0.09	33	2.18	2.05	-6	1.57	72	-0.08	11

[h] Station codes and countries are given in Table 5.

	Montseny	0.17	0.47	172	0.29	172	0.60	21	1.82	2.72	49	0.91	50	0.60	21
	Campisabalos	0.10	0.14	46	0.05	53	-	5	2.24	1.33	-41	1.28	57	-	5
In PM$_{10}$ summer	Birkenes	0.11	0.12	10	0.04	37	0.76	52	1.04	0.90	-13	0.27	26	0.81	52
	Melpitz	1.60	0.19	-88	1.41	88	0.59	183	2.58	1.93	-25	0.87	34	0.51	183
	Montseny	0.19	0.49	162	0.30	162	0.51	21	1.66	2.89	74	1.23	74	0.62	21
	Campisabalos	0.15	0.14	-9	0.08	52	-	10	2.26	1.48	-35	1.13	50	-	9
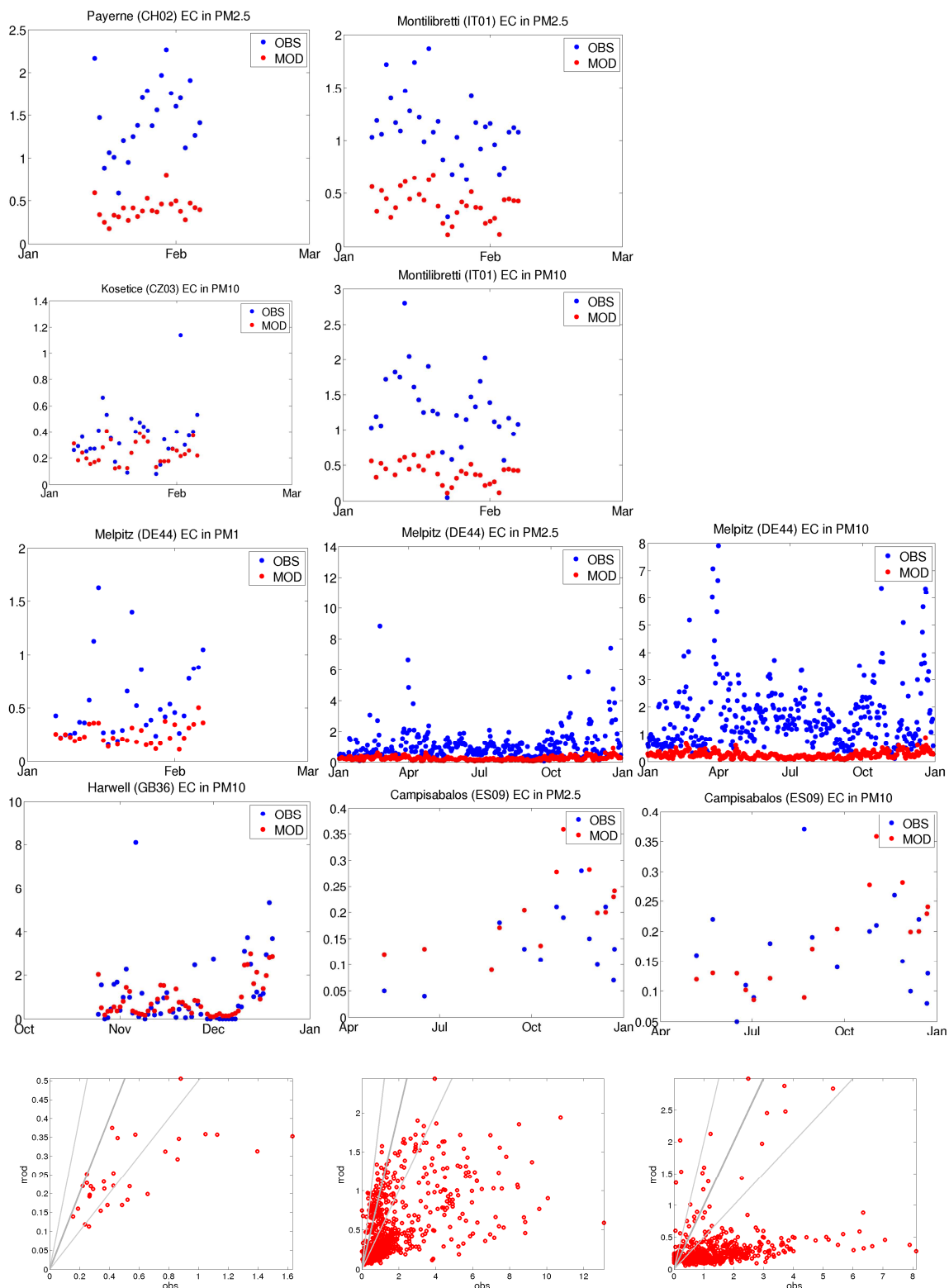
Figure A37. Observed and modeled time series for EC in PM₁, PM₂.₅ and PM₁₀ at measurement stations during 2007. Top row: EC in PM₂.₅ at Montelibretti, second row: EC in PM₁₀ at Kosetice and Montelibretti, third row: EC in PM₁, PM₂.₅ and PM₁₀ at Melpitz. Fourth row: EC in PM₁₀ at Harwell and EC in PM₂.₅ and PM₁₀ at Campisabalos . Bottom row: Scatter of observed and modeled diurnal averages of EC in PM₁ (left) PM₂.₅ (middle) and PM₁₀ (right) in 2007 (also includes Ispra; see Figure 15 for a time series plot for Ispra).
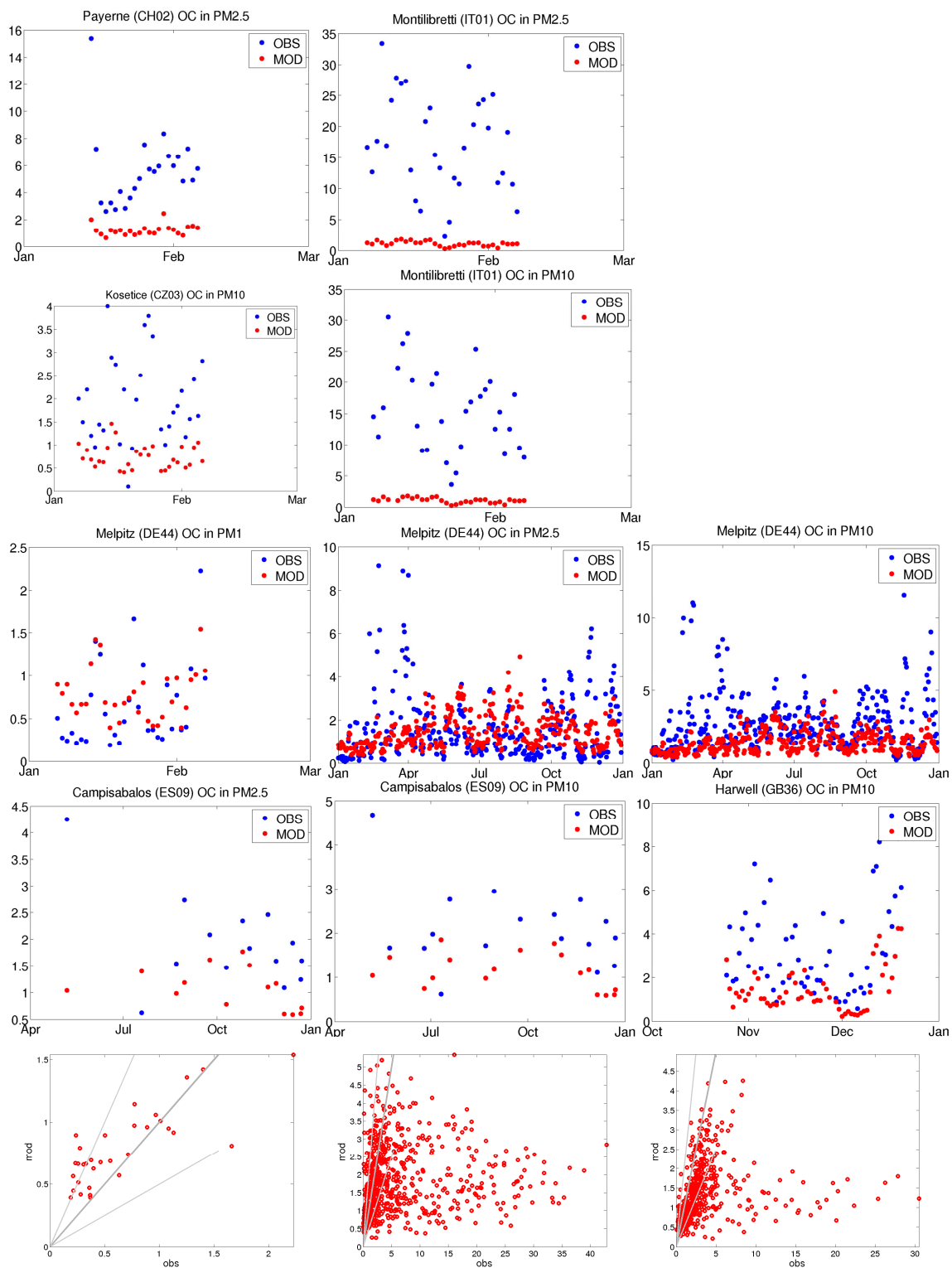
Figure A38. Top row: Observed and modeled diurnal average OC in PM₁, PM₂.₅ and PM₁₀ at measurement stations during 2007. Top row: OC in PM₂.₅ at Payerne and Montelibretti, second row: OC in PM₁₀ at Kosetice and Montelibretti, third row: OC in PM₁, PM₂.₅ and PM₁₀ at Melpitz. Fourth row: OC in PM₂.₅ at Campisabalos and OC in PM₁₀ at Campisabalos and Harwell. Bottom row: Scatter of observed and modeled diurnal averages of OC in PM₁ (left) PM₂.₅ (middle) and PM₁₀ (right) in 2007 (also includes Ispra; see Figure 15 for a time series plot for Ispra).

Table A21. Statistics from evaluation of daily mean modeled and observed PM$_1$ and PM$_{2.5}$ for the year 2007. Percentages are given in relation to observed mean. The rightmost three columns represent evaluation of modeled PM$_1$ and PM$_{2.5}$, excluding sea salt aerosol[i], versus measured PM$_1$ and PM$_{2.5}$.

			height		obs	mod	%bias	R	CV(RMSE) %	#days/ #stns	%bias	R	CV(RMSE) %
					PM$_1$ / PM$_{2.5}$ evaluation						**No sea salt mass in modeled PM$_1$ or PM$_{2.5}$**		
Spatial				PM$_{2.5}$	11.2	9.7	-14	0.64	38	27	-34	0.67	48
Austria	Illmitz	AT02	117	PM$_1$	11.4	9.6	-16	0.41	68	352	-16	0.41	68
				PM$_{2.5}$	16.2	11.1	-31	0.62	71	358	-36	0.63	73
Switzerland	Payerne	CH02	489	PM$_1$	9.3	6.2	-33	0.17	76	353	-41	0.35	78
				PM$_{2.5}$	12.5	8.8	-29	0.47	81	363	-39	0.57	82
	Rigi	CH05	1031	PM$_1$	6.1	5.9	-3	0.37	63	337	-11	0.45	63
				PM$_{2.5}$	8.0	8.2	3	0.60	67	344	-8	0.66	66
Czech Rep.	Kosetice	CZ03	534	PM$_{2.5}$	14.7	9.0	-39	0.04	79	198	-46	0.06	82
Germany	Waldhof	DE02	74	PM$_1$	6.5	8.0	23	0.07	89	330	-6	0.36	82
				PM$_{2.5}$	11.3	11.2	-1	0.20	79	328	-28	0.50	77
	Schauinsland	DE03	1205	PM$_{2.5}$	6.8	9.9	46	0.36	87	309	25	0.49	78
	Melpitz	DE44	86	PM$_1$	7.7	8.7	12	0.29	56	32	-23	0.18	69
				PM$_{2.5}$	17.3	10.3	-40	0.40	74	326	-51	0.58	77
Denmark	Lille Valby	DK41	10	PM$_1$	4.1	13.3	222	-0.15	207	29	41	0.27	56
				PM$_{2.5}$	12.6	11.8	-6	0.12	78	327	-36	0.00	88
Spain	Víznar	ES07	1265	PM$_{2.5}$	10.8	8.4	-22	0.29	63	340	-31	0.26	68
	Niembro	ES08	134	PM$_{2.5}$	11.7	9.0	-23	0.42	67	323	-38	0.51	72
	Campisabalos	ES09	1360	PM$_{2.5}$	6.9	6.0	-12	0.24	81	125	-25	0.33	82
	Cabo de Creus	ES10	23	PM$_{2.5}$	10.0	9.0	-10	0.55	49	333	-48	0.70	68
	Barcarrola	ES11	393	PM$_{2.5}$	8.2	8.6	4	0.42	56	339	-12	0.49	59
	Zarra	ES12	885	PM$_{2.5}$	8.8	8.2	-7	0.55	48	328	-21	0.59	54
	Paenausende	ES13	985	PM$_{2.5}$	6.4	7.2	11	0.32	62	340	-3	0.41	61

---

[i] Sea salt was included in the model simulation, but not included in the added mass of PM1 or PM2.5, thus some indirect effects of sea salt are still affecting the results.

Country	Site	Code	Alt	PM									
	Els torms	ES14	470	PM$_{2.5}$	12.3	9.9	-19	0.55	56	327	-30	0.61	61
	Risco Llamo	ES15	1241	PM$_{2.5}$	7.0	7.1	1	0.39	54	147	-10	0.48	55
	O Saviñao	ES16	506	PM$_{2.5}$	8.0	12.8	61	0.37	86	324	26	0.50	77
Finland	Virolahti II	FI17	4	PM$_1$	2.1	5.2	141	-0.15	169	28	94	-0.06	138
				PM$_{2.5}$	4.5	6.8	51	-0.08	122	30	-5	0.47	82
UK	Harwell	GB36	137	PM$_{2.5}$	19.0	12.4	-35	0.32	75	261	-61	0.55	86
	Auchencorth Moss	GB48	260	PM$_{2.5}$	7.6	13.0	71	0.02	142	326	-59	0.30	111
Ireland	Mace Head	IE31	15	PM$_{2.5}$	9.6	8.2	-14	0.35	65	294	-64	0.40	87
Italy	Montelibretti	IT01	48	PM$_{2.5}$	21.9	11.4	-48	0.04	75	334	-58	0.20	80
	Ispra	IT04	209	PM$_{2.5}$	25.8	15.1	-41	0.25	97	321	-43	0.26	98
Norway	Birkenes	NO01	175	PM$_1$	2.6	6.3	140	-0.01	187	120	16	0.25	92
Sweden	Vavihill	SE11	175	PM$_{2.5}$	8.8	10.0	13	0.14	68	100	-23	0.46	65
	Aspvreten	SE12	20	PM$_{2.5}$	6.7	5.7	-16	0.09	87	356	-46	0.43	88
Slovenia	Iskrba	SI08	520	PM$_{2.5}$	10.0	11.7	16	0.52	49	316	9	0.52	50
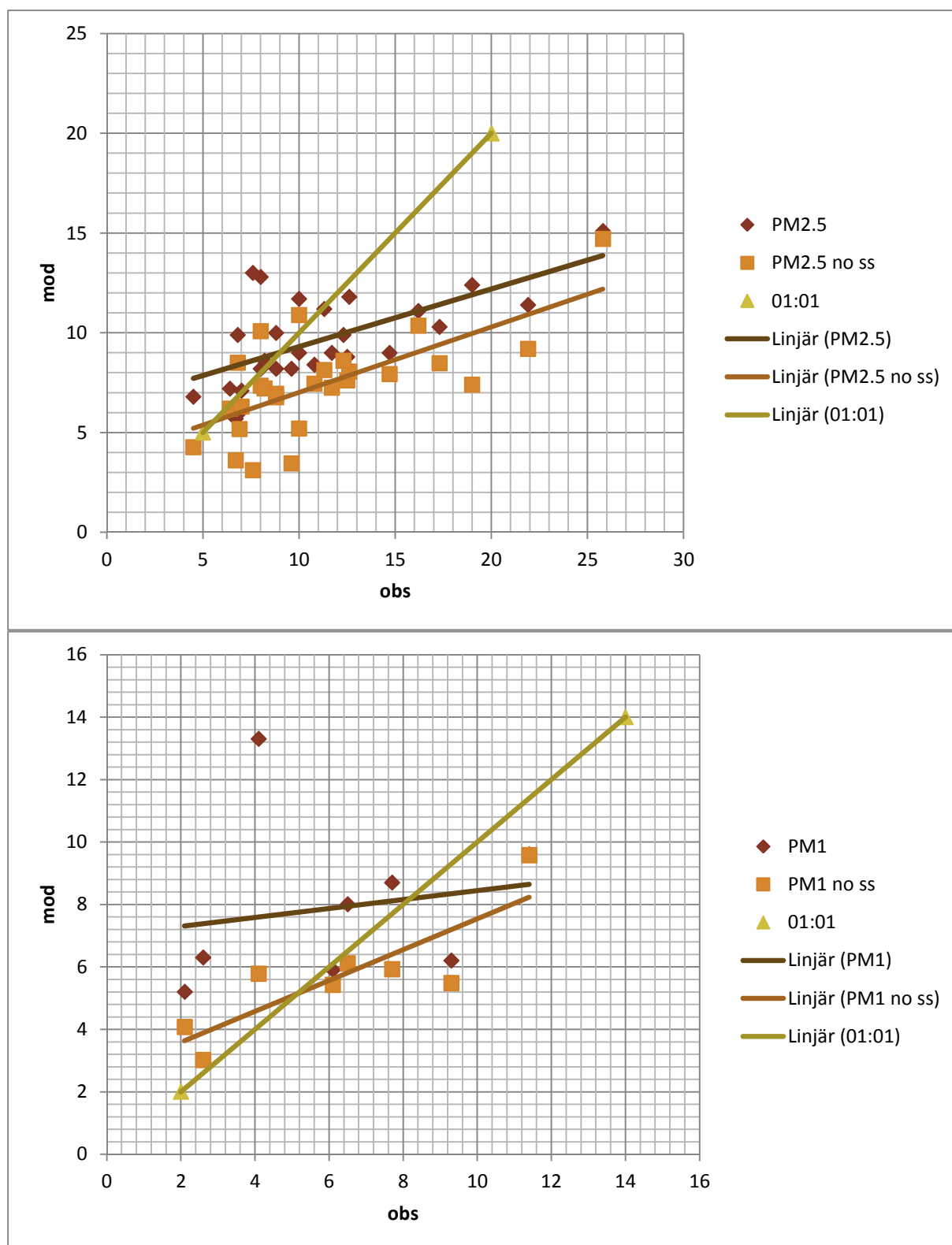
Figure A39. Scatter plots of mean modeled and observed PM₂.₅ (top) and PM₁ (bottom) as total and excluding sea salt mass at measurement sites in Europe (see Table A21).

PM1 DE44

PM2.5 DE44

DE44

PM1 DE02

DE02

PM2.5 DE02
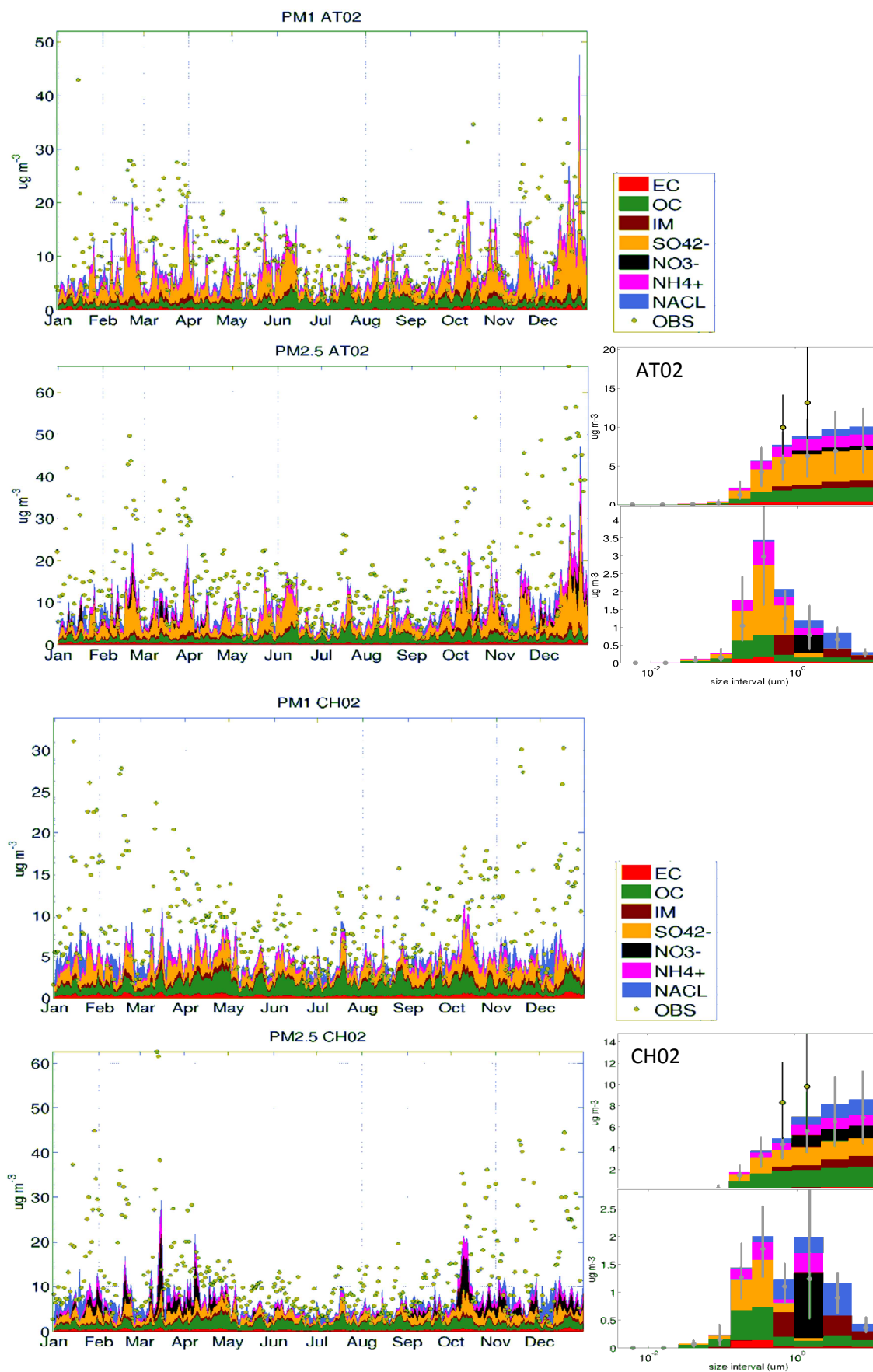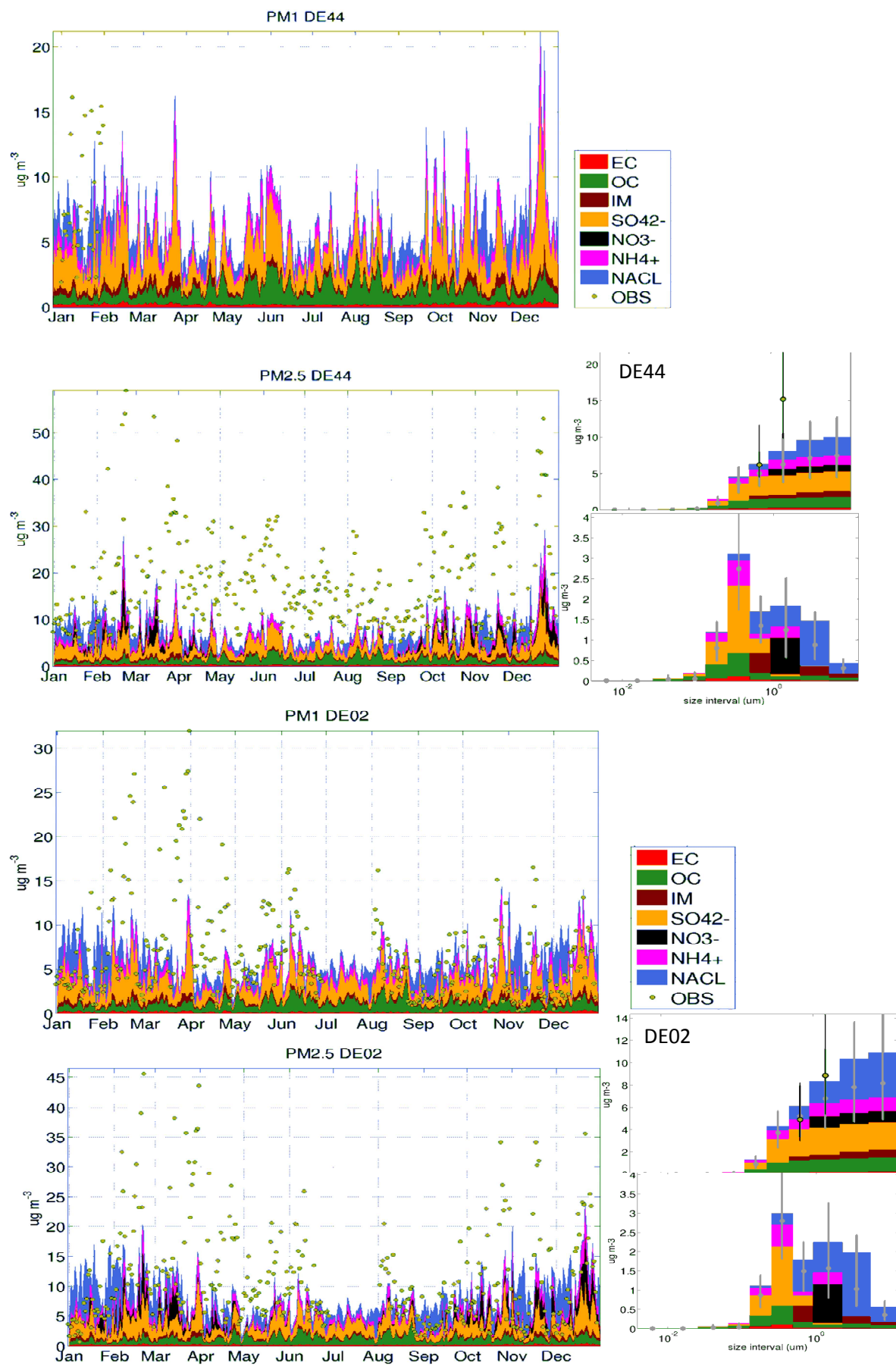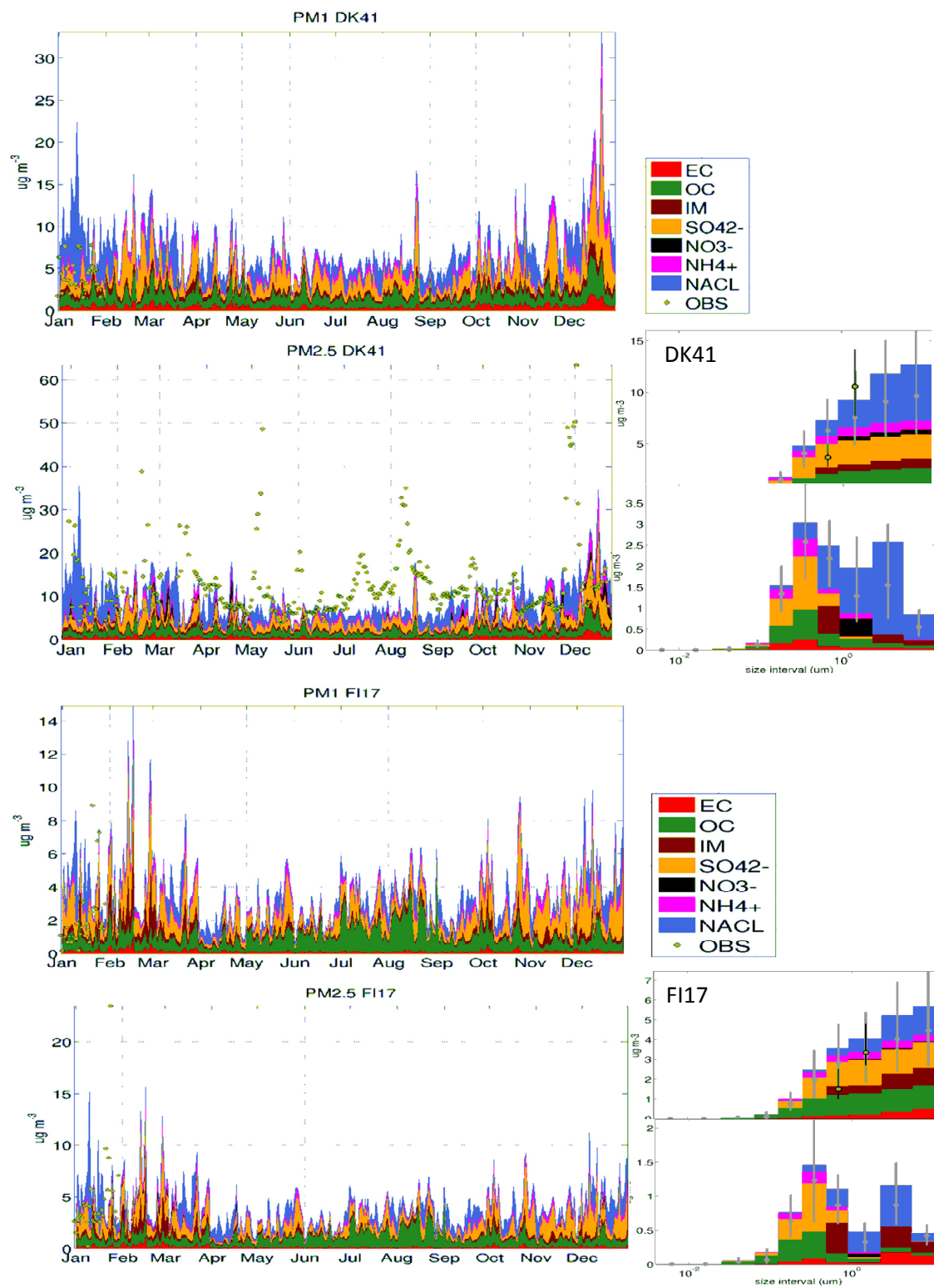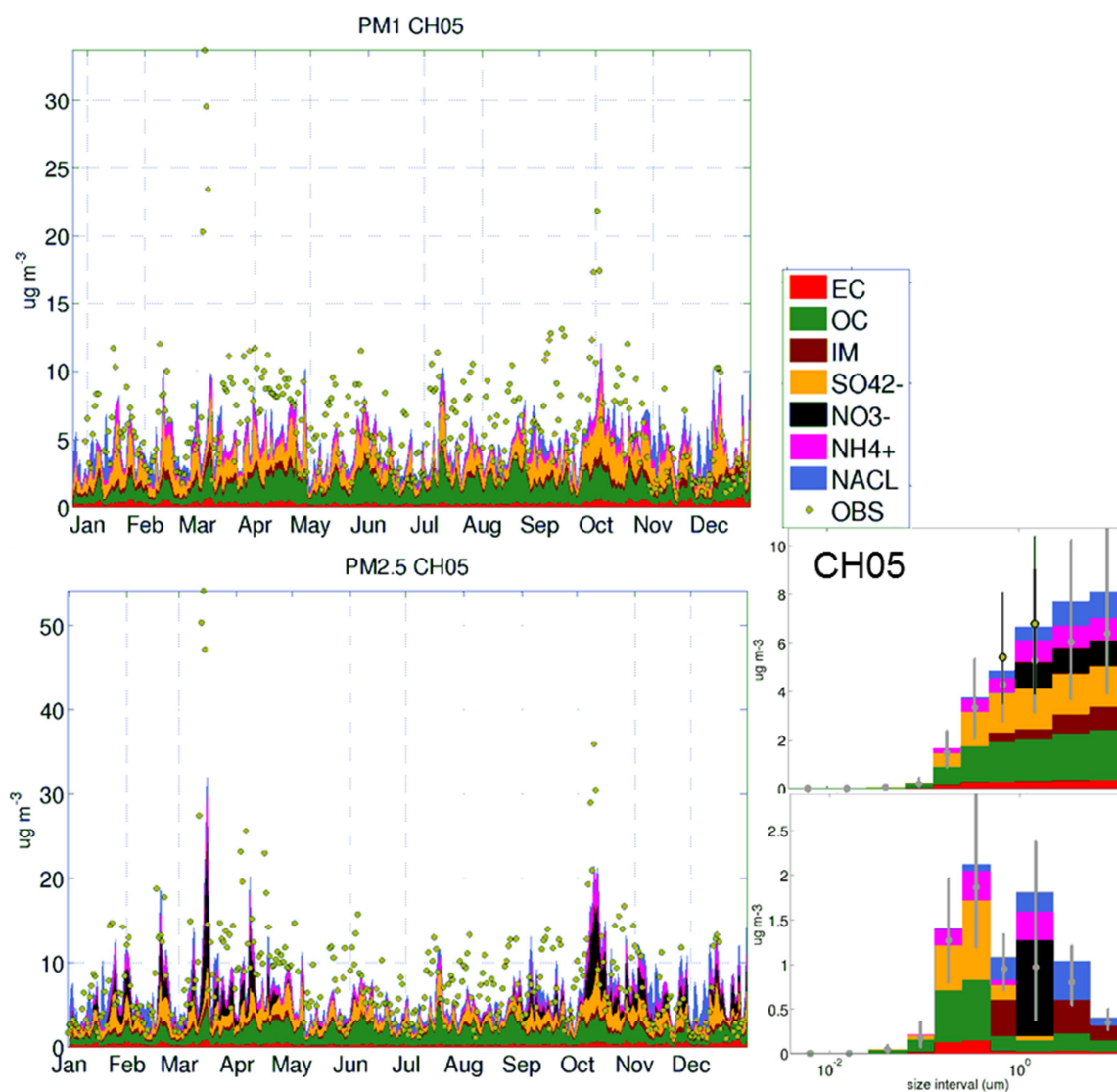
Figure A40. Modeled and observed PM₁ and PM₂.₅ at European measurement sites for 2007. Left: Observed (green dots) PM₁ and PM₂.₅ and modeled (surface plots) PM₁ (top) and PM₂.₅ (bottom) components (daily means). Right: Modeled annual mean PM component size distribution. Lower: mass per size bin; Upper: accumulated over size bins up to the higher end of an indicated interval. Modeled median and interquartile range (grey dots and error bars in right hand panels). Observed median and interquartile range for PM₁ and PM₂.₅ (green dot with black error bar in upper right panels). Colors, see legend.
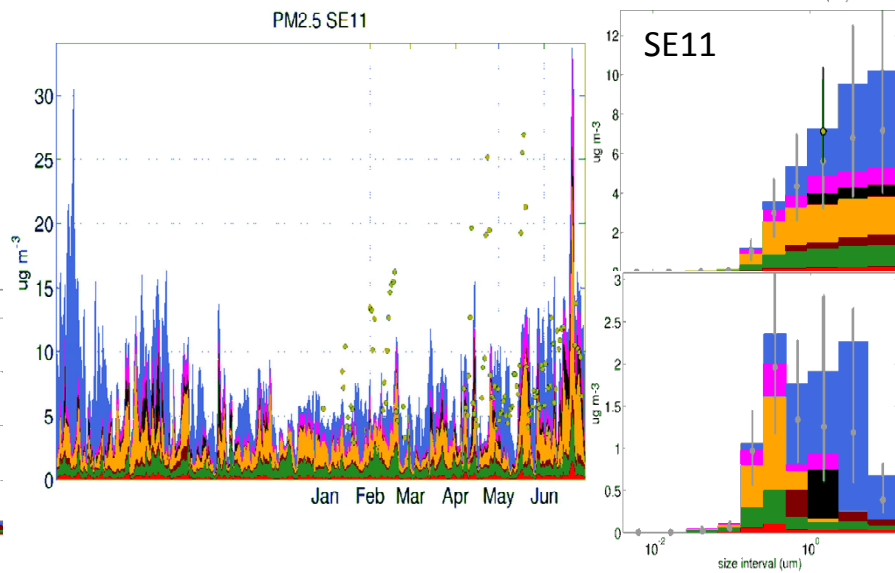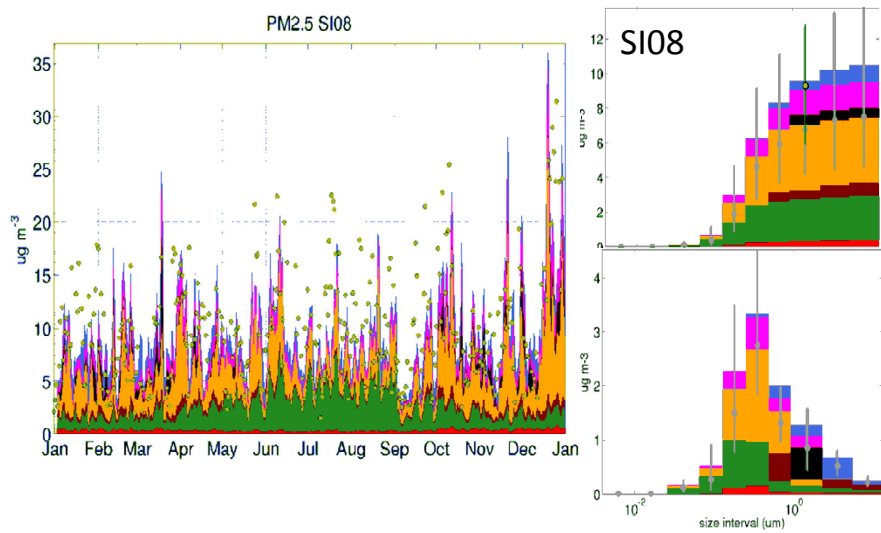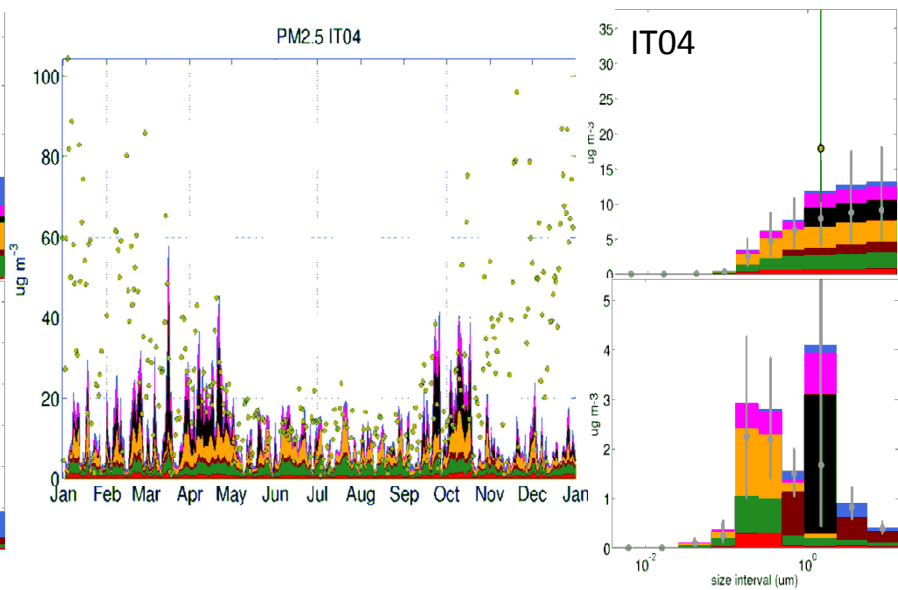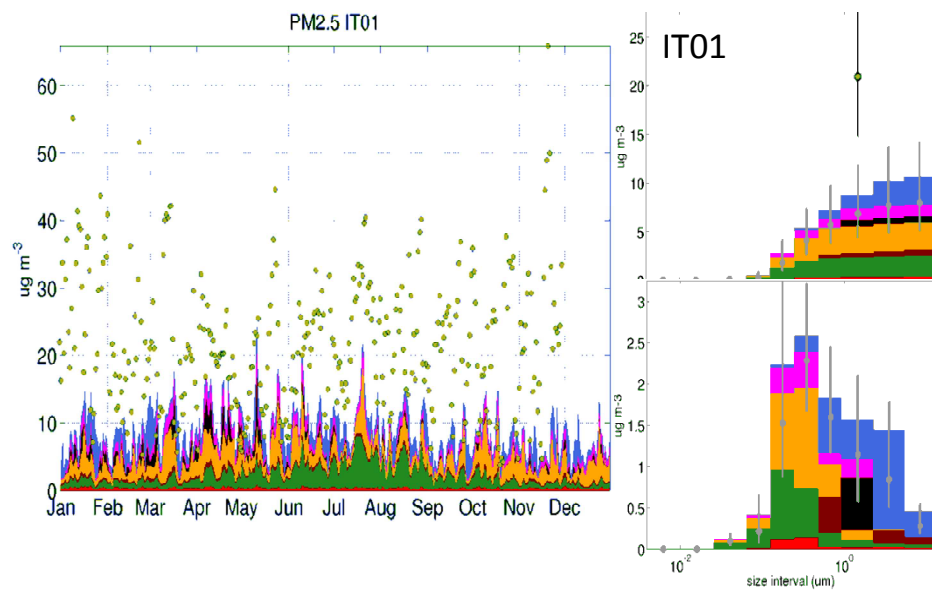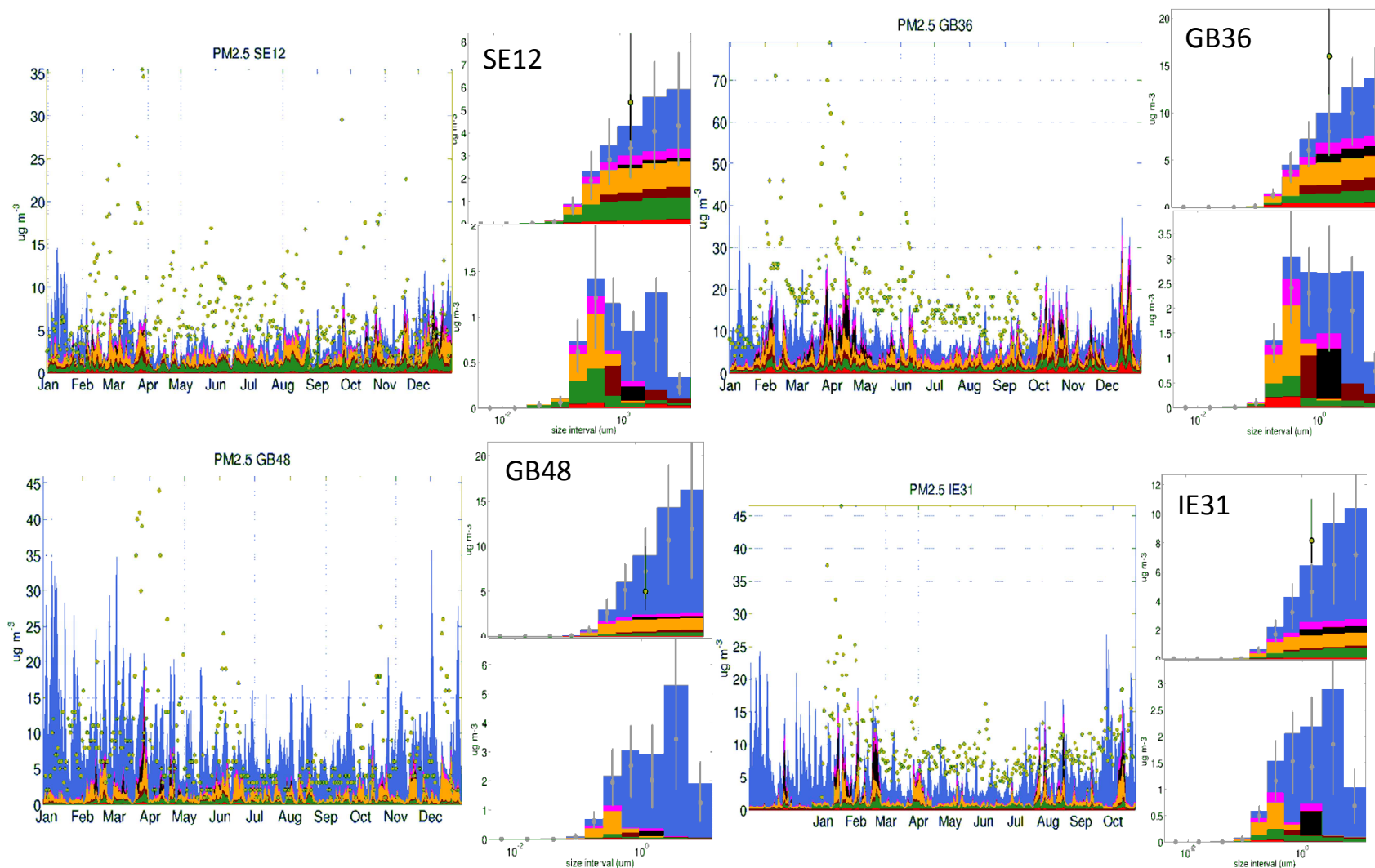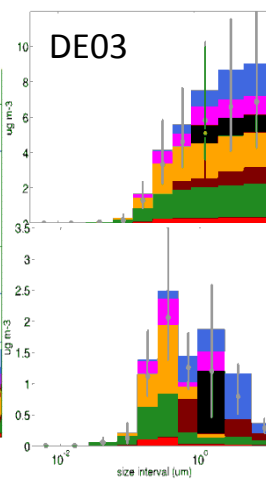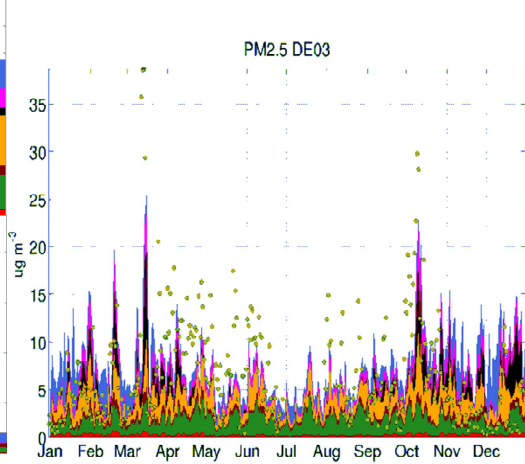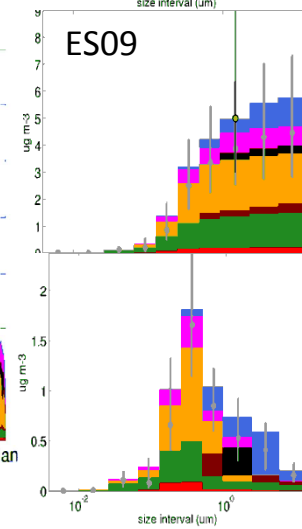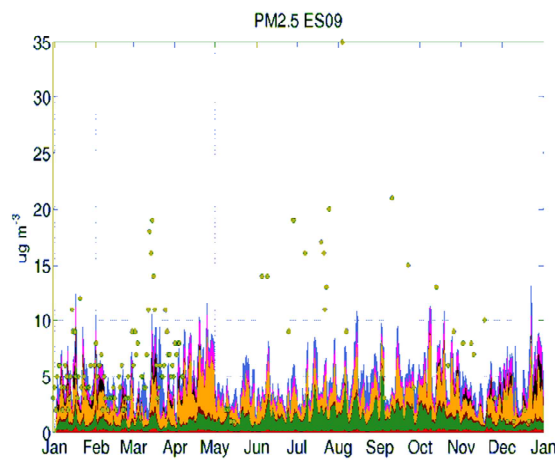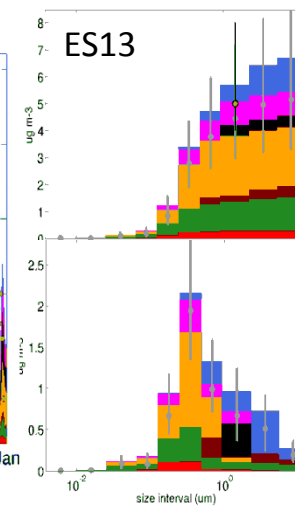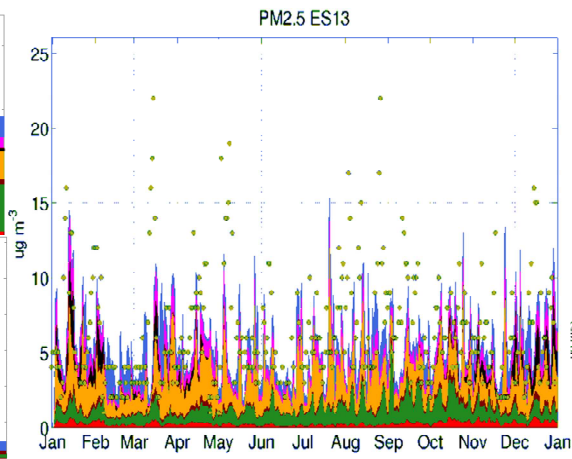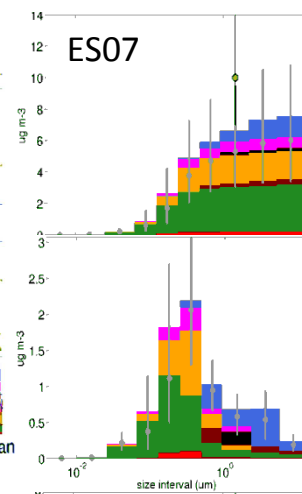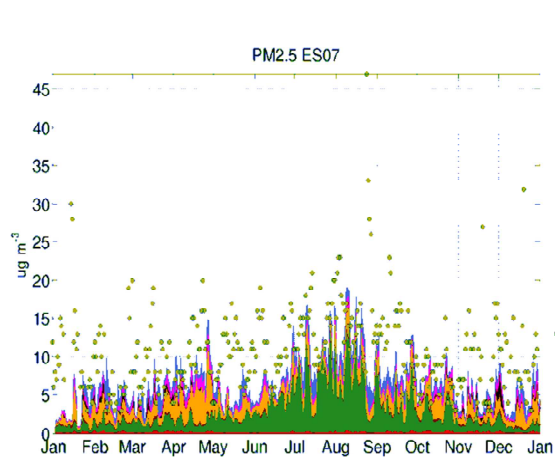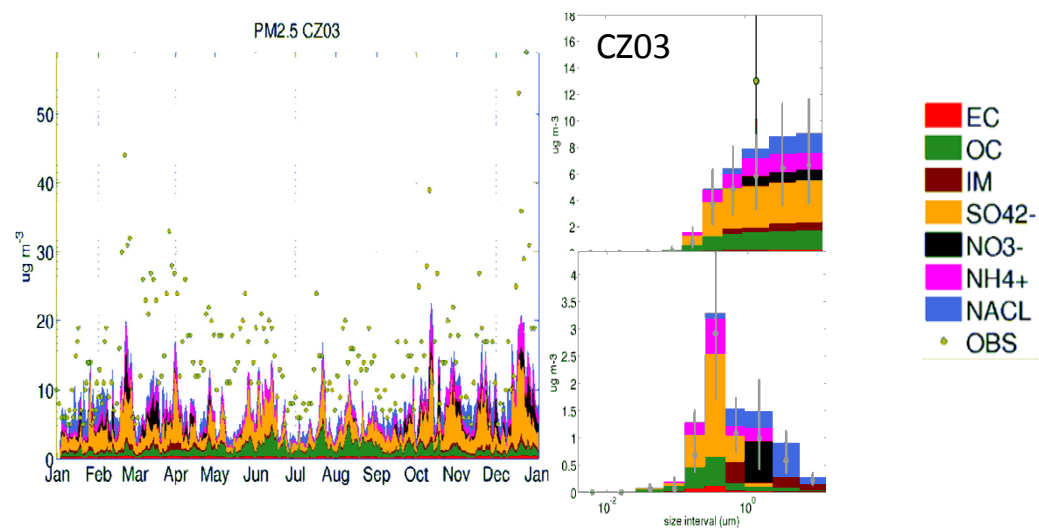
Figure A41. Modeled and observed PM$_{2.5}$ at European measurement sites for 2007. Large (left hand) panels: Observed (green dots) PM$_{2.5}$ and modeled (surface plots) PM$_{2.5}$ components (daily means). Smaller (right hand) panels: Modeled annual mean PM component size distribution. Lower, small: mass per size bin; Upper, small: accumulated over size bins up to the higher end of an indicated interval. Modeled median and interquartile range (grey dots and error bars in right hand panels). Observed median and interquartile range for PM$_{2.5}$ (green dot with black error bar in upper right panels). Colors, see legend (bottom right).
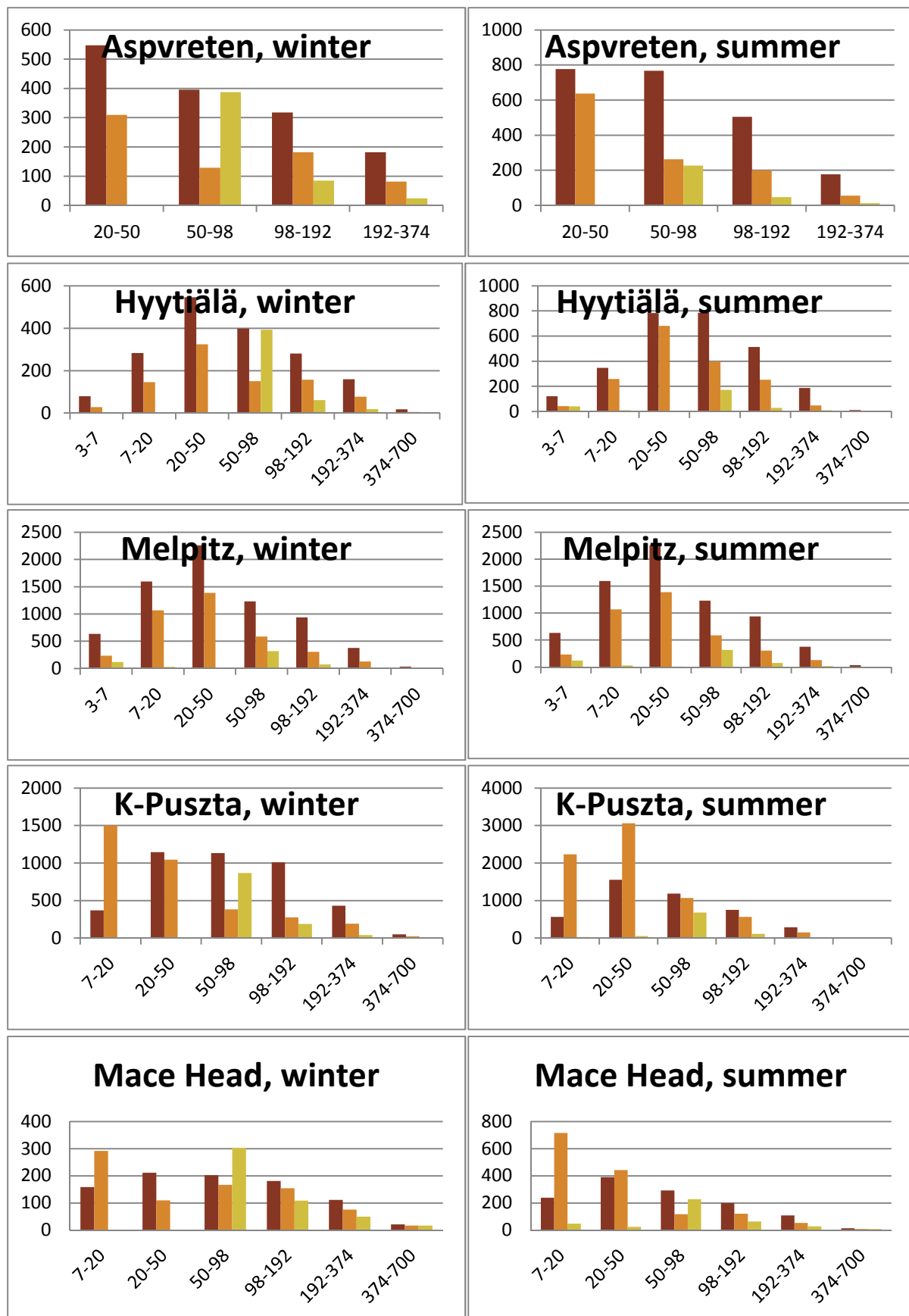
Figure A42. Particle number size distribution at five measurements sites in 2007. Left: winter half-year (Jan-Mar, Oct-Dec). Right: summer half-year (Apr-Sep). Measurements sites are from top to bottom: Aspvreten, Hyytiälä, Melpitz, K-Puszta, Mace Head. Observations are brown bars. Model versions are MATCH-SALSA (orange) and MATCH (yellow).
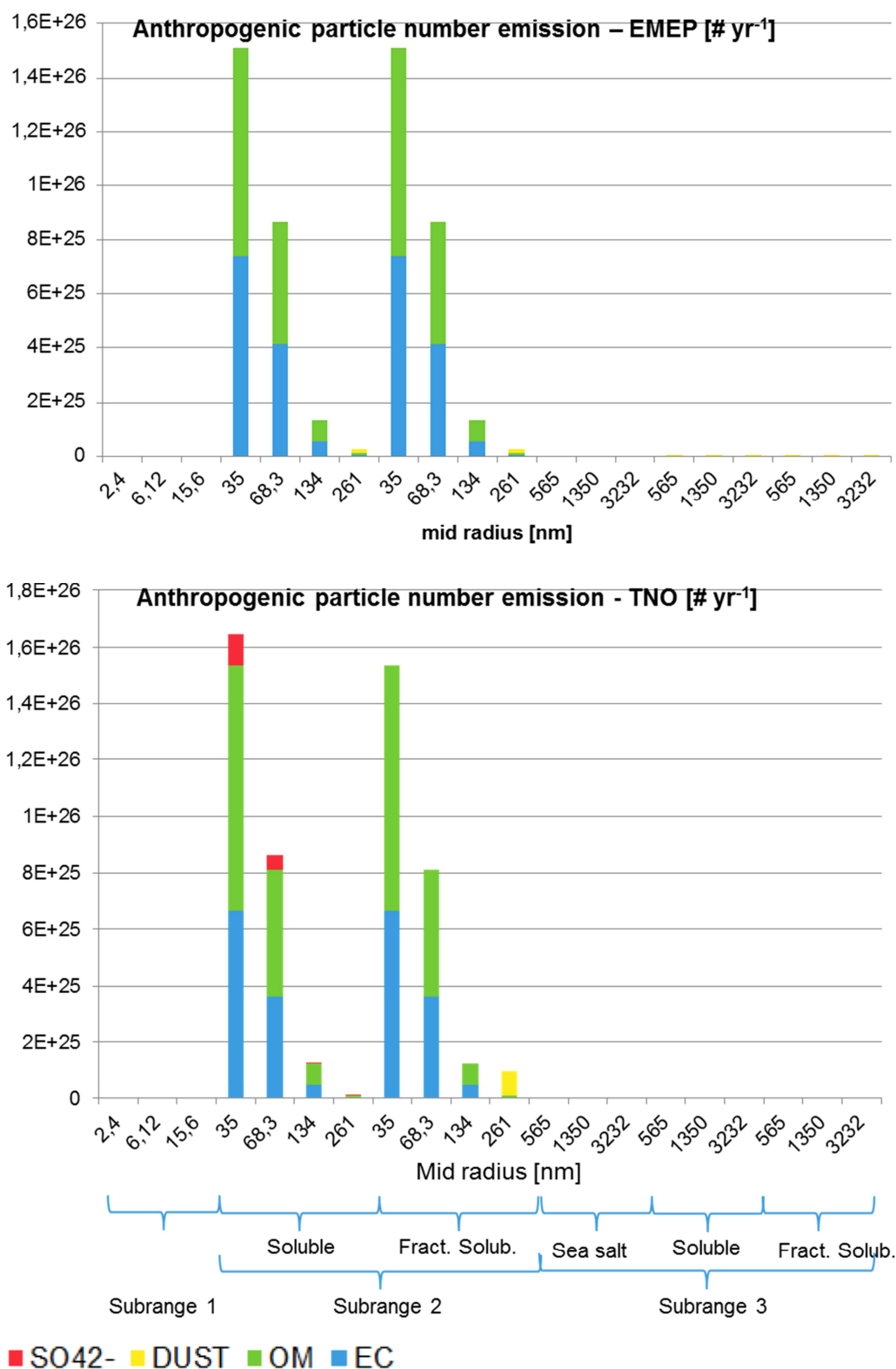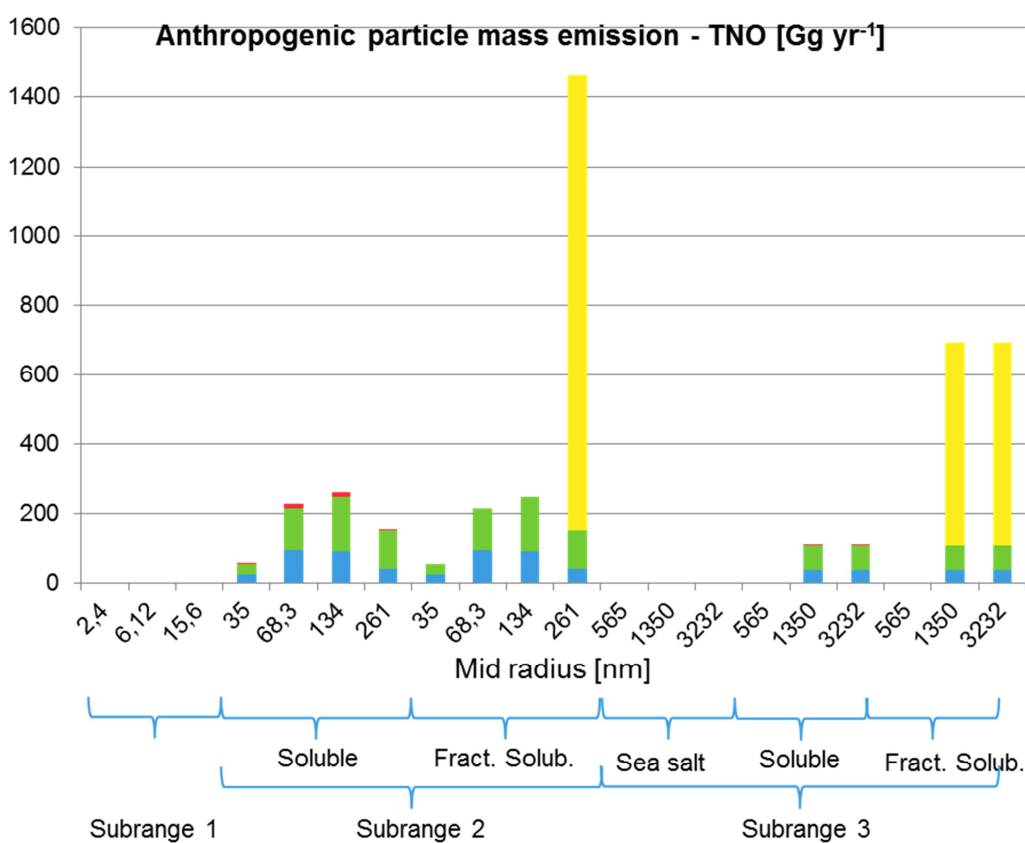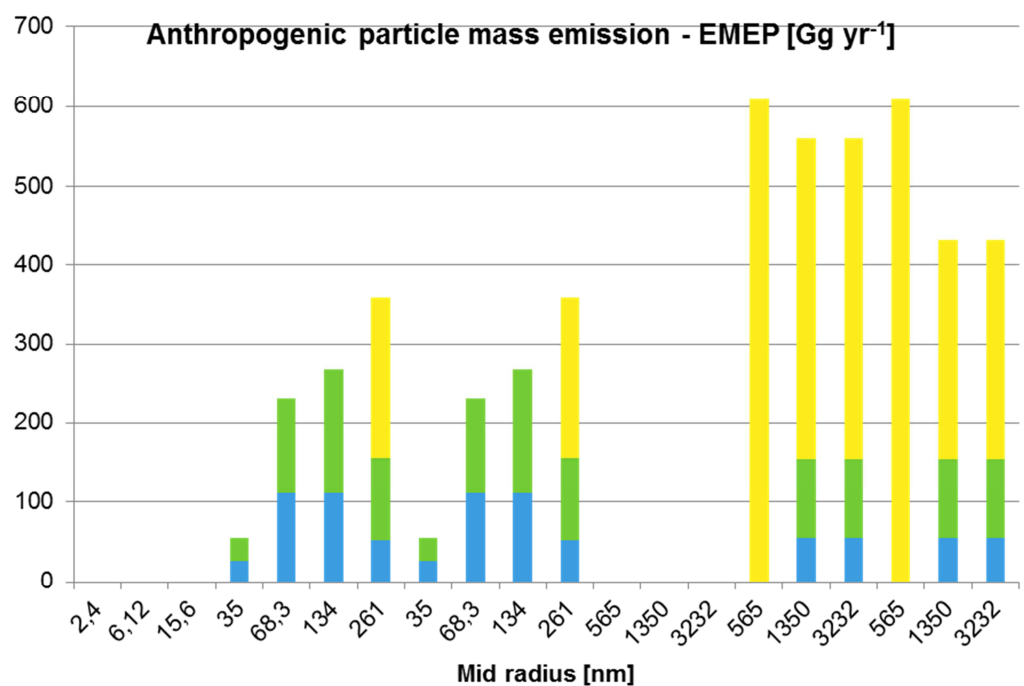
Appendix B
Emissions

Figure B43. Annual total anthropogenic, size resolved, particle number emissions (summed over the model domain) for 2007 with two different emission inventories, Top: EMEP expert emissions (used in wet scavenging sensitivity tests); Bottom: TNO-MACC inventory (used in all other simulations covered in this report). Particle number emissions due to primary sea salt are not included in the panels.

Figure B44. Annual total anthropogenic, size resolved, particulate mass emissions for 2007 (summed over the model domain) with two different emission inventories, Top: EMEP expert emissions (used in wet scavenging sensitivity tests); Bottom: TNO-MACC inventory (used in all other simulations covered in this report). Particle mass emissions due to primary sea salt are not included in the panels.
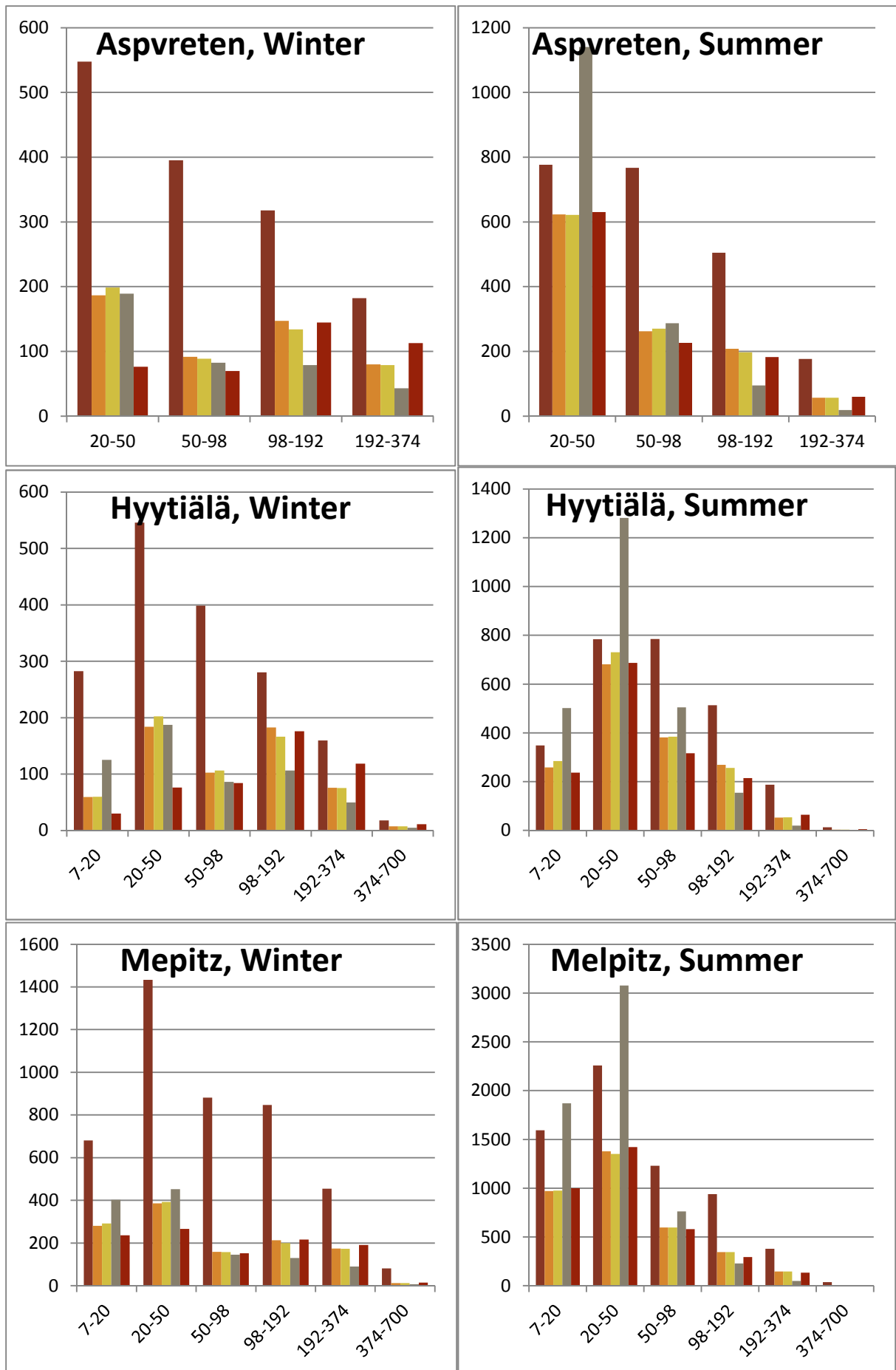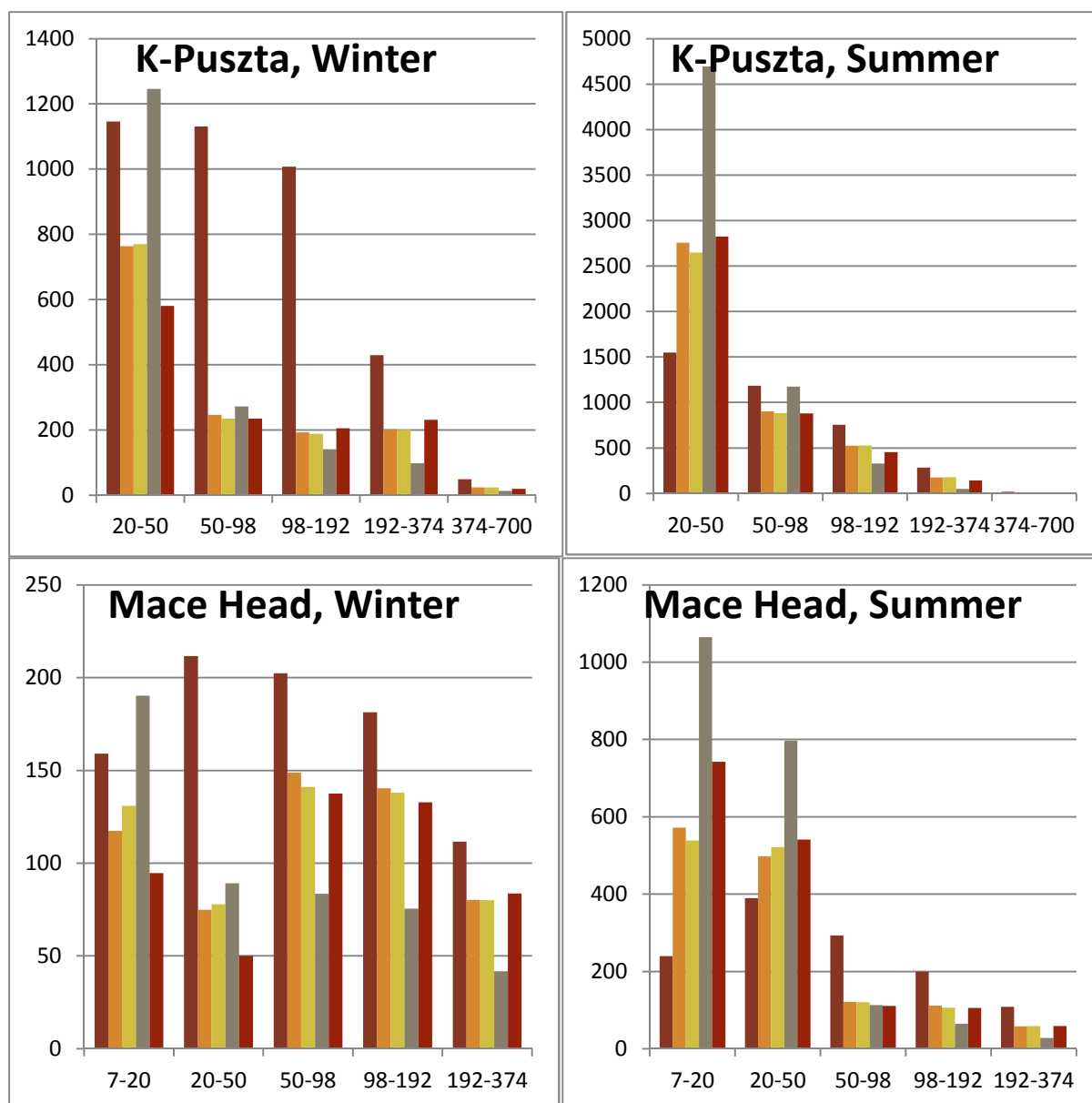
Appendix C
Sensitivity tests

Figure C45. Particle number concentration size distribution at five measurements sites in 2007: observed (brown) and four model versions (different treatments of wet deposition). The model versions are described in Table 14, where orange is baseE, yellow is cloud, grey is L1 and red is L2.

SMHI Publications

SMHI publish seven reportseries. Three of these, the R-series, are intended for international readers and are in most cases written in English. For the others the Swedish language is used.

Name of the series	Published since
RMK (Report Meteorology and Climatology)	1974
RH (Report Hydrology)	1990
RO (Report Oceanography)	1986
METEOROLOGI	1985
HYDROLOGI	1985
OCEANOGRAFI	1985
KLIMATOLOGI	2009

Earlier issues published in serie RMK

1　Thompson, T., Udin, I. and Omstedt, A. (1974)
Sea surface temperatures in waters surrounding Sweden.

2　Bodin, S. (1974)
Development on an unsteady atmospheric boundary layer model.

3　Moen, L. (1975)
A multi-level quasi-geostrophic model for short range weather predictions.

4　Holmström, I. (1976)
Optimization of atmospheric models.

5　Collins, W.G. (1976)
A parameterization model for calculation of vertical fluxes of momentum due to terrain induced gravity waves.

6　Nyberg, A. (1976)
On transport of sulphur over the North Atlantic.

7　Lundqvist, J.-E. and Udin, I. (1977)
Ice accretion on ships with special emphasis on Baltic conditions.

8　Eriksson, B. (1977)
Den dagliga och årliga variationen av temperatur, fuktighet och vindhastighet vid några orter i Sverige.

9　Holmström, I., and Stokes, J. (1978)
Statistical forecasting of sea level changes in the Baltic.

10　Omstedt, A. and Sahlberg, J. (1978)
Some results from a joint Swedish-Finnish sea ice experiment, March, 1977.

11　Haag, T. (1978)
Byggnadsindustrins väderberoende, seminarieuppsats i företagsekonomi, B-nivå.

12　Eriksson, B. (1978)
Vegetationsperioden i Sverige beräknad från temperaturobservationer.

13　Bodin, S. (1979)
En numerisk prognosmodell för det atmosfäriska gränsskiktet, grundad på den turbulenta energiekvationen.

14　Eriksson, B. (1979)
Temperaturfluktuationer under senaste 100 åren.

15　Udin, I. och Mattisson, I. (1979)
Havsis- och snöinformation ur datorbearbetade satellitdata - en modellstudie.

16 Eriksson, B. (1979)
Statistisk analys av nederbördsdata. Del I.
Arealnederbörd.

17 Eriksson, B. (1980)
Statistisk analys av nederbördsdata. Del II.
Frekvensanalys av månadsnederbörd.

18 Eriksson, B. (1980)
Årsmedelvärden (1931-60) av nederbörd,
avdunstning och avrinning.

19 Omstedt, A. (1980)
A sensitivity analysis of steady, free
floating ice.

20 Persson, C. och Omstedt, G. (1980)
En modell för beräkning av
luftföroreningars spridning och deposition
på mesoskala.

21 Jansson, D. (1980)
Studier av temperaturinversioner och
vertikal vindskjuvning vid Sundsvall-
Härnösands flygplats.

22 Sahlberg, J. and Törnevik, H. (1980)
A study of large scale cooling in the Bay of
Bothnia.

23 Ericson, K. and Hårsmar, P.-O. (1980)
Boundary layer measurements at Klock-
rike. Oct. 1977.

24 Bringfelt, B. (1980)
A comparison of forest evapotranspiration
determined by some independent methods.

25 Bodin, S. and Fredriksson, U. (1980)
Uncertainty in wind forecasting for wind
power networks.

26 Eriksson, B. (1980)
Graddagsstatistik för Sverige.

27 Eriksson, B.(1981)
Statistisk analys av nederbördsdata. Del
III. 200-åriga nederbördsserier.

28 Eriksson, B. (1981)
Den "potentiella" evapotranspirationen i
Sverige.

29 Pershagen, H. (1981)
Maximisnödjup i Sverige (perioden
1905-70).

30 Lönnqvist, O. (1981)
Nederbördsstatistik med praktiska
tillämpningar.
(Precipitation statistics with practical
applications.)

31 Melgarejo, J.W. (1981)
Similarity theory and resistance laws for
the atmospheric boundary layer.

32 Liljas, E. (1981)
Analys av moln och nederbörd genom
automatisk klassning av AVHRR-data.

33 Ericson, K. (1982)
Atmospheric boundary layer field
experiment in Sweden 1980, GOTEX II,
part I.

34 Schoeffler, P. (1982)
Dissipation, dispersion and stability of
numerical schemes for advection and
diffusion.

35 Undén, P. (1982)
The Swedish Limited Area Model. Part A.
Formulation.

36 Bringfelt, B. (1982)
A forest evapotranspiration model using
synoptic data.

37 Omstedt, G. (1982)
Spridning av luftförorening från skorsten i
konvektiva gränsskikt.

38 Törnevik, H. (1982)
An aerobiological model for operational
forecasts of pollen concentration in the air.

39 Eriksson, B. (1982)
Data rörande Sveriges temperaturklimat.

40 Omstedt, G. (1984)
An operational air pollution model using
routine meteorological data.

41 Persson, C. and Funkquist, L. (1984)
Local scale plume model for nitrogen
oxides. Model description.

42 Gollvik, S. (1984)
Estimation of orographic precipitation by
dynamical interpretation of synoptic model
data.

43 Lönnqvist, O. (1984)
Congression - A fast regression technique
with a great number of functions of all
predictors.

44 Laurin, S. (1984)
Population exposure to SO and NO_x from
different sources in Stockholm.

45 Svensson, J. (1985)
Remote sensing of atmospheric tempera-
ture profiles by TIROS Operational
Vertical Sounder.

46 Eriksson, B. (1986)
Nederbörds- och humiditetsklimat i
Sverige under vegetationsperioden.

47 Taesler, R. (1986)
Köldperioden av olika längd och
förekomst.

48 Wu Zengmao (1986)
Numerical study of lake-land breeze over
Lake Vättern, Sweden.

49 Wu Zengmao (1986)
Numerical analysis of initialization
procedure in a two-dimensional lake
breeze model.

50 Persson, C. (1986)
Local scale plume model for nitrogen
oxides. Verification.

51 Melgarejo, J.W. (1986)
An analytical model of the boundary layer
above sloping terrain with an application to
observations in Antarctica.

52 Bringfelt, B. (1986)
Test of a forest evapotranspiration model.

53 Josefsson, W. (1986)
Solar ultraviolet radiation in Sweden.

54 Dahlström, B. (1986)
Determination of areal precipitation for the
Baltic Sea.

55 Persson, C., Rodhe, H. and De Geer, L.-E.
(1986)
The Chernobyl accident - A meteorological
analysis of how radionucleides reached
Sweden.

56 Persson, C., Robertson, L., Grennfelt, P.,
Kindbom, K., Lövblad, G. och Svanberg,
P.-A. (1987)
Luftföroreningsepisoden över södra
Sverige 2 - 4 februari 1987.

57 Omstedt, G. (1988)
An operational air pollution model.

58 Alexandersson, H. and Eriksson, B. (1989)
Climate fluctuations in Sweden
1860 - 1987.

59 Eriksson, B. (1989)
Snödjupsförhållanden i Sverige -
Säsongerna 1950/51 - 1979/80.

60 Omstedt, G. and Szegö, J. (1990)
Människors exponering för
luftföroreningar.

61 Mueller, L., Robertson, L., Andersson, E.
and Gustafsson, N. (1990)
Meso-   scale objective analysis of near
surface temperature, humidity and wind,
and its application in air pollution
modelling.

62 Andersson, T. and Mattisson, I. (1991)
A field test of thermometer screens.

63 Alexandersson, H., Gollvik, S. and
Meuller, L. (1991)
An energy balance model for prediction of
surface temperatures.

64 Alexandersson, H. and Dahlström, B.
(1992)
Future climate in the Nordic region -
survey and synthesis for the next century.

65 Persson, C., Langner, J. and Robertson, L.
(1994)
Regional spridningsmodell för Göteborgs
och Bohus, Hallands och Älvsborgs län. (A
mesoscale air pollution dispersion model
for the Swedish west-coast region. In
Swedish with captions also in English.)

66 Karlsson, K.-G. (1994)
Satellite-estimated cloudiness from NOAA AVHRR data in the Nordic area during 1993.

67 Karlsson, K-G. (1996)
Cloud classifications with the SCANDIA model.

68 Persson, C. and Ullerstig, A. (1996)
Model calculations of dispersion of lindane over Europe. Pilot study with comparisons to easurements around the Baltic Sea and the Kattegat.

69 Langner, J., Persson, C., Robertson, L. and Ullerstig, A. (1996)
Air pollution Assessment Study Using the MATCH Modelling System. Application to sulfur and nitrogen compounds over Sweden 1994.

70 Robertson, L., Langner, J. and Engardt, M. (1996)
MATCH - Meso-scale Atmosperic Transport and Chemistry modelling system.

71 Josefsson, W. (1996)
Five years of solar UV-radiation monitoring in Sweden.

72 Persson, C., Ullerstig, A., Robertson, L., Kindbom, K. and Sjöberg, K. (1996)
The Swedish Precipitation Chemistry Network. Studies in network design using the MATCH modelling system and statistical methods.

73 Robertson, L. (1996)
Modelling of anthropogenic sulfur deposition to the African and South American continents.

74 Josefsson, W. (1996)
Solar UV-radiation monitoring 1996.

75 Häggmark, L. Ivarsson, K.-I. and Olofsson, P.-O. (1997)
MESAN - Mesoskalig analys.

76 Bringfelt, B., Backström, H., Kindell, S., Omstedt, G., Persson, C. and Ullerstig, A. (1997)
Calculations of PM-10 concentrations in

Swedish cities- Modelling of inhalable particles

77 Gollvik, S. (1997)
The Teleflood project, estimation of precipitation over drainage basins.

78 Persson, C. and Ullerstig, A. (1997)
Regional luftmiljöanalys för Västmanlands län baserad på MATCH modell-beräkningar och mätdata - Analys av 1994 års data

79 Josefsson, W. and Karlsson, J.-E. (1997)
Measurements of total ozone 1994-1996.

80 Rummukainen, M. (1997)
Methods for statistical downscaling of GCM simulations.

81 Persson, T. (1997)
Solar irradiance modelling using satellite retrieved cloudiness - A pilot study

82 Langner, J., Bergström, R. and Pleijel, K. (1998)
European scale modelling of sulfur, oxidized nitrogen and photochemical oxidants. Model development and evaluation for the 1994 growing season.

83 Rummukainen, M., Räisänen, J., Ullerstig, A., Bringfelt, B., Hansson, U., Graham, P. and Willén, U. (1998)
RCA - Rossby Centre regional Atmospheric climate model: model description and results from the first multi-year simulation.

84 Räisänen, J. and Döscher, R. (1998)
Simulation of present-day climate in Northen Europé in the HadCM2 OAGCM.

85 Räisänen, J., Rummukainen, M., Ullerstig, A., Bringfelt, B., Hansson, U. and Willén, U. (1999)
The First Rossby Centre Regional Climate Scenario - Dynamical Downscaling of CO_2-induced Climate Change in the HadCM2 GCM.

86 Rummukainen, M. (1999)
On the Climate Change debate

87 Räisänen, J. (2000)
    CO_2-induced climate change in northern
    Europé: comparison of 12 CMIP2
    experiments.

88 Engardt, M. (2000)
    Sulphur simulations for East Asia using the
    MATCH model with meteorological data
    from ECMWF.

89 Persson, T. (2000)
    Measurements of Solar Radiation in
    Sweden 1983-1998

90 Michelson, D. B., Andersson, T.,
    Koistinen, J., Collier, C. G., Riedl, J.,
    Szturc, J., Gjertsen, U., Nielsen, A. and
    Overgaard, S., (2000)
    BALTEX Radar Data Centre Products and
    their Methodologies

91 Josefsson, W. (2000)
    Measurements of total ozone 1997 – 1999

92 Andersson, T. (2000)
    Boundary clear air echos in southern
    Sweden

93 Andersson, T. (2000)
    Using the Sun to check some weather radar
    parameters

94 Rummukainen, M., Bergström, S., Källén,
    E., Moen, L., Rodhe, J. and Tjernström, M.
    (2000)
    SWECLIM – The First Three Years

95 Meier, H. E. M. (2001)
    The first Rossby Centre regional climate
    scenario for the Baltic Sea using a 3D
    coupled ice-ocean model

96 Landelius, T., Josefsson, W. and Persson,
    T. (2001)
    A system for modelling solar radiation
    parameters with mesoscale spatial
    resolution

97 Karlsson, K.-G. (2001)
    A NOAA AVHRR cloud climatology over
    Scandinavia covering the period 1991-
    2000

98 Bringfelt, B., Räisänen, J., Gollvik, S.,
    Lindström, G., Graham, P. and Ullerstig,
    A., (2001)
    The land surface treatment for the Rossby
    Centre Regional Atmospheric Climate
    Model - version 2 (RCA2)

99 Kauker, F. and Meier, H. E. M., (2002)
    Reconstructing atmospheric surface data
    for the period 1902-1998 to force a
    coupled
    ocean-sea ice model of the Baltic Sea.

100 Klein, T., Bergström, R. and Persson, C.
    (2002)
    Parameterization of dry deposition in
    MATCH

101 Räisänen, J., Hansson, U., Ullerstig A.,
    Döscher, R., Graham, L. P., Jones, C.,
    Meier, M., Samuelsson, P.and Willén, U.
    (2003)
    GCM driven simulations of recent and
    future climate with the Rossby Centre
    coupled atmosphere - Baltic Sea regional
    climate model RCAO

102 Tjernström, M., Rummukainen, M.,
    Bergström, S., Rodhe, J. och Persson, G.,
    (2003)
    Klimatmodellering och klimatscenarier ur
    SWECLIMs perspektiv.

103 Segersson, D. (2003)
    Numerical Quantification of Driving Rain
    on Buildings

104 Rummukainen, M. and the SWECLIM
    participants (2003)
    The Swedish regional climate modeling
    program 1996-2003. Final report.

105 Robertson, L. (2004)
    Extended back-trajectories by means of
    adjoint equations

106 Rummukainen, M., Bergström S., Persson
    G., Ressner, E (2005)
    Anpassningar till klimatförändringar

107 Will not be published

108 Kjellström, E., Bärring, L., Gollvik, S.,
    Hansson, U., Jones, C., Samuelsson, P.,
    Rummukainen, M., Ullerstig, A., Willén,

U., Wyser, K., (2005)
A 140-year simulation of European climate with the new version of the Rossby Centre regional atmospheric climate model (RCA3).

109 Meier, H.E.M., Andréasson, J., Broman, B., Graham, L. P., Kjellström, E., Persson, G., and Viehhauser, M., (2006)
Climate change scenario simulations of wind, sea level, and river discharge in the Baltic Sea and Lake Mälaren region – a dynamical downscaling approach from global to local scales.

110 Wyser, K., Rummukainen, M., Strandberg, G., (2006)
Nordic regionalisation of a greenhouse-gas stabilisation scenario

111 Persson, G., Bärring, L., Kjellström, E., Strandberg G., Rummukainen, M., (2007).
Climate indices for vulnerability assessments

112 Jansson, A., Persson, Ch., Strandberg, G., (2007)

2D meso-scale re-analysis of precipitation, temperature and wind over Europe - ERAMESAN

113 Lind, P., Kjellström, E., (2008)
Temperature and Precipitation changes in Sweden; a wide range of model-based projections for the 21st century

114 Klein, T., Karlsson, P-E., Andersson, S., Engardt, M., Sjöberg, K (2011)
Assessing and improving the Swedish forecast and information capabilities for ground-level ozone